BRILLOUIN SPECTROSCOPIC STUDIES OF THE ELASTIC PROPERTIES OF ARTIFICIAL AND NATURAL ICE SAMPLES

PETER HENRY GAMMON

BRILLOUIN SPECTROSCOPIC STUDIES OF THE ELASTIC PROPERTIES OF ARTIFICIAL AND NATURAL ICE SAMPLES

by

Peter Henry Gammon, B.Sc. (Hons.), M.Sc.

A Thesis submitted in partial fulfillment
of the requirements for the degree of
Doctor of Philosophy

Department of Physics
Memorial University of Newfoundland

April 1981

St. John's Newfoundland

ABSTRACT

The method of Brillouin spectroscopy has been used to measure the dynamic elastic moduli of local homogeneous regions in ice samples representing four different environments of formation. These included artificial ice frozen from distilled water, clear monocrystalline glacial ice, bubbly lake ice and sea ice. Results show Brillouin spectroscopy to be an effective technique for accurately measuring the small scale elastic properties (between inclusions) of natural ice samples.

The four samples studied were found to have identical microscopic elastic properties, that is, the respective measured sets of elastic moduli showed agreement within experimental uncertainty. Accordingly, the elastic properties of homogeneous monocrystalline ice have been found not to vary with sample age, with impurities present at the time of freezing or with crystal quality. The bulk elastic properties of ice remain of course, subject to modification by differing crystal grain textures and by the presence of inclusions of various sorts.

Weighted mean adiabatic elastic moduli for homogeneous monocrystalline ice (equivalently, local regions in polycrystalline or heterogeneous ice) have been calculated from the combined Brillouin spectroscopic data for the four types of samples. The values at -16°C were determined to be $c_{11} = 139.29 \pm .41$, $c_{12} = 70.82 \pm .39$, $c_{13} = 57.65 \pm .23$, $c_{33} = 150.10 \pm .46$, $c_{44} = 30.14 \pm .11$ (units of 10^8 N/m^2 or kbar). A simplified linear temperature correction relation for the elastic

moduli has been determined from Brillouin data obtained at -3°C and at -16°C. A full range of derived elastic parameters for monocrystalline ice and for homogenedus isotropic polycrystalline ice has been calculated.

The values for elastic moduli obtained in the present work are subject to smaller overall uncertainty than are values obtained by previous authors. Agreement of the present results with previous measurements is generally good but not in all cases within experimental uncertainty. Unnoticed systematic error in previous measurements provides the most probable explanation for the discrepancies. However, variation of elastic moduli induced by unusual sample preparation techniques cannot be entirely ruled out. Prior to the present application of Brillouin spectroscopy no single technique for measuring the elastic moduli of ice has been applied in a uniform manner to ice samples from several sources. Hence, the present results are unique in that their applicability to ice from a wide range of sources has been experimentally verified.

In a departure from the primary objective of the Brillouin spectroscopic studies (measurement of elastic moduli) the method has also been used to investigate the local acoustic properties of the crystal grain boundary region in a bicrystalline sample of river ice. Spectra from the boundary region showed a distinct and unexpected asymmetry in the Brillouin frequency shifts of the upshifted versus the downshifted longitudinal components. The precise physical processes underlying the observations have not been determined. However, it has been verified that the effect was not instrumental. Interaction between bulk and surface acoustic modes propagating in the grain

boundary region appears to provide a plausible line of explanation. Additional theory and experimental work, continuing from the present work can be expected to yield valuable direct information on the structure and physical properties of the crystal grain boundary region in polycrystalline ice.

ACKNOWLEDGEMENTS

In carrying out the work leading to the completion of this thesis, I benefitted from the kind assistance and support of a number of people. Here I would like to acknowledge their help, cooperation and interest in this work.

My supervisors, Dr. H. Kiefte and Dr. M.J. Clouter were generous in sharing both their considerable expertise in the technique of Brillouin spectroscopy and their fine set of experimental apparatus. Their appreciation of the value of extending techniques usually reserved for pure research into the realm of practical applications was instrumental in making this project possible.

The work on natural ice was motivated to a large extent by the keen interest of Dr. W.W. Denner in finding genuinely new technology to aid in unravelling the complex mechanical properties of sea ice. His insight and guidance throughout are sincerely appreciated. Some of the ice samples used in this work were provided through the courtesy of Dr. G. Lemieux and Dr. S. Ackley at the U.S. Army Cold Regions Research and Engineering Laboratory, Hanover, New Hampshire.

The assistance of Dr. J.C. Lewis in translating some of the German literature on ice elasticity is gratefully acknowledged. I must also express my gratitude to Mrs. Dallas Strange for her expert typing of the thesis manuscript.

Finally, I would like to thank my wife, Daisy, for her constant patience and support in what seemed at times to be an endless

occupation capable of swallowing up every spare minute. Her determination to help me see this project through extended beyond just moral support. I am thus proud to acknowledge her tangible assistance in carrying out this work including, as just one example, her dictation to me of thousands of elements of Brillouin spectroscopic data over the telephone. This procedure not only bypassed interface problems between incompatible electronic hardware (see Chapter 5) but also was sometimes almost fun. Thanks a million, Daisy.

TABLE OF CONTENTS

LIST OF TABLES

LIST OF FIGURES

CHAPTER 1

BACKGROUND AND OBJECTIVES

1.1 Introductory Remarks

Solid H_2O, or ice, is one of the most abundant minerals on the surface of the earth. It is also, in terms of chemical composition, one of the simplest minerals. The combination of these two properties, natural abundance and chemical simplicity, has made ice among the most well studied of all solids. Ice research has been undertaken from many viewpoints ranging from theoretical studies of crystal physics or lattice dynamics to applied research into the interaction of ice with offshore structures. Even with this breadth of approach and with the undoubted importance attached to understanding the physical properties of ice, much research must yet be done before basic results obtained via the methods of mathematics, physics and chemistry can be extended reliably into the realm of engineering applications. The work to be presented here, while limited to what is probably the least complex and most well understood aspect of the mechanical behaviour of ice, is intended to yield a step in that important direction.

Ice, as it occurs in the natural environment, is a transparent crystalline substance possessing hexagonal symmetry. The triangular shape of the water molecule, which is preserved in the ice crystal structure, is in part responsible for the relative complexity of the ice unit cell. This incorporates a net total of four

oxygen atoms and eight hydrogen atoms. The oxygen atoms are arranged such that the four nearest neighbours of a given oxygen atom lie at the vertices of a nearly regular tetrahedron. The hydrogen atoms (protons) have mean positions lying approximately along the lines joining nearest neighbour oxygen atoms but are not centred, instead dividing the O-O distance in the ratio of about 1:2. One proton lies along each nearest neighbour O-O bond and two protons are associated with each oxygen atom. The H-O-H bond angle in free H_2O, 105^o, is near the tetrahedral angle, 109.5^o, thus allowing water molecules to undergo only a small change in shape when incorporated into the hexagonal ice crystal structure. Additional description of the crystal structure of the normal phase of ice, including diagrams, can be found in the texts by Fletcher[1] or by Hobbs[2] or in the review article by Glen.[3]

The hexagonal phase of ice, found in the natural environment and designated ice Ih, is only one of a large number of polymorphs of solid H_2O. These polymorphs including amorphous ice, the metastable cubic phase ice Ic, and the high pressure and/or low temperature phases ice II to ice IX, have ranges of thermodynamic stability which lie outside the range of temperatures and pressures encountered in the natural environment. They are thus observed only in the laboratory but are nevertheless of interest in terms of analyzing the nature of the hydrogen bond which links adjacent molecules in each of the various phases of ice. In passing, it might be noted that a possible commercial application of knowledge of the existence and properties of the high pressure polymorphs of ice lies in the timely engineering problem of the demolition of icebergs by explosives. A

review of work regarding ice polymorphs along with the phase diagram for ice can be found in the article by Whalley[4] or in the references[1,2,3] cited above relating to crystal structure. Work to date has concentrated mainly on the crystallographic and thermodynamic properties of the ice polymorphs other than ice Ih. It can be noted that the Brillouin spectroscopic techniques to be discussed in relation to the present work are readily adaptable to the investigation of the elastic properties of several of the polymorphs.

Ice Ih (henceforth used interchangeably with "ice") is presumed to belong to the space group $P6_3/mmc$, that is, the crystal is presumed to possess maximal symmetry within the hexagonal system. Ice demonstrates optical birefringence but has one of the smallest differences in ordinary and extraordinary refractive indices (see Sec. 3.3) of all materials. Crystal grain boundaries in a polycrystalline ice chip are thus visible when viewed through crossed polaroid filters, even when the chip is several millimetres thick. The mechanical properties of ice are among the most complex of any common material. The reaction of pure monocrystalline ice to stress includes an elastic or recoverable component, a plastic or irrecoverable component, an anelastic or delayed recoverable component and brittle behaviour or fracture. The time rate of change of stress or strain along with the instantaneous values of stress or strain determine the relative importance of the various mechanisms of ice deformation. The relative importance of these mechanisms may also be strongly influenced by the crystal quality and purity of an ice sample. The article by Glen[5] reviews the mechanical properties of monocrystalline and polycrystalline pure ice while the review article

by Weeks and Assur[6] focuses on the mechanical properties of frozen ocean water or sea ice. The text by Hobbs[2] includes a lengthy chapter on the mechanical properties of ice as does the text by Michel.[7]

1.2 Elasticity in Ice

The present work deals entirely with the elastic properties of homogeneous ice. A mechanical deformation is said to be elastic when the deformed body returns to its exact original configuration upon removal of the pressure or stress which caused the deformation. Elastic deformation conserves mechanical energy. That is, the mechanical energy required to deform an elastic body can be entirely recovered in the process of allowing the body to relax back to its original shape. In almost all solid media, including ice, elastic behaviour is accurately described by a linear relation known as Hooke's law:

$$\sigma_{ij} = \sum_{k=1}^{3} \sum_{l=1}^{3} c_{ijkl}\, e_{kl} \qquad (1\text{-}1)$$

In equation (1-1), σ denotes the stress tensor. This is a 3 x 3 Cartesian tensor with elements σ_{ij} equalling the j'th component of the force acting on a unit element of surface area normal to coordinate i. The σ_{ij} have units of pressure. The elements of the strain tensor, e_{kl}, specify the spatial rate of change of the displacement of an infinitesimal volume of material from its initial (unstrained) position. The e_{kl} are dimensionless. The linear coefficients, c_{ijkl}, are elements of a 3 x 3 x 3 x 3 (4th rank) Cartesian tensor and are known as the elastic stiffness constants. Knowledge of these constants for a given crystalline medium completely determines the elastic reaction of that medium to an arbitrary stress configuration.

The c_{ijkl} have units of pressure. Further details of the theory of elasticity in anisotropic (crystalline) media can be found in numerous texts[8,9,10,11] or in the thesis by Gammon.[12]

General symmetry conditions along with specific conditions imposed by hexagonal symmetry allow the 81 elastic constants appearing in (1-1) to be expressed in terms of five independent constants when dealing with hexagonal crystalline media. The five constants are usually taken to be c_{11}, c_{12}, c_{13}, c_{33} and c_{44} where the c_{ij} denote elements of a 6 x 6 matrix. The form of this elastic stiffness constant matrix and its inverse, the elastic compliance constant matrix, for hexagonal media is given in each of the five references[8,9,10,11,12] cited above in relation to crystal elasticity theory. The elastic constants c_{ij} equal the tensor elements c_{ijkl} with the following correspondence of subscripts.

11 → 1	23 or 32 → 4	
22 → 2	13 or 31 → 5	(1-2)
33 → 3	12 or 21 → 6	

In making the correspondence (1-2) the four subscripts of the tensor elements are divided into two pairs comprising the first two and the second two subscripts, respectively. The correspondence (1-2) and the normal form of the matrix c_{ij} are both dependent on the choice of a Cartesian coordinate system fixed with the z axis parallel to the 6-fold axis (c axis) of the hexagonal monocrystalline medium. Henceforth, this axis specification will be assumed. The rotation angle of the x and y axes about the c axis can be specified arbitrarily as noted below.

The condition that the elastic modulus tensor be invariant under rotation of $\pi/3$ about $\hat{c}$, necessitated by hexagonal symmetry, gives rise to complete cylindrical isotropy in the elastic properties of ice. Hence, when dealing strictly with elasticity, directions relative to the crystallographic axes need be specified only in terms of the angle versus the crystal c axis. This angle, henceforth denoted γ, completely determines the directional dependence of the elastic behaviour of hexagonal media. For example, sound velocity in monocrystalline ice depends only on the angle γ between the direction of propagation and the crystal c axis.

The elastic properties of polycrystalline ice can be determined from the elastic constants of monocrystalline ice if the sizes, shapes and orientations of the crystal grains constituting the polycrystalline sample are known. In practice, knowledge of crystal grain structure for large polycrystalline samples is invariably statistical in nature and an appropriate averaging procedure must be used to determine bulk elastic properties from the elastic constants of monocrystalline ice. One such averaging procedure, developed by Voigt[13] for arbitrary hexagonal media assumes uniform random orientations of the c axes of small grains comprising a polycrystalline sample. This assumption leads to isotropy in the elastic properties of the bulk. These elastic properties can thus be expressed in terms of any two independent classical elastic parameters, for instance, Young's modulus and Poisson's ratio. Explicit equations giving Young's modulus and Poisson's ratio for polycrystalline ice in terms of the elastic constants c_{ij} for monocrystalline ice are stated, based on the model of Voigt,[13] in the article by Penny.[14] Equivalent

results are obtained using the averaging procedure of Sec. 6.2. This procedure has the advantage of being readily adaptable to the case of preferred or nonrandom grain orientation as may often be appropriate when dealing with natural ice samples. The elastic constants of monocrystalline ice can be used to determine limiting values for the range of variation of the elastic properties of homogeneous polycrystalline ice samples.

Natural ice samples may be heterogeneous in composition, that is, they may contain inclusions of material other than ice. Such inclusions usually consist of air or water vapour (air bubbles, internal cracks, etc.) or liquid water (Tyndall figures, brine cells, brine channels, etc.). Liquid inclusions are significant only in ice frozen from salt water (sea ice) or in fresh water ice at temperatures very near the melting point. Solid particulate inclusions may be present in ice frozen from water containing suspended matter or in sea ice at temperatures low enough ($< -25^{\circ}C$) to precipitate significant quantities of dissolved ionic compounds. Analysis of the complex and significant effects of inclusions on the elastic properties of natural ice lies outside the scope of the present work. To date, most investigations in this area have focused on the elastic and other mechanical properties of sea ice. This work is reviewed in the text by Doronin and Kheisin[15] and in the article by Weeks and Assur.[6] An explicit measurement of the dependence of Young's modulus for polycrystalline sea ice on porosity has been reported by Langleben.[16]

The elastic properties of ice dominate mechanical behaviour when the rapid application of moderate stress results in moderate strain. The quasi-static deformation measurements of Gold,[17] using

homogeneous polycrystalline ice at temperatures between -3°C and -40°C, indicated apparently pure elastic reaction when a maximum stress of 10^6 N/m^2 was applied for less than 10 s. The resultant strain was of the order of 10^{-4}. Tensile stress or shear stress of the order of 10^7 N/m^2 is usually associated with the occurrence of fracture in ice.[2] Accordingly, a rough estimate for the elastic limit of homogeneous ice is 10^7 N/m^2 stress or 10^{-3} strain (see Chapter 6 for values of elastic parameters) when stress is applied rapidly. For stress of appreciable duration, an elastic limit of 10^5 N/m^2 stress or 10^{-4} strain seems appropriate based on the observations of Gold.[17] Under pure hydrostatic stress, no obvious limit exists beyond which linear elastic deformation ceases. However, the region of phase stability of ice Ih ends at a pressure approximating 2×10^8 N/m^2 at temperatures below -20°C and transformation to liquid water occurs at lower hydrostatic stress when the temperature exceeds -20°C (see phase diagram[4]).

The aspect of the mechanical behaviour of ice most nearly determined by elastic properties only, is vibration or sound propagation. At frequencies exceeding 1 Hz, stress duration is considerably less than the time required to induce significant nonelastic deformation. Thus, mechanical vibrations in ice, excepting those of ultra-low frequency (less than 1 Hz) or those of extreme intensity (peak stress greater than 10^7 N/m^2) are almost purely elastic in nature. Virtually all common sources of acoustic vibrations fall within this range.

While knowledge of the elastic properties of ice may be used to determine acoustic properties, it is more common for sound velocity

measurements to be used in determining elastic moduli. The equations linking acoustic propagation velocities to the density and elastic moduli of a solid medium are derived by equating the mass times the acceleration of a differential volume element with the elastic force applied to that element, determined via Hooke's law. The procedure leads to the vanishing of the determinant of a 3 x 3 dynamical matrix having elements which are linear combinations of the elastic moduli and the product of the density with the square of the sound velocity. The zero determinant in turn implies an equation which is cubic in the square of the sound velocity, thus yielding, in the general case, three distinct expressions for the magnitudes of the velocities of acoustic waves. These velocity expressions are associated with three orthogonal polarizations or particle displacement vectors. The acoustic mode with polarization parallel to the propagation direction is referred to as longitudinal or compressional while the two orthogonal modes with polarization normal to the propagation direction are referred to as transverse or shear. In anisotropic (crystalline) media, the three acoustic modes each have velocity which is, in general, dependent on direction relative to crystal symmetry and the two transverse modes have distinct propagation velocities. In isotropic (polycrystalline or amorphous) media, no directional dependence in sound velocity exists and the two shear modes have equal velocity.

Detailed discussion of the propagation of elastic vibrations in solids can be found in numerous texts. These include Landau and Lifshitz[8] (derivation of determinantal equation for anisotropic media, complete analysis for isotropic media), Malvern[18] (complete

analysis for isotropic media), Musgrave[11] (complete analysis for anisotropic media), and McSkimin[19] (emphasis on application to ultrasonic measurements). An outline of the derivation of the sound velocity equations for hexagonal crystalline media is included, along with the equations in explicit form, in the thesis by Gammon.[12] These equations have been reproduced, in slightly modified form, in the present thesis (Sec. 2.2).

There are several direct practical applications for data regarding the acoustic properties of ice. For example, acoustic measurements have been used in studying the annual variations in the properties of sea ice and the variations from point to point in the ice cover.[15] The thickness of both fresh water ice and ocean ice may be measured by acoustic techniques. Acoustic (seismic) studies of glaciers are used to infer composition and structure of large ice masses. Detection of ice in the ocean by ultrasonic (sonar) techniques requires analysis of the phenomenon of acoustic reflection at the ice-water interface. Clearly, many more existing or potential applications could be enumerated.

As noted above, the mechanical reaction of ice to quasi-static stress is only partly elastic. Creep,[20] or plastic yield may be the dominant mechanism of deformation even at very low stress ($\sim 10^5$ N/m^2), given sufficient time. Nevertheless, knowledge of the elastic properties of ice is important in analyzing mechanical deformation in almost all cases. This importance stems from the fact that the first reaction of ice to any mechanical stress is purely elastic and that subsequent nonelastic deformation will be governed by the stress field established within the ice by elastic forces.

Thus, for example, in analyzing the collision of a floating ice mass with an offshore structure, one would proceed by assuming that the initial deformation following impact was entirely elastic. By way of the equations of elasticity, the resultant stress and strain within the ice would then be determined. Analysis of subsequent mechanical deformation, for instance plastic yield and fracture propagation, would be based on this initial determination of stress and elastic strain. Continuous reevaluation of the stress field due to internal elastic strain would be required as nonelastic deformation of the ice mass proceeded. Similar reasoning applies in analysis relating to ice dynamics, that is, the interaction of floating ice masses with one another under the influence of aerodynamic and hydrodynamic stress. Thus the equations underlying models for forecasting ice cover (for example, the AIDJEX[21] model) usually include Hooke's law and the elastic moduli of ice.

Values for the elastic moduli of ice find application in theoretical and experimental studies of other ice properties. For example, in the analysis of creep, or plastic yield, the internal stress field causing the creation or migration of dislocations is determined from the applied external stress and an assumed distribution of existing dislocations, via the elastic moduli. The migration of dislocations is the principal mechanism of creep in ice. A discussion of the general theory of dislocations in crystals and their relation to the theory of elasticity is given in the text by Landau and Lifshitz.[8] Theoretical and experimental aspects of creep in ice are reviewed by Weertman.[20]

The elastic moduli of ice are ultimately determined by the forces between water molecules in the ice crystal structure. Hence, via the theories of lattice dynamics, an assumed model for the molecular configuration of ice and the forces of interaction between molecules can be used to predict values for the elastic moduli. Comparison of these values with those determined experimentally provides a test for the assumed model. Alternatively, parameters (atomic force constants) in the model may be fitted to measured elastic data. Application of these techniques is illustrated in the articles by Penny,[14] by Haridasan and Govindarajan,[22] and by Renker and Blanckenhagen.[23]

1.3 Previous Studies of the Elastic Properties of Monocrystalline Ice

(i) Before 1940

Work on the elastic properties of ice up until 1940 is reviewed in the text by Dorsey.[24] Most measurements were made using static techniques applied to polycrystalline samples. A few dynamic (sound velocity) measurements were also carried out using polycrystalline samples. These yielded values for Young's modulus and Poisson's ratio which were reasonably consistent with one another, the primary source of scatter likely arising from preferred grain orientation in the samples. The static measurements showed much more scatter and tended to yield values of Young's modulus about one third of those yielded by the dynamic measurements. Error was likely due to plastic yielding (creep) of the samples. Dorsey[24] comments that the static measurements as of 1940 were "mainly of historical interest." The dynamic measurements were insufficiently

precise to identify any directional variation in the elastic moduli of ice.

(ii) Penny

In 1948, Penny[14] reported a quasi-theoretical determination of the elastic moduli of monocrystalline ice. The approach involved utilizing a set of assumptions regarding the arrangement of atoms in the ice unit cell and the corresponding interatomic forces to yield, in effect, the directional dependence of the monocrystalline elastic properties. Experimentally determined values for the polycrystalline elastic moduli of ice were required in the analysis. The result consisted of the five elastic moduli c_{ij} appropriate for monocrystalline ice.

Two assumptions were made by Penny[14] regarding the atomic arrangement of the ice unit cell. Firstly, perfect tetrahedral coordination of the oxygen atoms was assumed. Secondly, the hydrogen atoms were assumed to lie at the midpoints of nearest neighbour O-O bonds. The first assumption was in only small disagreement with existing x-ray crystallographic data while the second assumption differed more substantially from data subsequently obtained from nuclear magnetic resonance studies and from neutron scattering studies in frozen D_2O.[2] The final assumption used by Penny was to include only nearest neighbour interactions in the dynamical model. In view of the open structure of ice Ih and the fact that hydrogen bonding occurs only between nearest neighbour oxygen atoms, this assumption was apparently quite reasonable.

Penny's analysis, which was based on the ordinary theory of lattice dynamics, led to the expression of the five elastic moduli

of ice in terms of two atomic force constants. These force constants were, in turn, fitted to experimental data. Hence, the net result of the analysis was to determine three relations among the five elastic constants of ice. The experimental data used by Penny consisted of the acoustic measurements of Young's modulus and Poisson's ratio for polycrystalline ice by Northwood.[25] These values were linked to the monocrystalline elastic constants via the averaging procedure of Voigt.[13] The results obtained by Penny were thus dependent to a significant extent on the accuracy with which the model of Voigt described the grain structure and hence the elastic properties of the polycrystalline samples studied by Northwood.[25] Without this and other sources of experimental uncertainty, the values for the elastic moduli quoted by Penny would have been in remarkably good agreement with values obtained by subsequent acoustic experiments on monocrystals (see Sec. 6.3).

(iii) Jona and Scherrer

The first experimental determination of the full set of elastic moduli of monocrystalline ice was reported by Jona and Scherrer[26] in 1952. The samples employed were monocrystals of ice at $-16^{\circ}C$, artificially formed from water of unstated purity. The Schaefer-Bergmann method was used to measure the elastic constants. This is a combined optical acoustic technique which facilitates precise measurement of acoustic wavelength in transparent media. Sound waves of a variety of polarizations and propagation directions are induced in a sample with an attached quartz transducer. A monochromatic light beam is then used to probe the sample. The light transmitted by the sample and incident on a screen or photographic

film is divided into a set of concentric geometrical figures as a result of diffraction by acoustically induced periodic spatial variations in refractive index. The acoustic wavelength is determined from the angle through which the light is diffracted. The sound velocity is then deduced using the known frequency of vibration of the transducer. A description of the method, along with several samples of Schaefer-Bergmann patterns can be found in the text by Huntington.[10] The application of the Schaefer-Bergmann technique to ice by Jona and Scherrer[26] yielded reasonably precise values for all five elastic moduli at -16°C (see Sec. 6.3). These values were used to test the three theoretical relations of Penny.[14] Agreement was within experimental uncertainty.

(iv) Green and MacKinnon

In 1956, Green and MacKinnon[27] measured the transit times of compressional and shear acoustic pulses along the c axes of monocrystalline, cylindrical ice samples. These measurements yielded values for c_{33} and c_{44} which were in turn used in calculating the other three elastic moduli by way of the three theoretical relations of Penny.[14] The samples tested were frozen from distilled water and were presumably held at -16°C although this was not stated. Estimated uncertainty in the measured elastic constants was about 3% while the uncertainty in the three calculated elastic constants was about 14%, not including possible error in the theoretical equations. Agreement with the values of Jona and Scherrer[26] was approximately within experimental uncertainty.

(v) Bass, Rosseberg and Ziegler

A measurement of the complete set of elastic compliance constants s_{ij} of monocrystalline ice was reported by Bass, Rosseberg and Ziegler[28] in 1957. The samples used were monocrystalline bars and plates of ice machined from artificially grown bulk samples of unstated purity. Sample temperatures ranging from $-2^{o}C$ to $-30^{o}C$ were used in making the measurements. Hence temperature dependence curves were determined for the compliance moduli. The method of measurement involved observing nodal patterns induced by resonant acoustic vibrations in the monocrystalline bars and plates. The patterns, observed in transmitted polarized sodium light were interpreted to yield the compliance constants. For purposes of comparison with other measurements, the matrix $[s_{ij}]$ obtained by Bass, Rosseberg and Ziegler[28] must be inverted to obtain the elastic stiffness constant matrix $[c_{ij}]$. This process significantly increases uncertainty in the results.

(vi) Bogorodskii (natural ice)

The first measurement of the full set of elastic moduli for monocrystalline natural ice was reported by Bogorodskii[29] in 1964. The samples consisted of large clear monocrystals extracted from bulk ice samples from Lake Ladoga in the U.S.S.R. The monocrystals were extracted by dusting the surface of the bulk samples with "red lead" (presumably Pb_3O_4) and taking advantage of preferential melting (hence penetration of red lead) at grain boundaries which occurred when the bulk samples were left exposed to sunlight for two or three hours. The elastic moduli were determined from measurements of acoustic pulse transit time in three crystallographic directions.

Uncertainty in the measured acoustic velocities approximated 5%, giving rise to uncertainty of the order of 10% in the elastic moduli. These relatively large uncertainties preclude detailed comparison of the measurements of Bogorodskii[29] on natural ice samples with other more precise measurements on artificial ice samples.

(vii) Other work before 1965

The elastic moduli of artificial ice at temperatures ranging from -20°C to very near the melting point were measured by Brockamp and Querfurth[30] in 1964. An ultrasonic pulse method was used. The resulting values (see Chapter 6) were in fairly good agreement with those of Jona and Scherrer.[26] An unexpected drop of about 5% in the elastic moduli was observed at temperature very near melting. Also in 1964, the temperature dependence of two of the elastic moduli of ice, c_{11} and c_{33}, was investigated by Zarembovitch and Kahane[31] using the Schaefer-Bergmann method. The agreement of the measurements at -16°C with those of Jona and Scherrer[26] was excellent.

(viii) Proctor

The first comprehensive investigation of the elastic moduli of ice at low temperatures was reported by Proctor[32] in 1966. Monocrystalline samples frozen from distilled, degassed water were tested over a temperature range from -223°C (50°K) to -23°C (250°K). The complete set of elastic moduli was measured over a smaller range, -213°C to -163°C. An ultrasonic method of measurement was used. The method involved the timing of two consecutive acoustic pulses such that cancellation among the reflections of the pulses within the ice sample occurred. The pulse separation was then used to

determine the round trip transit time in the sample and hence the sound velocity. The resulting elastic modulus data were fitted with a quadratic least squares temperature dependence curve. Extrapolation of this curve to $0^{\circ}K$ facilitated calculation of the Debye temperature for ice (equations and outline of reasoning are given by Huntington[10]). Hobbs[2] points out that the resultant value is in good agreement with heat capacity measurements and with calculations from x-ray data.

(ix) Dantl

In 1967 Dantl[33,34,35] reported results of measurements of the elastic moduli of ice over the broad temperature range, $-140^{\circ}C$ to $-.7^{\circ}C$. Frequency dependence over the range 5 MHz to 140 MHz was also investigated. Particular caution was exercised in forming the monocrystalline ice samples utilized in the measurements. These were grown slowly from water prepared in a quartz multiple distillation apparatus. Tests for pH and conductivity were performed on the water samples prior to freezing and showed minimal acidity along with conductivity approaching the ideal minimum value for pure water (see Dorsey[24]). Although results of a complete water analysis were either not obtained or not reported, the samples were described by Dantl as being "extremely pure." Following freezing, the monocrystalline ice samples were aged for at least eight months at a temperature near the melting point before being used in the acoustic experiments.

The elastic moduli of the ice samples were measured by Dantl using a combination of two acoustic techniques. The first of these was a conventional pulse echo technique where the round trip transit time of an acoustic pulse emitted by a quartz transducer bonded to

the ice sample was measured versus a calibrated electrical delay line. This technique was rapid in its application and was hence well suited to making the large number of measurements required in determining the temperature dependence of the five elastic moduli. However, the technique was felt by Dantl to yield possible large error in absolute measurements of the elastic moduli (see Sec. 6.3). Relative measurements, on the other hand, were not subject to this uncertainty. Thus, while the pulse echo method was presumed accurate in specifying the shapes of the temperature and frequency dependence curves, the overall heights of the curves required checking by a second technique.

A double pulse interference method[33,36,37] involving cancellation of successive pulses by reflections within the ice sample (in some respects similar to the method of Proctor[32]) was used by Dantl to check several of the sound velocity measurements obtained using the pulse echo technique. This method was apparently assumed by Dantl to yield no significant uncertainty in velocity measurement. The checks performed indicated that correction of the initial pulse echo results was not required (see Sec. 6.3).

The measurements of Dantl were interpreted to yield least squares quadratic temperature dependence curves for the elastic moduli of ice over the range $-140^{\circ}C$ to $0^{\circ}C$. The curves revealed a very gradually decelerating increase in the moduli with decreasing temperature. The slope of the curves in the neighbourhood of the melting point was of the order of 1.5 parts per thousand per $^{\circ}C$. No significant frequency dependence of the elastic moduli of ice was noted by Dantl.

Perhaps the most striking observation which stems from the comprehensive set of measurements carried out by Dantl relates to the absolute or systematic values obtained for the elastic constants. These averaged about 5% below values obtained by other previous authors. On the other hand, the relative values of the five elastic moduli, and the temperature dependence curves were in generally good agreement with previous measurements (see Sec. 6.3 and discussion by Hobbs[2]). The tendency of each of the elastic moduli measured by Dantl to run about 5% below corresponding values measured by other authors, in particular Jona and Scherrer,[26] could not be accounted for by estimated experimental uncertainty in the respective sets of results.

Dantl[33,34,35] attributed the apparently low elastic moduli of the samples studied to sample-to-sample variation in the elastic properties of ice. That is, a fundamental difference in elastic properties of the aged pure ice samples used by Dantl versus the unaged samples used by other authors was hypothesized to exist. The tentative explanation offered by Dantl was as follows. During freezing a significant spatial variation in electrical potential develops along a growing ice crystal. This effect has been studied and verified by Workman and Reynolds[38] and is attributed to selective incorporation of impurity ions into the ice crystal structure. The resultant electric field was thought by Dantl to lead to preferential (nonrandom) orientation of the H_2O dipoles constituting the ice crystal. This preferential orientation in turn leads to long range dipole-dipole interactions between water molecules which, in effect, tend to pull the crystal structure together slightly. Molecules in

the denser structure interact more strongly yielding increased elastic moduli. Dantl then argues that during aging at or near the melting point, the potential accumulated during crystal growth drains off and the H_2O dipoles reassume random orientations. The density and elastic moduli thereby decrease with age. No samples studied previous to the work of Dantl had been deliberately aged for long periods prior to measurement of their elastic moduli.

Dantl substantiates his arguments by pointing out variations in measurements of ice density, in particular, a tendency for ice of minimum age to have maximum density.[39] A reported observation of piezoelectricity, in ice,[40] presumably related to the breaking of $P6_3/mmc$ crystal symmetry by preferential dipole orientation was also noted by Dantl. This effect was observed to disappear a few days after freezing.

(x) Discussion of Dantl's observations

Some of the arguments of Dantl appear improbable in view of various results quoted in the literature. For instance, in a review of crystallography of ice, Kamb[41] points out that neutron crystallographic data for ice Ih indicate that polar structure (long range ordering of H_2O dipoles) is not present. However, Kamb[41] acknowledges that tests on freshly formed samples, quenched rapidly to low temperature, have not been carried out. Nevertheless, it appears that without special precautions taken to preserve a possible polar structure induced at the time of freezing, a purely nonpolar structure is most probable. In this light, Hobbs[2] concludes that ". . . although various other space groups have been suggested from time to time, there now seems little doubt that the correct space group

(for ice Ih) is $P6_3/mmc$." The arguments of Dantl[33,34,35] run basically converse to the above, that is, they imply that without special precautions to remove a polar structure (for instance, aging eight months near the melting point) ice Ih will be polar in nature and hence be piezoelectric, have high density and have high elastic moduli.

As indicated by Dantl, measurments of the piezoelectric effect in ice have yielded contradictory results.[2] Dantl interprets these as evidence of a polar structure in some samples. Probably the most convincing test for piezoelectricity in ice to date, that of Teichmann and Schmidt,[42] yielded a null result. Nevertheless, the existence of piezoelectricity in freshly formed ice crystals remains a possibility. The effect may, however, arise from causes other than polar structure, for instance electric charges on dislocations.[3] Furthermore, observation of the effect would appear to require deliberate effort on the part of the investigator in order to prevent its disappearance by annealing. This contrasts with measurements of elastic moduli where the high moduli thought by Dantl to be associated with a polar structure have been observed, in the absence of special precautions, by several authors.[26,28,29,30,31] A similar argument can be applied to experimental determinations of the zero point entropy of ice. Values in excellent agreement with a theoretical value based on assumed disorder in proton-arrangement, have been determined.[1,2] The resultant implied statistical distribution of H_2O dipole moments rules out a polar structure in the samples studied.

Sample-to-sample variation in the density of ice has been more closely studied than has variation in the properties discussed

above. In a careful experiment, Butkovich[43] measured the specific gravity of several unflawed monocrystals of naturally occurring glacial ice (see Chapters 3 and 4). The large sizes and exceptional quality of the monocrystals indicated very prolonged annealing at the melting point. The measured densities were highly self-consistent and were in good agreement with several measurements on control samples (age not quoted) of polycrystalline "commercial" ice. The precise density measurements of Ginnings and Corruccini[44] using freshly formed polycrystalline ice (presumably aged no more than a few minutes) yielded a value differing by substantially less than one part in 10^4 from the average of the measurements of Butkovich[43] (see Sec. 3.3). While sample-to-sample variation in ice density remains a possibility, comparison of the measurements noted above demonstrates that there is no definite correlation between density and sample age. Camp[45] has attempted to verify the above hypothesis directly by noting the change in volume of a freshly formed ice sample held for 60 days at $-4^{\circ}C$. A null result was obtained and an upper limit of 2.5×10^{-6}/day set on the rate of fractional volume change of ice. The fractional density variation required to yield a 2% change in elastic moduli is hypothesized by Dantl to be about 1.8×10^{-3}.

In summary it can be noted that the measurements of Dantl,[33,34,35] when compared with those of other authors, imply a sample-to-sample variation in the elastic moduli of ice. The explanation put forth by Dantl, while difficult to discount completely, seems improbable in light of existing data, especially with regard to the time dependence of ice density. It may thus be advisable to

look for some other explanation, for instance differences in impurity concentration or in crystal quality (distribution of point defects, dislocations, etc.). Alternatively, unnoticed systematic error in sets of measurements made in different laboratories using different techniques may account for all or part of the apparent variations in the elastic moduli of ice. This possibility is discussed in detail in Sec. 6.3. To a large extent, the present work has been motivated by the uncertainties arising from the points discussed above.

Following 1967, and until the present work, no measurements of the full set of elastic moduli of ice have been carried out. The results of Dantl have been widely accepted as the standard values for the elastic moduli of ice.

In 1964, the full set of elastic moduli of frozen D_2O were measured over a wide range of temperatures by Mitzdorf and Helmreich.[46] The apparatus and techniques used were similar to those of Dantl. The elastic constants of frozen D_2O were found to differ from the corresponding elastic constants of frozen H_2O by amounts ranging from 5% to 20%. All elastic constants excepting c_{13} were found to be greater in frozen D_2O.

1.4 Brillouin Spectroscopy

Brillouin spectroscopy is a purely optical technique for studying the acoustic properties of materials. While the method has found application in studies of a wide range of liquid and solid media, including layer compounds, liquid crystals, semiconductors and metals,[47,48,49,50] the discussion below relates mainly to its application in studying transparent crystalline media, in particular, ice. The basic principle underlying the method of Brillouin spectroscopy

can be interpreted classically as being similar to that underlying the Schaefer-Bergmann method. That is, acoustic vibrations propagating in a transparent solid cause (or may be considered equivalent to) fluctuations in intermolecular spacing or density which in turn lead to local variations in refractive index. These variations are capable of scattering light. Unlike the Schaefer-Bergmann method, however, Brillouin spectroscopy does not necessitate the use of an external source of monochromatic acoustic vibrations (transducer). Rather, the acoustic waves observed by Brillouin spectroscopy are thermally induced and hence arise spontaneously within a sample. The observed vibrations form part of the broad spectrum of propagating excitations (phonons) which is present in any solid material at temperatures above absolute zero.[51]

The most commonly used arrangement for observing Brillouin scattering in transparent media involves an intense, highly collimated and highly monochromatic laser light source, incident on a sample and making an angle, α (scattering angle), with the axis of an optical dispersion and detection system. The scattering angle is quite frequently (as in the present work) chosen to be 90°. The optical detection system is designed to limit observed light both in spatial and directional extent. That is, only light emanating from a small region of the sample (diameter typically a fraction of 1 millimetre) and travelling in one precisely defined direction (angular divergence typically a fraction of one degree) is allowed to reach the detecting optics.

The light scattered by propagating elastic vibrations in a transparent medium is subject to certain physical constraints. From

a simplistic classical point of view these may be interpreted as follows. Firstly, scattering is specular, that is, the light is apparently reflected in a mirror-like manner from the plane wavefronts of acoustic vibrations. These wavefronts lie normal to the acoustic propagation direction. Secondly, an interference condition is satisfied. Accordingly, the wavelength of the observed acoustic vibrations must be such that the optical path difference for light reflected by two adjacent wavefronts equals one optical wavelength. Thus only a single wavelength is selected from the broad spectrum of acoustic vibrations spontaneously present in the sample. Finally, the light scattered by a propagating elastic vibration is effectively Doppler shifted by an amount corresponding to the rate of change of optical path from the light source to the detector. The optical path change results from movement of the reflecting surface (acoustic wavefront). Thus the observed Doppler shift is directly proportional to acoustic propagation velocity.

The physical constraints outlined above lead to the following relation between sound velocity and frequency shift of Brillouin scattered light.[12,52]

$$V = \Omega\lambda/2n \sin(\alpha/2) \qquad (1\text{-}3)$$

Equation (1-3) is known as the Brillouin equation. In equation (1-3), V denotes sound velocity, Ω denotes Brillouin frequency shift, λ denotes wavelength of incident light, n denotes refractive index of a transparent medium, and α denotes scattering angle.

The frequency shifts yielded by equation (1-3) are typically a very small fraction ($\sim 10^{-5}$) of the frequency of the incident

radiation. Hence, accurate spectroscopic analysis of Brillouin scattered light requires an instrument capable of very high resolution. A Fabry-Perot interferometer is commonly used for this purpose. The relative intensity of Brillouin scattered light is governed by the dependence of the polarizability (hence dielectric constant, and refractive index) of a medium on strain. This dependence, expressed in terms of coefficients (Pockels coefficients) in a fourth rank tensor linking polarizability with elastic strain, varies significantly between media. Low Brillouin scattering intensity necessitates a sophisticated optical detection system in many instances.

Frequent and varied use has been made of the technique of Brillouin spectroscopy since the mid-nineteen sixties, immediately following the invention of the laser. The technique has thus been well reviewed in the literature.[47,48,49,50] A detailed analysis of the underlying physical processes giving rise to Brillouin scattering is inherently quantum mechanical in nature. The article by Benedek and Fritsch[52] provides a complete review of these processes. Nevertheless, the classical discussion given above successfully accounts for those aspects of the Brillouin scattering phenomenon which are important in practical application of the technique for acoustic velocity measurement. Several Brillouin spectroscopic experiments utilizing apparatus and techniques very similar to those used in the present work have been carried out and reported in the literature.[12,50,53,54,55,56] These experiments were primarily aimed at measurement of the elastic moduli of various transparent media which are difficult to obtain in single crystal form. One Brillouin spectroscopic study of ice prior to the present work has been reported.[57]

The experiment was aimed at investigating an anomaly in the temperature dependence of the elastic moduli of ice at low temperatures.

1.5 Advantages and Objectives of the Present Work

The principal objective of the present work is to measure the elastic moduli of artificial and natural ice samples by Brillouin spectroscopy. By applying a uniform experimental technique to ice samples from different sources, possible sample-to-sample variation in the elastic moduli can be identified. The method of Brillouin spectroscopy is particularly well suited to such a study. The three principal advantages of this method, to be discussed below, relate to (i) inherently good precision in measurement; (ii) relative simplicity of identification and evaluation of systematic error; and (iii) highly localized region of observation.

(i) The precision of sound velocity measurements obtained by Brillouin spectroscopic techniques is inherently limited only by the precision with which the frequency shifts of the Brillouin components can be measured. With the optical setup used in the present work, uncertainties of a few tenths of one per cent in frequency shift measurement are typical (see Chapters 3 and 4). The resultant uncertainty in velocity compares well with the uncertainties typical of conventional acoustic measurement techniques (see Sec. 6.3). The primary advantage of Brillouin spectroscopy lies, however, in the ease with which large numbers of acoustic velocity measurements at different crystallographic orientations can be obtained. Since bonding of a transducer to the sample is not required, a single crystal can be rotated to a large number of arbitrary orientations and the sound velocity in corresponding crystallographic directions measured.

Furthermore, the velocities of one or two or sometimes three acoustic components can be measured simultaneously in one direction from one Brillouin spectrum. Accordingly, a good statistical distribution of sound velocity measurements over crystal orientations is obtained.

(ii) In contrast to the precision (relative uncertainty), the accuracy (absolute uncertainty) of a set of Brillouin spectroscopic sound velocity measurements depends on several terms appearing in the Brillouin equation (see Sec. 3.3). Uncertainty in any of these terms can lead to systematic error. However, due to the mathematical simplicity of the Brillouin equation and the physical simplicity of the parameters included in that equation, systematic error can be readily and reliably evaluated. This represents a potential advantage over conventional acoustic techniques where sources of systematic error may be subtle and hence difficult to estimate accurately (see Sec. 6.3). Accordingly it is among the primary objectives of the present work to carry out a thorough and reliable determination of uncertainty in the measurements obtained. The error analyses accompanying previously reported values of the elastic moduli of ice are decidedly lacking in detail in most instances. This makes comparison among the various quoted results somewhat dubious.

(iii) A highly localized region of observation is inherent in the method of Brillouin spectroscopy. The region of the sample within which the elastic moduli are actually measured lies at the intersection of the incident beam path and the axis of the optical detection system. The location of this region (much less than 1 mm^3 in volume) can be varied readily and controlled accurately (see Chapters 4 and 5). Thus, the samples studied can be small and completely irregular in shape.

Minimal sample preparation (see Sec. 4.2) is required. Perhaps the greatest advantage, however, lies in dealing with heterogeneous natural ice samples. Conventional acoustic techniques typically require samples considerably greater than 1 cm^3 in volume. The measured elastic properties then represent an average over the entire sample volume. If inclusions are present, the resultant values for the elastic moduli will not represent the fundamental properties of the ice matrix, but rather will be determined in part by the sizes, shapes, content and distribution of the inclusions. Such data may, of course, be of interest, but is clearly subject to sample-to-sample variation. Interpretation of the data will ultimately require a description of the elastic properties of the ice matrix, which may or may not vary from one sample to another. It is an objective of the present work to measure the elastic properties of the ice matrix in a sample of heterogeneous sea ice. This is possible with Brillouin spectroscopy since the region of observation can be chosen to avoid the various inclusions present in the sample.

For the reasons noted above, detailed study of the elastic properties of the ice matrix in heterogeneous natural ice has not been reported previously. Estimates of these elastic properties have, however, been inferred by extrapolation of curves showing the dependence of the isotropic (polycrystalline) elastic moduli on porosity. The zero porosity intercept of these curves has been interpreted to yield the elastic moduli of the ice matrix. Similar reasoning has frequently been applied to other nonelastic mechanical properties of heterogeneous ice. A review of the theory and experimental results can be found in the article by Weeks and Assur[6] and in the article by

Schwarz and Weeks.[58] In general detailed comparison of such results with precise measurements of the elastic moduli of homogeneous monocrystalline pure ice is not possible. Rough comparison suggests that the elastic properties of the ice matrix in sea ice resemble those of fresh water ice.[15] Uncertainty of the order of 10% to 20% exists in making the comparisons, however.

The high level of impurities present at the time of freezing of sea ice may modify the elastic or other mechanical properties of the ice matrix. The precise distribution of impurities within the microstructure of sea ice is very difficult to measure and has not been determined. It is well known, however, that the process of freezing and subsequent annealing of ice leads to the reduction of most ionic impurity concentrations dissolved within the crystal structure to part per million levels (see text by Hobbs[2] or Sec. 6.1). Much less is known about potential maximum nonequilibrium impurity concentrations or about the precise mechanism by which impurity ions are accommodated within the ice crystal structure. The mechanism of diffusion of impurity ions or molecules through the ice crystal structure is also not well understood.[3] This leaves open the possibility of relatively high concentrations of impurities in the ice matrix in sea ice due to diffusion from nearby regions of brine accumulation.

Studies aimed specifically at determinihg the mechanism of accommodation of impurities in ice have been carried out. Measurements of the electrical properties of ice doped with HF, NH_3 and NH_4F have shown that these substances can apparently be incorporated substitutionally in the ice crystal structure.[2] Concentrations of up to 4000 ppm by weight of NH_4F (believed to be the ionic compound most

soluble in ice) can be dissolved in monocrystalline ice by freezing stirred solutions of NH_4F in water at uniform rates.[59] The solubility and incorporation mechanism of HCl in ice have been investigated by Young and Salomon[60] who found that 7 ppm by weight HCl could be dissolved in monocrystalline ice without clouding the crystals. Very gradual freezing rates were used. Up to half of the HCl at this concentration was thought to have entered the crystal structure substitutionally. Little work appears to have been done on the incorporation mechanisms and peak dissolved concentrations of impurities in rapidly frozen ice. The principal reason for this probably lies in the heterogeneous nature of such samples. The impurities tend to concentrate in liquid inclusions and at the crystal grain boundaries which are invariably present in rapidly frozen ice samples.

Glen[3] points out that because of the open nature of the ice crystal lattice, the possibility of interstitial accommodation of impurity molecules must not be neglected. Perhaps the best experimental evidence for this occurrence is provided by the work of Kahane, Klinger and Philippe[61] who noted that 2 cm^3 (atmospheric pressure) of either He or Ne were absorbed into a 1 cm^3 monocrystalline ice sample at $-25^{\circ}C$ (under an applied pressure of 1.25×10^7 N/m^2). No change in the bulk crystal structure was noted. The absorbed concentrations corresponded to approximately 1 molecule of inert gas for each 570 molecules of H_2O.

While the above brief discussion (for a more extensive review, see the text by Hobbs[2]) indicates that a variety of impurities may be dissolved in ice in possibly several different ways, no effort has yet been made to determine the effects of impurities on the elastic

properties. It may be argued that the typically low dissolved impurity concentrations will lead to a negligible effect on the elastic moduli. However, as noted above there is no definite evidence that the concentrations are always low, particularly in rapidly frozen polycrystalline ice. Furthermore, as noted by Hobbs,[2] impurities which tend to be excluded from the ice crystal structure are precisely those which are highly disruptive to the molecular arrangement of ice. Thus such impurities, when present in low concentrations, may nevertheless yield significant distortion of the overall crystal structure.

The present work is not specifically a study of the effect of impurities on the elastic moduli of ice. Such a study would logically involve measurement of the elastic moduli of frozen ultrapure water samples doped with controlled amounts of specific chemicals. What can be learned from the present work, however, is whether the impurities likely to be incorporated in ice forming in the natural environment have significant effects on the elastic moduli. This result will be of primary interest to those using elastic modulus data in engineering applications.

1.6 Thesis Organization

The organization of this thesis is as follows. Chapter 2 deals with two important aspects of data analysis required in interpreting the results of the Brillouin spectroscopic measurements on ice. Each of the two sections of Chapter 2 is basically self-contained in the sense that the results presented are applicable in processing data from a range of experiments differing substantially from the present experiment. Chapter 3 includes the complete

description of the experimental setup used in measuring the elastic moduli of artificial ice along with a description of the technique and presentation of the results. Chapter 4 describes the technique for measuring the elastic moduli of three types of natural ice and presents the results. Reference is made to Chapter 3 for all those aspects of the technique and apparatus which did not differ from those used in the artificial ice experiment. Brillouin spectroscopy at an ice crystal grain boundary is described in Chapter 5. This chapter is self-contained in terms of the phenomenon studied and the discussion of the results. The studies discussed in Chapter 5 would ideally have been greatly expanded in scope and detail. However, this was not possible within the context of the present work. Chapter 6 compares the Brillouin spectroscopic measurements of the elastic moduli of ice both with themselves and with measurements of other authors. A complete tabulation of the derived elastic properties of ice likely to be utilized in future engineering and scientific applications is also included in Chapter 6.

CHAPTER 2

PROBLEMS OF CRYSTAL ORIENTATION

2.1 An Algorithm for Determining the Orientation of Monocrystalline Samples by the Analysis of Laue X-ray Diffraction Data

The study of anisotropic properties of single crystals (for example, elastic properties) often necessitates transforming vector or tensor quantities from a laboratory frame of reference into a more physically meaningful reference frame related to crystal symmetry. This procedure requires knowledge of the orientation of the crystallographic axes in monocrystalline samples. A useful method of determining crystal orientation is the technique of Laue x-ray diffraction. This method utilizes a collimated polychromatic x-ray beam which, after diffraction within a crystalline sample and subsequent photographic detection, reveals the orientation of crystallographic planes in a laboratory frame of reference. Details of the theory and experimental methods frequently used in obtaining Laue data[12,62,63,64] along with relevant aspects of elementary crystallography[12,51,65] can be found in the references.

Laue data generally consist of the cartesian coordinates of spots formed on a plane sheet of photographic film by several diffracted x-ray beams arising, effectively, from the simultaneous specular reflection of the incident beam by various crystallographic planes. In the transmission Laue method, where the sample lies between the x-ray source and the camera, the orientation of a

reflecting plane is linked to its corresponding Laue spot position by the transformation given below:

$$x' = 2xyL/(2y^2 - 1)$$
$$z' = 2yzL/(2y^2 - 1) \qquad (2\text{-}1)$$

Equivalently:

$$x = x'\left[1 + L/(x'^2 + z'^2 + L^2)^{\frac{1}{2}}\right]^{\frac{1}{2}} / (2x'^2 + 2z'^2)^{\frac{1}{2}}$$
$$y = -\left[1 - L/(x'^2 + z'^2 + L^2)^{\frac{1}{2}}\right]^{\frac{1}{2}} / 2^{\frac{1}{2}} \qquad (2\text{-}2)$$
$$z = z'\left[1 + L/(x'^2 + z'^2 + L^2)^{\frac{1}{2}}\right]^{\frac{1}{2}} / (2x'^2 + 2z'^2)^{\frac{1}{2}}$$

In the above transformations, L denotes the distance from the centre of the crystal to the film surface, while x' and z' are the co-ordinates of a Laue spot measured on the film surface relative to an origin defined by the point at which the undeflected x-ray beam strikes the film. The direction cosines of the normal to the reflecting plane are given by x, y and z where the incident x-ray beam travels in the positive y-axis direction and the x and z axes are taken to be parallel to the x' and z' axes, respectively.

The first step in calculating the orientation of a mono-crystal from Laue data is to establish a cartesian coordinate system fixed in the crystal. Let the three translation vectors defining a unit cell have coordinates (q_{11}, q_{12}, q_{13}), (q_{21}, q_{22}, q_{23}) and (q_{31}, q_{32}, q_{33}) in this system. Then, all crystal structure information relevant to the present analysis is contained in a 3 x 3 matrix, Q, with elements q_{ij}. Additionally, Q fixes the orientation of the cartesian coordinate system relative to the unit cell axes.

Miller indices must be assigned to all planes giving rise to observed Laue spots in order to determine the orientation of the planes in the crystal frame of reference. Index assignment necessarily involves trial and error, with a self-consistent assignment being recognized by way of the mathematical relationships discussed below. The angle, δ, between two plane normals is given by the matrix expression,

$$\cos \delta = D_1 D_2 (h_1\ k_1\ l_1)\ (QQ^{\dagger})^{-1} \begin{bmatrix} h_2 \\ k_2 \\ l_2 \end{bmatrix} \qquad (2\text{-}3)$$

where $(h_u\ k_u\ l_u)$ are the Miller indices of plane u and the D_u denote the spacing between adjacent parallel crystallographic planes of form u. When the two planes are taken to have identical Miller indices, $\cos \delta = 1$ and equation (2-3) can be solved for the plane spacing, D.

The interplanar angle, δ, arising via (2-3) from the trial indexing of two planes can be compared with the interplanar angle determined directly from the Laue data with the aid of the transformations, (2-2). If the trial indexing appears valid, then a third plane can be indexed according to the matrix equation given below:

$$D_3 \begin{bmatrix} h_3 \\ k_3 \\ l_3 \end{bmatrix} = \frac{1}{1 - P_{12}^2}\ QM \begin{bmatrix} P_{13} - P_{12}\,P_{23} \\ P_{23} - P_{12}\,P_{13} \\ Det_{123} \end{bmatrix} \qquad (2\text{-}4)$$

where $M \equiv \begin{bmatrix} m_{11} & m_{21} & m_{12}m_{23} - m_{13}m_{22} \\ m_{12} & m_{22} & m_{13}m_{21} - m_{11}m_{23} \\ m_{13} & m_{23} & m_{11}m_{22} - m_{12}m_{21} \end{bmatrix}$

(2-4)
(Cont'd)

$$\begin{bmatrix} m_{u1} \\ m_{u2} \\ m_{u3} \end{bmatrix} = D_u Q^{-1} \begin{bmatrix} h_u \\ k_u \\ l_u \end{bmatrix}$$

$$P_{uv} = (x_u \; y_u \; z_u) \begin{bmatrix} x_v \\ y_v \\ z_v \end{bmatrix}$$

$$Det_{123} = \det \begin{bmatrix} x_1 & y_1 & z_1 \\ x_2 & y_2 & z_2 \\ x_3 & y_3 & z_3 \end{bmatrix}$$

In equation (2-4), $(x_u \; y_u \; z_u)$ denote the direction cosines of the normal to plane u calculated from the Laue data while $(h_u \; k_u \; l_u)$ denote the Miller indices assigned to plane u. The equation implicitly determines the orientation of the crystal specified by the trial indexing of planes 1 and 2 and then, using this orientation, indexes a third plane. Three interplanar angles, 1 ^ 2, 1 ^ 3 and 2 ^ 3 can subsequently be calculated from the Miller indices and compared with values determined from the Laue data thereby further testing the validity of the trial indexing.

With three or more crystal planes correctly indexed, the orientation of the crystal is over-specified thus necessitating use of a least squares method in calculating the orthogonal matrix (rotation) which links the laboratory and crystal coordinate systems.

The most convenient way in which to define a sum squared error term, χ^2, is as follows:

$$\chi^2 = \sum_{u=1}^{N} [(x_u - n_{1u})^2 + (y_u - n_{2u})^2 + (z_u - n_{3u})^2] \qquad (2\text{-}5)$$

In equation (2-5), the direction cosines of the normal to plane u, calculated from the Laue data, are given by (x_u, y_u, z_u) while (n_{1u}, n_{2u}, n_{3u}) denote the direction cosines of the normal to plane u determined from a specified crystal orientation and assignment of Miller indices. N is the number of Laue spots being considered. The n_{iu} are calculated using the relationship given below:

$$\begin{bmatrix} n_{1u} \\ n_{2u} \\ n_{3u} \end{bmatrix} = D_u R^{-1} Q^{-1} \begin{bmatrix} h_u \\ k_u \\ l_u \end{bmatrix} \qquad (2\text{-}6)$$

The orthogonal 3 x 3 matrix, R, in equation (2-6) transforms a vector expressed in the laboratory frame of reference into the coordinate system fixed in the crystal. Writing the sum squared error explicitly in terms of the lab-to-crystal-system rotation matrix, R, yields

$$\chi^2 = 2\,[N - \text{trace}(RT^{\dagger})] \qquad (2\text{-}7)$$

where the 3 x 3 matrix T is given by

$$T = \sum_{u=1}^{N} D_u Q^{-1} \begin{bmatrix} h_u \\ k_u \\ l_u \end{bmatrix} (x_u \; y_u \; z_u) \qquad (2\text{-}8)$$

To verify a minimum of χ^2 taken as a function of the elements, r_{ij}, of the matrix R, it is necessary to write the r_{ij} in

terms of three independent parameters. With the three parameters chosen to be Euler angles,[66] it is readily shown that the three first derivatives of χ^2 equal zero and a minimum for χ^2 results when R satisfies the matrix equation:

$$TR^{\dagger} = RT^{\dagger} \tag{2-9}$$

The following matrix iteration can be used to find R satisfying (2-9):

$$U^{(0)} = T$$

$$U^{(n+1)} = [U^{(n)} + V^{(n)}] / K^{(n)} \tag{2-10}$$

$$U^{(n)} \to R \quad \text{as} \quad n \to \infty$$

where $V_{ij}^{(n)} =$ cofactor $U_{ij}^{(n)}$

and $K^{(n)} = \{ \sum_{j=1}^{3} [U_{ij}^{(n)} + V_{ij}^{(n)}]^2 \}^{\frac{1}{2}}$

The iteration (2-10) is useful both in the final determination of crystal orientation and in the intermediate process of indexing subsequent crystal planes after two or more planes have been indexed by trial and error. It should be noted as a matter of practical importance that trial and error index selection becomes very inefficient and time-consuming, even on a large computer, if several planes are to be indexed simultaneously. Hence only two planes (the minimum number possible) should have trial Miller indices assigned arbitrarily, by sequential selection from lists. A third plane is most efficiently indexed through equation (2-4), while subsequent planes can be indexed by calculating a rotation matrix via (2-10)

and then using the relationship given below:

$$D \begin{bmatrix} h \\ k \\ l \end{bmatrix} = QR \begin{bmatrix} x \\ y \\ z \end{bmatrix} \qquad (2\text{-}11)$$

In equation (2-11), (x, y, z) denote the direction cosines, determined from the Laue data, of the normal to the plane with Miller indices (h k l). Use of equation (2-11) minimizes the risk of error in index assignment resulting from scatter in the Laue data.

Equations such as (2-4) and (2-11), which are used to calculate Miller indices from Laue spot coordinates cannot be written so as to yield the indices directly in integer form. Rather, index ratios of the form (Dh Dk Dl) are invariably calculated. Furthermore, these ratios include uncertainty due to error in measurement of the spot coordinates.

The ratios can be converted to Miller indices by using the following procedure. Let

$$(p_1\ p_2\ p_3) \equiv (Dh/A\ Dk/A\ Dl/A) \qquad (2\text{-}12)$$

where: $A \equiv \max(|Dh|, |Dk|, |Dl|)$

Then, the absolute values of p_1, p_2 and p_3 are arranged in increasing order of magnitude to yield the ordered set (m, n, 1). The pair of ratios (m, n) is subsequently compared with a list of pairs (m'_j, n'_j) generated from the list of all Miller index sets, $(h'_g\ k'_g\ l'_g)$ considered possible to designate observed Laue reflecting planes. The pairs (m'_j, n'_j) are determined from the $(h'_g\ k'_g\ l'_g)$ by arranging the lesser two of $|h'_g/A'_g|$, $|k'_g/A'_g|$, $|l'_g/A'_g|$ in ascending order. The

A'_g are given by $A'_g \equiv \max(|h'_g|, |k'_g|, |l'_g|)$.

When the pair (m'_*, n'_*) which minimizes $(m-m'_j)^2 + (n-n'_j)^2$ has been located, the set $(m'_*, n'_*, 1)$ is rearranged to yield an ordering equivalent, in terms of the magnitudes of the elements to that of the set $(|p_1|, |p_2|, |p_3|)$. The resulting set now takes the form $(|h/B|, |k/B|, |l/B|)$ where B is an unknown positive integer. The Miller indices are finally given by,

$$(h\ k\ l) = (B'|h/B|\,\mathrm{sgn}(p_1)\quad B'|k/B|\,\mathrm{sgn}(p_2)\quad B'|l/B|\,\mathrm{sgn}(p_3)) \tag{2-13}$$

where $$\mathrm{sgn}(p) = \begin{cases} 1 & p > 0 \\ 0 & p = 0 \\ -1 & p < 0 \end{cases}$$

The value of B' is taken to be the smallest positive integer yielding integral values for h, k and l in the expression (2-13).

A convenient check of the validity of Miller indices assigned using the above procedure can be made by calculating the angle, α, between the plane normal specified by the indices through equation (2-6) and the plane normal (x, y, z), determined from the Laue data.

$$\cos\alpha = (n_1\ n_2\ n_3)\begin{bmatrix} x \\ y \\ z \end{bmatrix} \tag{2-14}$$

If the value of α exceeds a given error limit, then it can be assumed that excessive error occurred in locating spots on the Laue photograph or that the trial indexing leading to the assumed rotation matrix was invalid.

Any algorithm to determine crystal orientation by the methods described above must include a finite list of sets of allowed Miller indices. The list should contain all sets of Miller indices which might designate crystal planes having sufficient x-ray scattering power to give rise to observable spots on a Laue photograph. Inclusion of unnecessary sets of indices is preferably avoided since these increase the number of possibilities in the trial and error portion of the algorithm and increase the requirements for accuracy in measuring Laue spot coordinates. Generally, lower Miller indices denote crystal planes of higher molecular density and hence greater x-ray scattering power. Thus, an efficient list begins with sets of low Miller indices (although list may be modified by structure factor considerations). No a priori rule for terminating the list can be stated. This depends on the substance being analyzed and on the nature of the Laue diffraction setup. When, for practical reasons, the list is left incomplete, it may be preferable to omit some Laue spots in making an initial determination of crystal orientation. The omitted spots can subsequently be indexed using a longer index list along with a preliminary estimate for the appropriate rotation matrix.

A list of allowed Miller indices can be generated from a much shorter list of index ratios, (m_j', n_j'), defined as indicated in the text preceding equation (2-13). The sets, $(m_j', n_j', 1)$ are converted to sets of integers using a multiplicative constant and the resulting elements permuted and alternated in sign to yield all possible Miller index arrangements. This procedure reduces the volume of numerical data which must be stored when the algorithm is programmed

for implementation on a computer.

The initial trial and error process of selecting Miller indices for the first crystal plane under consideration can be shortened by taking advantage of crystal symmetry. Only the form to which the first plane belongs must be specified and any index assignment lying within this form will give rise to a symmetrically equivalent determination of crystal orientation. Evaluation of the plane spacing, D, provides a useful check for the symmetrical equivalence of two index sets. All planes in one form have equal D, although in a few cases the converse of this statement is not true. Coincidental equality of the plane spacing in different forms should be noted before using repeated D as a criterion for rejecting trial indices selected for a first crystal plane. Indices selected for a second plane must be specified exactly.

An algorithm for determining the orientation of a monocrystal of arbitrary symmetry from Laue x-ray diffraction data is outlined in the flow chart shown in Fig. 2.1. This algorithm, utilizing the equations and techniques described above, was programmed on a Hewlett-Packard 9825 microcomputer. The routine was then tested and verified by calculating orientations for randomly oriented samples of NaCl (cubic), $BaSO_4$ (orthorhombic) and $CuSO_4.5H_2O$ (triclinic). The program has subsequently been translated to BASIC for use on a PDP 11/70 timeshare computer system.* All Laue data arising from the present work on ice was analyzed using the H.P. 9825 orientation program. The program was also used extensively in calculating crystal

*Translation carried out by Ian Hare, undergraduate student at Memorial University of Newfoundland, 1980.

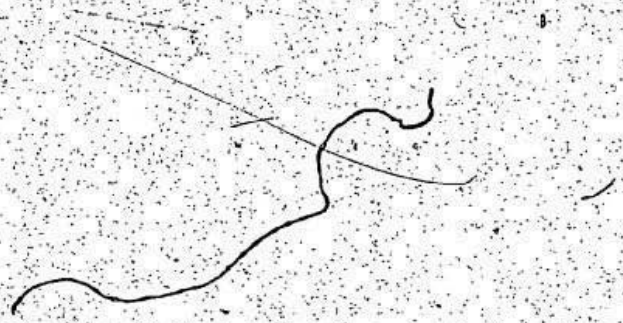

Fig. 2.1. Flow chart for algorithm to determine monocrystal orientation from Laue x-ray diffraction data.

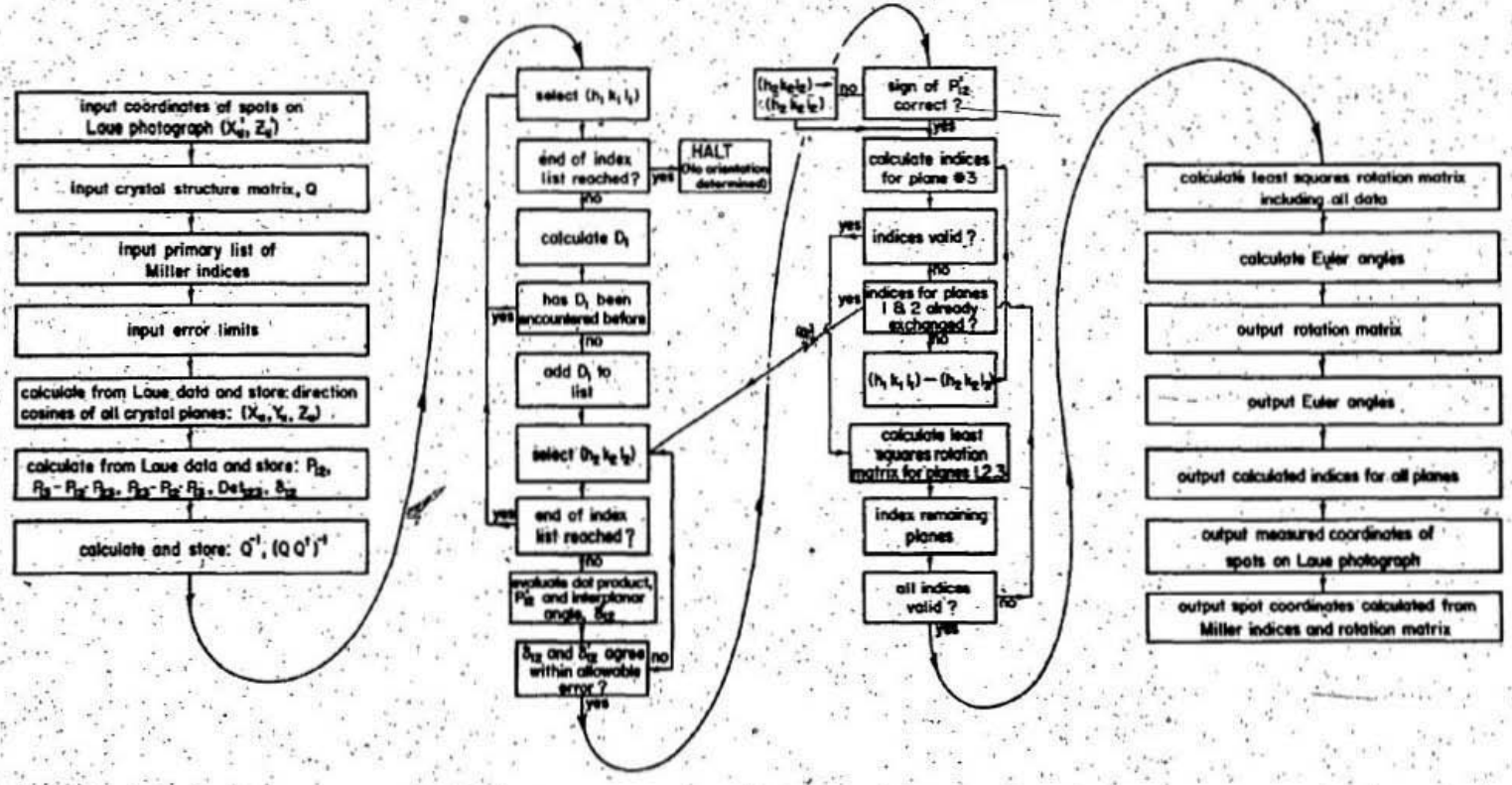
input coordinates of spots on Laue photograph (X'_s, Z_s)
input crystal structure matrix, Q
input primary list of Miller indices
input error limits
calculate from Laue data and store: direction cosines of all crystal planes: (X_s, Y_s, Z_s)
calculate from Laue data and store: P_{12}, $P_{13} - P_{12} \cdot P_{23}$, $P_{23} - P_{12} \cdot P_{13}$, Det_{123}, δ_{12}
calculate and store: Q^{-1}, $(Q\,Q^T)^{-1}$
select (h_1 k_1 l_1)
end of index list reached?
yes
HALT (No orientation determined)
no
calculate D_1
has D_1 been encountered before
yes
no
add D_1 to list
select (h_2 k_2 l_2)
end of index list reached?
yes
no
evaluate dot product, P'_{12} and interplanar angle, δ_{12}
δ_{12} and δ_{12} agree within allowable error?
no
yes
(h_2 k_2 l_2) — (h_2 k_2 l_2)
no
sign of P'_{12} correct?
yes
calculate indices for plane ③3
indices valid?
yes
no
indices for planes 1 & 2 already exchanged?
yes
no
(h_1 k_1 l_1) — (h_2 k_2 l_2)
calculate least squares rotation matrix for planes 1,2,3
index remaining planes
all indices valid?
no
yes
calculate least squares rotation matrix including all data
calculate Euler angles
output rotation matrix
output Euler angles
output calculated indices for all planes
output measured coordinates of spots on Laue photograph
output spot coordinates calculated from Miller indices and rotation matrix

Fig. 2.1

orientations for Brillouin experiments on doped argon crystals where, in many instances, the speed and simplicity of the analysis were essential in distinguishing between cubic and hexagonal phases.[67] Similarly, the program facilitated analysis of composite Laue photographs obtained in connection with the present ice grain boundary studies (see Chapter 5) when the incident x-ray beam intersected both crystals in a bicrystalline ice sample.

2.2 Analysis of Acoustic Data from Hexagonal Monocrystals of Unknown Orientation*

Although explicit knowledge of crystal orientation is highly desirable in interpreting acoustic data to yield elastic constants, it is not essential when a crystalline medium possesses hexagonal symmetry. Thus, acoustic data from hexagonal media can be fully analyzed even if it is impractical to determine crystal orientation as, for instance, in dealing with Brillouin spectroscopic data for individual grains in heterogeneous or polycrystalline materials. This can be demonstrated by first rewriting the usual equations[11,12] expressing the velocities of the three independent acoustic modes in the form indicated below:

$$2\rho V_L^2 = k_1 + k_2 \cos^2\gamma + [k_3^2 - k_4^2 \cos^2\gamma + k_5^2 \cos^4\gamma]^{\frac{1}{2}} \qquad (2\text{-}15)$$

$$2\rho V_{T2}^2 = k_1 + k_2 \cos^2\gamma - [k_3^2 - k_4^2 \cos^2\gamma + k_5^2 \cos^4\gamma]^{\frac{1}{2}} \qquad (2\text{-}16)$$

$$2\rho V_{T1}^2 = k_6 - k_7 \cos^2\gamma \qquad (2\text{-}17)$$

In the above equation, ρ denotes the density of the medium while V_L and V_{T2} denote the velocities of acoustic modes which are predominantly

*A synopsis of this section is in press.[68]

longitudinal and predominantly transverse, respectively. V_{T1} is the velocity of a purely transverse acoustic mode with polarization orthogonal to the mode with velocity, V_{T2}. γ is the angle between the sound propagation direction and the c axis of the hexagonal crystal. The k_i have units of pressure and are related to the five hexagonal elastic constants as indicated below:

$$k_1 = c_{11} + c_{44} \qquad k_2 = c_{33} - c_{11} \qquad k_3 = c_{11} - c_{44}$$

$$k_4 = [2(c_{11} - c_{44})(c_{11} + c_{33} - 2c_{44}) - 4(c_{13} + c_{44})^2]^{\frac{1}{2}} \tag{2-18}$$

$$k_5 = [(c_{33} - c_{11})^2 + 4(c_{11} - c_{44})(c_{33} - c_{44}) - 4(c_{13} + c_{44})^2]^{\frac{1}{2}}$$

$$k_6 = c_{11} - c_{12} \qquad k_7 = c_{11} - c_{12} - 2c_{44}$$

It is apparent that the angle γ can be eliminated from any pair of the equations, (2-15), (2-16) and (2-17). Acoustic data consisting of simultaneous velocity measurements of two independent acoustic modes propagating in a single crystallographic direction are required for this purpose. Such data will result, for example, from Brillouin spectroscopic measurements where, as is usually the case, more than one Brillouin component is observed on a single spectrum.

Accordingly, equation (2-17) can be solved for $\cos^2\gamma$ to yield:

$$\cos^2\gamma = (k_6 - 2\rho V_{T1}^2)/k_7 \tag{2-19}$$

Equation (2-19) can then be substituted into either of equations (2-15) or (2-16) yielding, after rearranging terms and squaring

both sides:

$$Y^2 + S_5XY - S_4Y - S_3X^2 + S_2X - S_1 = 0 \qquad (2\text{-}20)$$

The above equation is that of a hyperbola where X denotes $2\rho V_{T1}^2$ while Y denotes either $2\rho V_L^2$ or $2\rho V_{T2}^2$. These latter two components lie along separate branches of the hyperbola. The five coefficients, S_i can be linked to the five elastic constants, c_{ij}, by the one-to-one set of transformations given below.

$$c_{44} = \{S_2-S_4-[(S_2-S_4)^2 - 4S_1(S_3-S_5-1)]^{\frac{1}{2}}\} / [4(S_3-S_5-1)]$$

$$c_{11} = c_{44}(S_5-1-S_5^2/S_3) + S_4/2 - S_2S_5/(2S_3)$$

$$c_{12} = [c_{11}S_5 - S_4 + 2(c_{11} + c_{44})] / S_5 \qquad (2\text{-}21)$$

$$c_{33} = S_4/2 - c_{44}(S_5 + 1)$$

$$c_{13} = [(c_{11}-c_{44})(c_{33}-c_{44}) - S_3(c_{33}-c_{11})^2 / S_5^2]^{\frac{1}{2}} - c_{44}$$

Equivalently:

$$S_5 = 2(c_{33} - c_{11}) / (c_{11} - c_{12} - 2\,c_{44})$$

$$S_4 = 2(c_{11} + c_{44}) + (c_{11} - c_{12})S_5$$

$$S_3 = 4[(c_{11}-c_{44})(c_{33}-c_{44}) - (c_{13}+c_{44})^2] / (c_{11}-c_{12}-2\,c_{44})^2 \qquad (2\text{-}22)$$

$$S_2 = (c_{11} - c_{12} + 2\,c_{44})S_3 - 2\,c_{44}\,S_5$$

$$S_1 = 2\,c_{44}\,[(c_{11} - c_{12})(S_3 - S_5) - 2\,c_{11}]$$

Solving equation (2-20) for Y and summing the two roots yields the following relationship among three acoustic modes propagating in the same crystallographic direction:

$$2\rho(V_L^2 + V_{T2}^2 + S_5\,V_{T1}^2) - S_4 = 0 \qquad (2\text{-}23)$$

Equation (2-23) can be solved for $2\rho V_{T1}^2$ and the result substituted in equation (2-20) to yield a quadratic expression in the quantities $2\rho V_L^2$ and $2\rho V_{T2}^2$:

$$Y^2 + (2+S_5^2 / S_3)XY - (2S_4 - S_2S_5/S_3)Y + X^2 - (2S_4 - S_2 S_5 / S_3)X + [S_5(S_1S_5 - S_2S_4) / S_3 + S_4^2] = 0 \quad (2\text{-}24)$$

In the above expression, Y denotes $2\rho V_L^2$ while X denotes $2\rho V_{T2}^2$.

The elastic constants of a hexagonal crystal can be obtained by inverting equation (2-20) to yield the S_i and then determining the c_{ij} via the set of transformations, (2-21). The required data are the bulk density, ρ, and five or more pairs of acoustic velocity measurements of the form (V_{T1}, V_L) or (V_{T1}, V_{T2}). In using the method of least squares to invert (2-20), it is most computationally convenient to define the sum squared error as follows:

$$\chi_1^2 = \sum_i [Y_i^2 + S_5 X_i Y_i - S_4 Y_i - S_3 X_i^2 + S_2 X_i - S_1]^2 \quad (2\text{-}25)$$

The derivatives of χ_1^2 are then linear in the S_i and those values for the S_i which minimize χ_1^2 are given by the closed matrix expression below:

$$\begin{bmatrix} S_1 \\ S_2 \\ S_3 \\ S_4 \\ S_5 \end{bmatrix} = \begin{bmatrix} \sum_i 1 & -\sum_i X_i & \sum_i X_i^2 & \sum_i Y_i & -\sum_i X_i Y_i \\ \sum_i X_i & -\sum_i X_i^2 & \sum_i X_i^3 & \sum_i X_i Y_i & -\sum_i X_i^2 Y_i \\ \sum_i X_i^2 & -\sum_i X_i^3 & \sum_i X_i^4 & \sum_i X_i^2 Y_i & -\sum_i X_i^3 Y_i \\ \sum_i Y_i & -\sum_i X_i Y_i & \sum_i X_i^2 Y_i & \sum_i Y_i^2 & -\sum_i X_i Y_i^2 \\ \sum_i X_i Y_i & -\sum_i X_i^2 Y_i & \sum_i X_i^2 Y_i & \sum_i X_i Y_i^2 & -\sum_i X_i^2 Y_i^2 \end{bmatrix}^{-1} \cdot \begin{bmatrix} \sum_i Y_i^2 \\ \sum_i X_i Y_i^2 \\ \sum_i X_i^2 Y_i^2 \\ \sum_i Y_i^2 \\ \sum_i X_i Y_i^3 \end{bmatrix} \quad (2\text{-}26)$$

Where data of the form (V_{T2}, V_L) are to be included, a total sum squared error is conveniently defined by $\chi^2 = \chi_1^2 + \chi_2^2$ with

$$\chi_2^2 = \sum_j \{ (X_j+Y_j)^2 + (S_5^2/S_3)X_jY_j - (2S_4-S_2S_5 / S_3)(X_j+Y_j) + [S_5(S_1S_5 - S_2S_4) / S_3 + S_4^2]\}^2 \quad (2\text{-}27)$$

Since χ_2^2 has only three independent coefficients, at least two pairs of measurements containing V_{T1} must be included along with any measurements of the form (V_{T2}, V_L) in order to determine the five elastic constants. The derivatives of $(\chi_1^2 + \chi_2^2)$ are not linear in the S_i thereby necessitating use of a matrix iteration in minimizing χ^2. The iteration indicated below (Newton–Raphson method in five dimensions[69]) can be used for this purpose.

$$[S]^{m+1} = [S]^m - [T^{-1}]^m \cdot [F]^m$$

$$T_{ij}^m = \frac{\partial \chi^2}{\partial S_i \partial S_j} (S_1^m, S_2^m \ldots S_5^m) \quad (2\text{-}28)$$

$$F_i^m = \frac{\partial \chi^2}{\partial S_i} (S_1^m, S_2^m \ldots S_5^m)$$

For increasing m, $[S]^m$ will converge to those values of the S_i minimizing χ^2, providing $[S]^0$ is a sufficiently good initial estimate. Where possible, the preferred method of obtaining the initial estimate is to omit data of the form (V_{T2}, V_L) and then calculate $[S]^0$ via equation (2–26). It is straightforward to obtain reasonably concise explicit expressions for the matrix elements in equation (2-28). This procedure is simplified by making the change of variables, $S_5/S_3 \rightarrow S_5'$, following which χ^2 becomes a polynomial in the S_i. The explicit expressions for the matrix elements enable a simple and

rapidly executed algorithm to be used in minimizing χ^2. The appropriate algorithm has been constructed and programmed in BASIC on a PDP 11/70 computer. The program was subsequently used to determine the elastic constants of polycrystalline sea ice in connection with the present work (see Sec. 4.7).

CHAPTER 3

THE ELASTIC CONSTANTS OF ARTIFICIALLY GROWN ICE SINGLE CRYSTALS*

3.1 Crystal Growth Apparatus

The samples used in the Brillouin spectroscopic determination of the elastic moduli of artificial ice consisted of small unflawed monocrystals grown in a cylindrical quartz cell. The sample cell and associated cooling system were initially designed for use in Brillouin scattering studies of frozen cyclohexane and are described in detail in a publication associated with that work.[56] The similarity in relevant physical properties between water and cyclohexane was such that the sample housing apparatus could be used in the present work without significant modification. Hence, only a brief description of the system is included here.

The sample cell was the bottom 2 cm of a 3 mm i.d., 5 mm o.d. quartz tube, closed at the bottom with a polished quartz window. The tube was housed in an evacuated plexiglas cylinder mounted in a bearing assembly which allowed rotation of the cell and housing about the tube axis. This rotation axis coincided with the z direction in the laboratory frame of reference (see Fig. 3.1) and with the direction of the incident laser beam used in Brillouin spectroscopy. A scale on the outer housing indicated the angle of rotation of the

*A synopsis of this chapter has been published.[70]

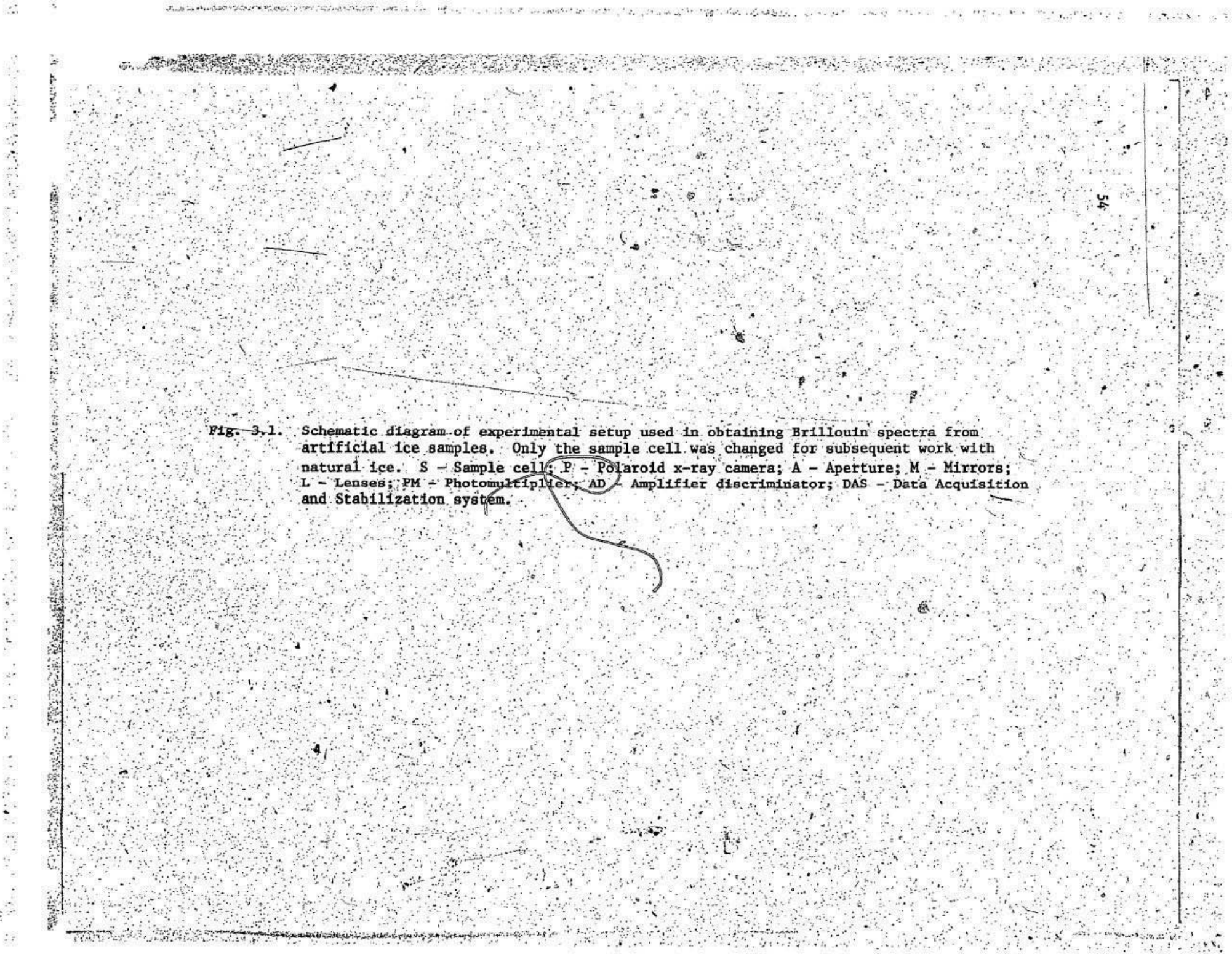

Fig. 3.1. Schematic diagram of experimental setup used in obtaining Brillouin spectra from artificial ice samples. Only the sample cell was changed for subsequent work with natural ice. S - Sample cell; P - Polaroid x-ray camera; A - Aperture; M - Mirrors; L - Lenses; PM - Photomultiplier; AD - Amplifier discriminator; DAS - Data Acquisition and Stabilization system.

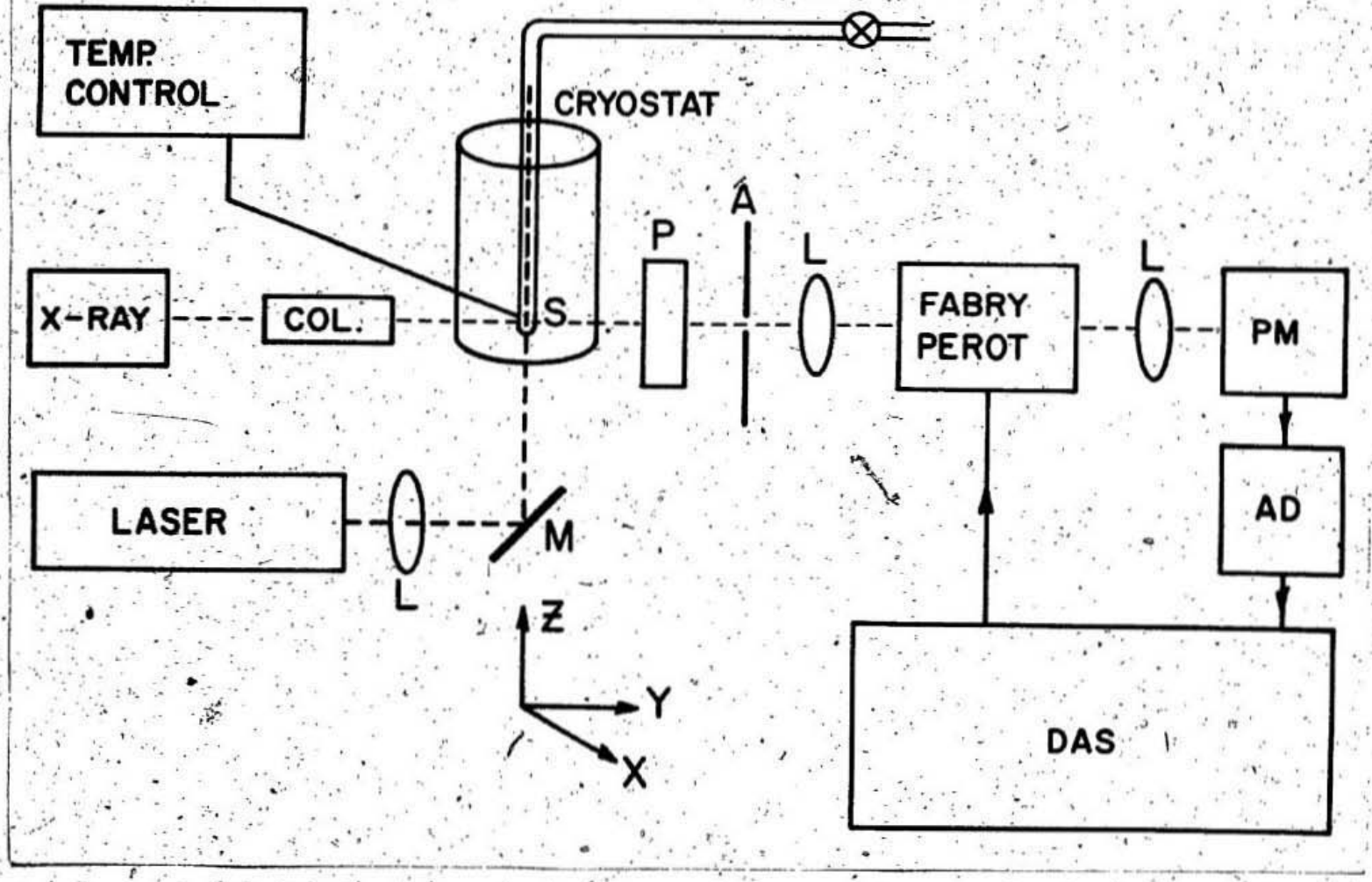
TEMP.
CONTROL
CRYOSTAT
P
A
L
L
X-RAY
COL.
S
FABRY
PEROT
PM
AD
LASER
L
M
Z
Y
X
DAS

Fig. 3.1

sample to within about .5 degree. The sample cell was cooled by two brass clips encircling the quartz tube at its bottom and at a point 2 cm above the bottom. The clips were connected via copper braids to a thermoelectric module which was, in turn, cooled by water flowing through an attached heat sink.

The temperature of the clip at the bottom of the cell was monitored with a GaAs temperature-sensing diode. The output of the diode was used to control heaters on the top and bottom clips through a feed-back circuit (Lakeshore DTC 500) which regulated the temperature at the bottom clip to within .1°C. A differential thermocouple was used to measure the temperature difference between the top and bottom clips. This temperature difference and hence the thermal gradient along the cell was controlled with a potentiometer which divided the heater current supply between the upper and lower heaters.

The absolute temperature of the sample was determined by calibration of the GaAs diode. Distilled water was frozen in the sample cell and then melted until the solid-liquid boundary was located midway between the two brass clips, in the approximate region where Brillouin scattering was subsequently to be observed. The temperature difference between the top and bottom clips was set at less than .5°C with the top clip being slightly warmer. This temperature difference equalled that which existed during the recording of the Brillouin spectra. The voltage across the temperature-sensing diode thereby corresponded to a sample temperature of 0°C. A relative calibration curve for the GaAs diode was subsequently used to determine the appropriate voltage readings for nearby temperatures. The estimated uncertainty in sample temperature was ±.2°.

A temperature of $-3^{\circ}C$ was chosen for the artificial ice samples used in the determination of elastic moduli. The principal reason for choosing a sample temperature near the freezing point was to minimize stress resulting from differential thermal contraction between the ice crystal and the quartz cell walls. Furthermore, the temperature calibration was most accurate near $0^{\circ}C$ and a value for the refractive index of ice, required in analysis of the Brillouin data, was quoted for $-3^{\circ}C$. The selected sample temperature lay within the range of temperatures most frequently associated with the occurrence of ice in the natural environment. Thus direct extension of the present results to include natural ice is simplified.

The water samples used in the Brillouin measurements were doubly distilled and had a conductivity of $1.07 \times 10^{-2}\ (\Omega m)^{-1}$ and a pH of 5.9 prior to freezing. The significant conductivity (300 times greater than that of melted ice samples used in elastic moduli determination by Dantl[35]) and slightly low pH (pH of 6.8 for sample used by Dantl[35]) were probably due to an equilibrium concentration of CO_2 dissolved in the water at atmospheric pressure. Dissolved gases were clearly present in the initial distilled sample as indicated by the numerous bubbles given off during freezing. Continuous pumping during the freezing process maintained a pressure not exceeding the equilibrium vapour pressure of water above the sample, thus aiding in the removal of dissolved gases. Analysis of the meltwater from the ice samples was not attempted due to their very small volume and the likelihood of reintroduction of atmospheric gases during handling.

3.2 Crystal Growth Procedure

Careful procedures were used to grow good quality single crystals of ice in the Brillouin scattering cell. A 3 cm high column of the doubly distilled, filtered water was injected into the bottom of the quartz tube using a thin plastic tube attached to a syringe. Both items were rinsed thoroughly with distilled water prior to use. The minimal presence of dust in the water sample in the cell was best indicated by the difficulty in obtaining ice nucleation. Often, the maximum cooling power of the thermoelectric modules, yielding a temperature close to $-20^{\circ}C$, was insufficient to solidify the sample. Waiting periods of several hours were frequently required before nucleation occurred although the process was greatly accelerated through the installation of a powerful 60 Hz vibrator on the mounting stand supporting the sample housing.

The initial freezing of the supercooled water sample yielded an optically flawed polycrystalline ice sample filling the entire cell. The temperature was then raised to near the freezing point and the heater current was diverted entirely to the top heater thereby yielding a maximum thermal gradient along the cell. This caused melting of the entire sample except for a layer less than .5 mm thick on the bottom window of the cell. This thin ice layer was annealed for a time period not less than 6 hours until inspection through crossed polaroid filters indicated that it was monocrystalline and free from any visible imperfections. The thermal gradient and cell temperature were then simultaneously reduced in gradual steps causing the ice crystal to grow up the cell at the rate of about 2 mm per hour. During growth, the crystal was checked

periodically both visually through crossed polaroids and by Laue x-ray diffraction to ensure complete absence of flaws. If flaws appeared, the sample was remelted and the growth procedure repeated. When the sample temperature reached $-3^{\circ}C$ and the thermal gradient reached a predetermined value corresponding to a temperature difference of less than $.5^{\circ}C$ between the top and bottom clips, the growth procedure was concluded. By this time a perfectly clear single crystal filled the entire cell.

3.3 Ice Crystal Orientation

Laue x-ray diffraction photographs were used to verify the crystal quality of the ice samples and to determine the orientation of their crystallographic axes in the laboratory frame of reference. The photographs were obtained using a Philips (MG 101) x-ray source, a lead collimator and a Polaroid XR-7 Land diffraction camera. The x-ray source, collimator and camera were aligned along the axis of the optical system used to collect scattered light. The distance from the film surface in the x-ray camera to the centre of the sample cell was 8.7 cm.

Disrupted or strained ice crystals were indicated by Laue spots which were small or irregular in shape or smeared or split into one or more parts. Good quality single crystals yielded oval shaped Laue spots of approximately uniform size. Accordingly, the Laue photographs provided a basis for selecting those crystals suitable for use in the Brillouin scattering experiments.

The orientations of the ice monocrystals were calculated from Laue photographs using the methods described in Chapter 2. Spot positions were measured by overlaying the photographs with a

finely ruled rectangular grid. The Cartesian coordinates of the centres of the diffracted spots were thereby determined to within an uncertainty of about .5 mm, corresponding to an angular uncertainty of about .3°. The required matrix, Q (see Sec. 2.1), defining the ice crystal structure and specifying the orientation of a Cartesian coordinating system fixed with respect to the crystallographic axes was taken to be the matrix given below.

$$Q = \begin{bmatrix} 1 & -.57735 & 0 \\ 0 & 1.15470 & 0 \\ 0 & 0 & 1.881 \end{bmatrix} \qquad (3.1)$$

The above matrix specifies hexagonal crystal structure with a c/a ratio of 1.629. The unit vectors, $\hat{i}$, $\hat{j}$ and $\hat{k}$ of the Cartesian coordinate system fixed in the crystal are normal to the (100), (120) and (001) crystal planes respectively.

No a priori list of crystal forms likely to give rise to observable spots on Laue diffraction photographs from ice was available. The list was thus created by trial and error and is given below. In order of decreasing frequency of observation, forms yielding observed spots on the 29 analyzed Laue photographs obtained from 4 artificial ice crystals were: {011}, {013}, {021}, {123}, {112}, {023}, {012}, {015}, {010}, {110}, {121}, {120}, {032}, {001}, {122}, {025}, {111}.

The input data for the HP 9825 program for determining crystal orientation consisted of the structure matrix, Q, and list of forms given above, along with the distance from the crystal to the x-ray film and the coordinates of the Laue spots. The output data

consisted of the least squares rotation matrix, R, defined as in equation (2-6) along with a set of Euler angles parameterizing R, a set of Miller indices for each Laue spot and calculated coordinates for each spot determined from the indexing and the least squares rotation matrix. The Euler angles[66] were defined so as to parameterize the rotation matrix in the manner indicated below:

$$R = \begin{bmatrix} \cos\phi\cos\psi-\sin\phi\cos\theta\sin\psi & \sin\phi\cos\psi+\cos\phi\cos\theta\sin\psi & \sin\theta\sin\psi \\ -\cos\phi\sin\psi-\sin\phi\cos\theta\cos\psi & -\sin\phi\sin\psi+\cos\phi\cos\theta\cos\psi & \sin\theta\cos\psi \\ \sin\phi\sin\theta & -\cos\phi\sin\theta & \cos\theta \end{bmatrix} \quad (3\text{-}2)$$

With the above parametrization of R, the angle between the crystal c axis and the laboratory frame z axis is given by θ while the angle between the c axis projected on the x-y plane and the y axis (coordinates denote laboratory frame) is given by ϕ. Hence, rotation of the sample about the axis permitted by the apparatus (laboratory frame z axis) varied ϕ in direct correspondence with the angle of rotation while leaving θ and ψ unchanged.

The incident laser beam used for Brillouin spectroscopy travelled in the positive direction along the laboratory frame z axis while the scattered light observed by the collecting optics travelled in the positive direction along the laboratory frame y axis. Thus, phonons giving rise to observed Brillouin scattering had wave-vectors with direction cosines $\pm(0, -2^{-\frac{1}{2}}, 2^{-\frac{1}{2}})$ and made an angle $\gamma \equiv \cos^{-1}[(\cos\phi\sin\theta+\cos\theta)/2^{\frac{1}{2}}]$ with the crystal c axis. Values of γ were calculated from the crystal orientations and used in fitting elastic constants to the Brillouin spectroscopic sound velocity measurements. Since a well determined fit depended on a good

distribution of γ values, an initial determination of crystal orientation was used in selecting subsequent angles of rotation of the sample cell which yielded widely distributed γ.

3.4 Optical Detection and Data Acquisition System

The basic layout of the optical system used in obtaining Brillouin spectra from the ice samples is illustrated in Fig. 3.1. The system has been described in detail in previous publications[12,53,54,55,56] and hence only a brief description of the principal components follows. The incident light source was a single mode argon ion laser (Spectra Physics 165-08) providing a power output of about 100 mW at a wavelength, λ, of 5.145×10^{-7} m. The effective width of the laser line was approximately 5 MHz. The laser light was focused near the scattering volume in the ice sample by a lens (focal length = 25.4 cm) and was deflected upwards through 90° by a mirror. Translation of this mirror in the direction of the incident beam (parallel to x axis) moved the reflected beam across the axis of the collecting optics and facilitated precise alignment of the incident beam with the point in the sample being observed. This alignment was checked and corrected from time to time using a thin card in the position normally occupied by the sample and defining the axis of the collecting optics with a He-Ne laser beam passed through the x-ray collimator. Slight error in the positioning of the incident beam yielded a greatly reduced intensity of observed Brillouin scattering.

The angle between the incident beam and the axis of the collecting optics corresponded to the angle through which the incident

beam was deviated by observed Brillouin scattering. This angle, α, appearing in the Brillouin equation, was set equal to 90^{o} by using a pentaprism to reflect the incident beam along the path of the He-Ne beam. The uncertainty in α determined by this procedure was estimated to be $\pm.2^{o}$.

The light scattered from the sample was collimated by a lens (focal length = 40 cm) before being analyzed by a piezoelectrically scanned triple-pass Fabry-Perot interferometer (Burleigh Instruments Inc. model RC-110). The angular radius of the cone of light reaching the interferometer was limited by an aperture to about $.5^{o}$. The interferometer utilized 93% reflectivity plates, flat to within $\lambda/200$, and typically yielded a finesse (ratio of free spectral range to instrumental half width) better than 50. The magnitude of the free spectral range (frequency separation between adjacent orders) was determined by precise measurement of the interferometer plate separation[12] to be 11.101 GHz with uncertainty smaller than .1%.

The voltage ramp used to repetitively scan the interferometer was provided by a Burleigh Instruments Inc. DAS 1 (Data Acquisition and Stabilization) system. The DAS unit included a digital sawtooth waveform generator and high voltage amplifier, along with a 1024 channel multichannel analyzer for data storage and display, and two independent electronic stabilization systems. The respective stabilization modules utilized negative feedback circuitry to compensate for drift in laser frequency or Fabry-Perot plate separation and to maintain optimally parallel plate alignment for indefinite time periods. The system made possible multiday continuous spectral accumulation times.

The spectral data were accumulated in the multichannel analyzer in the form of photon count versus channel number. The photon count corresponded to light transmitted by the interferometer, detected by a photomultiplier tube (ITT FW 130) and processed through an amplifier discriminator (PAR 1120). See Fig. 3.1. The channel number was linearly related to the amplitude of the ramp waveform and hence via the separation of the Fabry-Perot plates to the frequency of the transmitted light.

The DAS system included two optional features, sometimes used in obtaining or analyzing Brillouin spectra from ice. A segmented time base feature allowed the slope of the digital ramp to be reduced over a set interval of channels thereby increasing spectral accumulation time in the interval by a factor between 2 and 99 relative to the remaining channels. An arithmetic module incorporating a three-point smoothing feature allowed simultaneous resetting of the count in every channel according to the formula $[C(I-1) + 2C(I) + C(I+1)] / 4 \rightarrow C(I)$ where $C(I)$ denotes the count in channel number I. This smoothing function, which could be applied iteratively, reduced relative scatter among nearby channels and increased apparent signal to noise ratio without significantly modifying the shape of spectral components, providing the number of iterations was small compared to the half width (expressed in channels) of the spectral components.

3.5 Experimental Observations

A total of 30 Brillouin spectra were obtained from four single crystals of artificial ice. The spectral accumulation times averaged about 6 hours although some spectra were accumulated over

time periods exceeding 24 hours in order to resolve low intensity Brillouin components scattered by transverse acoustic modes in ice. A typical Brillouin spectrum from artificial ice, showing all three acoustic components is shown in Fig. 3.2. The intensity of the unshifted (laser) component typically exceeded that of the longitudinal Brillouin components by a ratio of about 300 to 1. This high ratio was primarily the result of the inherently low intensity of the Brillouin spectrum of ice. The analogous ratio in the Brillouin spectrum of methanol, obtained using the same optical setup, was 2 to 1. While some of the unshifted light was undoubtedly the result of Rayleigh scattering in ice, the fact that the laser beam travelling in the sample was completely invisible indicated that the relative contribution from Rayleigh scattering was small. Most of the unshifted light was therefore attributable to stray reflections from the walls of the sample cell.

The instrumental linewidth was typically about 0.2 GHz and the widths of the transverse Brillouin components tended not to differ significantly from this value. The longitudinal components were significantly broadened, however, having widths ranging from 0.3 to 0.6 GHz. Some of the broadening was due to the finite range in scattering angle for light entering the collecting optics. An angular width of 0.5^{o} in the cone of light admitted to the collecting optics would account for a broadening, via the Brillouin equation, of more than 0.1 GHz in the longitudinal components. Flaws in the optics preceding the interferometer could cause a wider cone of light to be admitted and hence lead to further broadening.

This effect apparently caused broadening of the components in several spectra when a thin but irregular film of oil accumulated

Fig. 3.2. 3-hour Brillouin spectrum from artificial ice at -3°C (crystal 2, $\gamma = 24.9^{\circ}$). L designates the longitudinal Brillouin component and T_1 and T_2 the transverse components associated with the unshifted component U. A total time of 10 s was spent accumulating counts in each MCA channel. See text for further description.

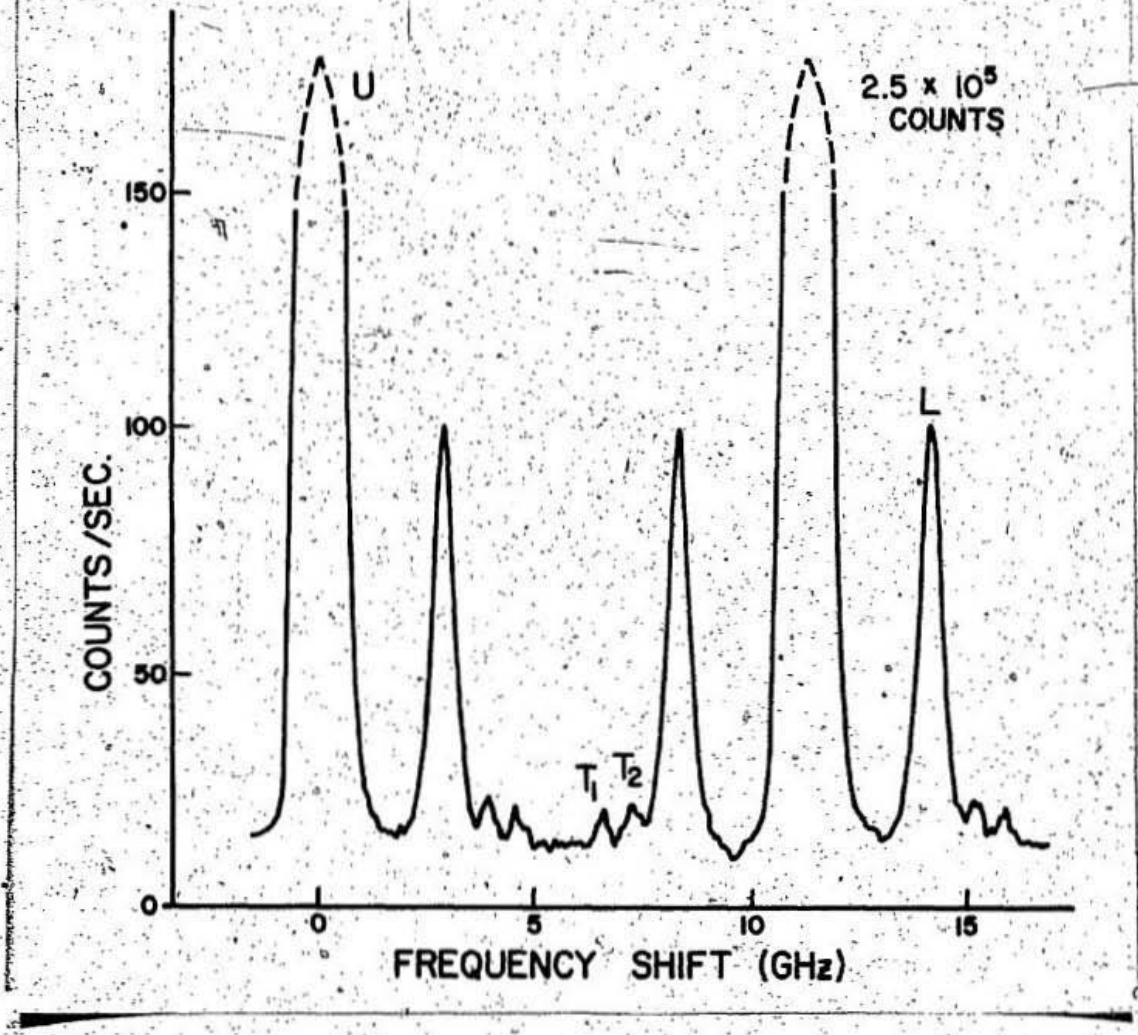
U
2.5 x 10^5
COUNTS
150
100
50
0
COUNTS/SEC.
L
T1
T2
0
5
10
15
FREQUENCY SHIFT (GHz)

Fig. 3.2

on the outside surface of the sample cell. The oil drained from the heat sink compound used to provide thermal contact between the cell walls and the brass clips which cooled the cell. As well as broadening the components, it reduced the apparent intensity of Brillouin scattering and caused small absolute deviations in the scattering angle which in turn led to increased scatter in the Brillouin frequency shift measurements. The film was removed before growing the second of the four ice crystals and did not appear to recur. Due to the similarity in values for the widths of the Brillouin and instrumental lines as well as the uncertainty caused by a significant range in the scattering angle and the difficulty in making precise linewidth measurements, no analysis of real Brillouin linewidths was carried out in connection with the present work.

Brillouin spectra were generally accumulated until the longitudinal component and one or both transverse components were sufficiently well resolved to allow their peak frequencies to be determined to within an estimated uncertainty of ±1 channel. Since one free spectral range corresponded to about 390 channels, this was equivalent to an uncertainty of ±.03 GHz in the frequency shift measurements.

Because the frequency shifts of the longitudinal components, averaging about 13.7 GHz, exceeded the spectral free range, the components overlap into the adjacent order. The frequency shifts of the transverse components, averaging about 7.0 GHz, exceed 50% of the spectral free range. Hence, transverse components are associated with the more distant of the two adjacent unshifted components. These relationships are indicated in Fig. 3.2 and remained

unchanged throughout the work discussed here and in the following chapters.

The Brillouin spectra from artificial ice included a significant background component arising from a combination of several sources. Photomultiplier dark count (about 1 count/second) generally accounted for less than 10% of the background. The largest contribution appeared to come from the very broad but relatively intense Raman components in the ice spectrum. Raman scattering made the incident laser beam in the ice crystal clearly visible when viewed through an orange coloured glass filter. When recording many of the spectra, an interference filter with a 10^4 GHz bandpass centred at the laser frequency was placed between the sample and the interferometer to block the Raman scattered light. However, use of the filter also reduced the observed Brillouin intensity by more than one third and was thus not always an advantage. Another significant contribution to background count resulted from stray laser light or room light from other sources which bypassed the interferometer and illuminated the photomultiplier directly. Accordingly, precautions were taken to minimize sources of extraneous light.

The finite contrast of the Fabry-Perot interferometer gave rise to a curvature in the background spectrum between the unshifted components. However, with the usually observed intensity ratio of the unshifted components relative to the Brillouin components in the spectra from artificial ice, background curvature due to finite contrast was not significant when operating the interferometer in the triple pass mode.

3.6 Determination of Elastic Constants and Uncertainties

The 30 Brillouin spectra obtained from 4 single crystals of artificial ice at $-3^{\circ}C$ yielded 65 Brillouin frequency shift measurements. These are tabulated versus crystal orientation in Table 3.1. Acoustic propagation velocities were determined from the frequency shift measurements via the Brillouin equation (equation (1-3)). Hence, values for the three linear coefficients λ, $1/n$ and $1/\sin(\alpha/2)$ were required in the analysis of the Brillouin data.

The laser wavelength λ was 5.145×10^{-7} m with negligible uncertainty. The scattering angle α was $90^{\circ} \pm .2^{\circ}$ yielding a value of $1.4142 \pm .17\%$ for the term $1/\sin(\alpha/2)$. The refractive index n of ice at $-3^{\circ}C$ for light of wavelength 5.145×10^{-7} m was determined by linear interpolation from values given in the International Critical Tables.[71] The index was taken to be $n = 1.312 \pm .001$, where the uncertainty is included primarily to account for the very slight birefringence ($n^{o} = 1.3117 \pm .0003$, $n^{e} = 1.3131 \pm .0003$) of hexagonal ice. The effect of birefringence on the Brillouin spectra appeared negligible. The coefficient $1/n$ had a value of $0.7622 \pm .08\%$. Acoustic velocity V and Brillouin frequency shift Ω were thus related by the equation given below (m k s units);

$$V = (2.773 \times 10^{-7} \pm .19\%)\Omega \qquad (3\text{-}3)$$

The velocities of the three acoustic modes in hexagonal media are related to density, ρ, propagation direction, γ, and the elastic constants, c_{ij}, by the equations (2-15), (2-16) and (2-17). Each of these equations is of the form,

$$f(c_{ij}, \cos^2\gamma) = 2\rho V^2 \qquad (3\text{-}4)$$

TABLE 3.1

BRILLOUIN SPECTROSCOPIC DATA FOR ARTIFICIAL ICE, $-3^{o}C$

Crystal #	Euler Angles (deg.) ϕ	θ	ψ	γ(deg.)	Brillouin Frequency Shifts (GHz) L	T_1	T_2
1	60.7	67.9	81.5	54.1	13.49	-	-
	79.5	68.1	81.1	67.5	13.68	-	7.27
	38.9	68.5	81.2	39.5	13.62	6.62	-
	13.8	68.5	81.8	26.1	13.74	6.49	7.24
	106.4	68.0	81.2	85.4	14.00	-	6.60
	93.8	67.7	81.0	77.0	13.68	-	6.76
	48.7	68.2	81.6	45.9	13.34	-	-
	28.5	68.0	82.3	32.7	13.71	6.56	-
	3.5	68.7	82.0	23.9	14.08	6.56	-
	84.9	67.4	81.1	70.7	13.86	-	7.04
	72.8	67.3	81.8	62.2	13.73	-	7.40
	54.6	67.9	81.7	49.8	13.56	-	-
	43.5	68.0	82.0	42.2	13.56	-	-
	21.6	68.2	82.1	29.2	13.92	6.61	7.55
	105.2	68.0	81.0	84.7	13.80	-	6.46
2	197.3	114.4	247.0	24.9	13.98	6.52	7.19
	223.5	114.7	247.9	40.4	13.59	6.64	7.75
	248.4	115.0	248.0	57.7	13.52	-	7.56
	258.0	115.1	248.2	64.3	13.64	-	7.25
	275.5	115.3	248.7	76.1	13.81	-	6.77
3	3.8	58.9	248.9	14.2	14.25	6.52	-
	19.6	58.5	249.0	20.4	14.14	6.54	7.03
	42.0	58.0	248.4	34.9	13.70	-	7.61
	53.7	57.8	248.4	43.1	13.58	-	7.85
	67.9	57.6	248.1	52.9	13.51	6.79	7.69
	79.9	57.6	247.5	61.1	13.61	6.81	7.37
4	277.8	95.1	91.8	89.7	13.91	-	6.46
	277.8	98.1	91.8	89.7	13.92	-	6.46
	287.6	98.8	92.0	84.1	13.90	6.90	6.53
	316.6	98.9	92.3	66.5	13.64	6.83	7.21

where $f = f_1 + f_2$ with f_1 being linear in the elastic constants and f_2^2 being a mixed quadratic in the elastic constants. Hence values obtained for the elastic constants by inverting (2-15), (2-16) and (2-17) depend linearly on the density and on the squares of the Brillouin frequency shifts.

The density of ice at $-3^{\circ}C$ was taken to be 917.5 ± 1.5 kg/m^3, based on several values given in the literature. These values showed a small dependence on the purity, age, and crystal quality of a given sample and on the method of measurement. A review of ice density measurements prior to 1940, along with a comment on their variability, can be found in the text by Dorsey.[24] Further comments on variations in ice density are given by Dantl and Gregora,[39] who argue that density tends to decrease with sample age (see also Sec. 1.3x). Butkovich,[43] however, suggests that while tiny recognizable variations exist, the density of uniform, optically clear ice is basically constant.

The density value quoted in the International Critical Tables[71] for ice at $0^{\circ}C$ is $916.8 \pm .5$ kg/m^3. An experiment utilizing the Bunsen Ice Calorimeter yielded a value of $916.71 \pm .05$ kg/m^3 for the density of freshly formed polycrystalline ice at $0^{\circ}C$.[44] Specific gravity measurements (by immersion in 2, 2, 4-trimethylpentane) on several high quality monocrystals of pure ice from the Mendenhall Glacier gave an average value of 917.18 kg/m^3 for the density at $-3.5^{\circ}C$.[43] An x-ray crystallographic determination of the lattice parameters of tiny ice crystals frozen from droplets of distilled water implied a density of $918.7 \pm .7$ kg/m^3 at $-10^{\circ}C$.[72] Table 3.2 was formed by correcting each of the four density values mentioned

TABLE 3.2

FOUR DETERMINATIONS OF THE DENSITY OF ICE Ih

Source	Density (kg/m^3) ($-3^{\circ}C$)	Reference
Critical examination of available data	917.2	71
Bunsen ice calorimeter	917.14	44
Specific gravity of Mendenhall ice	917.11	43
X-ray crystallography	917.7	72

above to the value appropriate for $-3^{\circ}C$ using the thermal expansion data of Butkovich[73] (see equation (4-1)). The density value chosen for use in the present analysis includes sufficient uncertainty to encompass all reliable published measurements. The value is biased slightly above the mean of the values in Table 3.2 in view of the observation of Dantl and Gregora[39] regarding the greater density of freshly formed ice samples.

The .16% uncertainty allowed in the density of ice, combined with the above determined uncertainties in scattering angle and refractive index, yielded a systematic uncertainty of ± .41% in values of ρV^2 and hence in values of the elastic constants determined from the Brillouin data. Further (nonsystematic) uncertainty in the elastic constants resulted from error in the measurement of Brillouin frequency shifts, slight variations in the scattering angle and uncertainty in the orientations of the crystals. The combined effect of these uncertainties was included in an empirical error term, calculated for each individual elastic constant via the least squares fit routine discussed below. The dynamic elastic moduli of monocrystalline artificial ice at $-3^{\circ}C$ were determined by Brillouin spectroscopy to have the following values. The uncertainty has been divided into its nonsystematic and systematic components.

$$\left.\begin{aligned} c_{11} &= 136.96 \pm .15\% \\ c_{12} &= 69.66 \pm .50\% \\ c_{13} &= 56.28 \pm .37\% \\ c_{33} &= 147.02 \pm .20\% \\ c_{44} &= 29.59 \pm .30\% \end{aligned}\right\} \times (10^8 \pm .41\%)\,N/m^2$$

The elastic constants listed above represent a least squares fit to the 65 Brillouin frequency shift measurements listed in Table 3.1. The relevant sum squared error term, χ^2, is defined in equation (3-5):

$$\chi^2(c_{ij}) = \frac{1}{N-5} \sum_{k=1}^{N} \left[\frac{\Omega_k^{meas.} - \Omega^{calc.}(\gamma_k, c_{ij})^2}{\sigma_k} \right] \qquad (3\text{-}5)$$

In the above equation, N denotes the total number of frequency shift measurements, N-5 is the number of degrees of freedom, $\Omega_k^{meas.}$ denotes the k'th measured frequency shift while $\Omega^{calc.}$ denotes frequency shift calculated via the Brillouin equation and equation (2-15) or (2-16) or (2-17) for the appropriate acoustic mode propagating with angle γ relative to the c axis of an ice crystal with assumed elastic constants, c_{ij}. The standard deviation of the k'th frequency shift measurement is given by σ_k.

An existing FORTRAN program was used to minimize χ^2 as a function of the five elastic constants. The program had been used previously in the analysis of Brillouin data from several hexagonal substances and was described in the thesis by Landheer.[74] Its principal features included a modified Newton-Raphson iteration for finding the zeros of the first derivatives of χ^2, along with an analytic routine for determining the propagation of error. The error analysis required reasonable estimates for the values of the standard deviations, σ_k. Since there was no clear criterion for estimating a separate value for each Brillouin spectrum, similar spectra were assumed to yield identical uncertainties in frequency shift measurements. Accordingly, the spectra were divided into two groups, the

first of these comprising spectra from the first ice crystal, and the second comprising spectra from the three subsequent crystals. Variations in scattering angle caused by the oil film mentioned in the previous section yielded significantly increased error in frequency shifts determined from the first crystal.

The standard deviations in the frequency shift measurements were calculated empirically, using the statistical criterion that χ^2 have an expectation value of unity when $\sigma_k \equiv \sigma$ = one standard deviation. A separate fit was required for data from each of the two groups of spectra. The empirical standard deviation for frequency shift data from the first crystal was found to be .093 GHz. This value significantly exceeded probable error due to imprecise measurement of the peak frequencies (.03 GHz or 1 channel) and thus primarily reflected variations in the scattering angle. The empirical standard deviation for frequency shift data from the subsequent three crystals was found to be .026 GHz. A final simultaneous least squares fit to both sets of data, appropriately weighted with the respective standard deviations, yielded the elastic constants and the nonsystematic uncertainties quoted above.

To illustrate the distribution of the Brillouin data and their relative uncertainties, curves of the form Ω vs. γ, specified by the least squares elastic constants, are plotted along with the experimental data in Fig. 3.3. These curves completely determine the elastic properties of ice and hence are used in subsequent graphical comparisons of the elastic properties of artificial ice with those of the natural ice samples discussed in the following chapter (see also Chapter 6).

Fig. 3.3. Data for artificial ice at -3°C. Measured Brillouin frequency shifts Ω (indicated by crosses) and calculated frequency shifts (indicated by solid curves) versus the angle γ between the crystal c (hexagonal) axis and the direction of sound propagation. Heights of vertical bars indicate empirical standard deviation in frequency shift measurements. Curves specified by least squares elastic constants via equation (2-15) (L), equation (2-16) (T_2) and equation (2-17) (T_1) along with Brillouin equation (1-3) or (3-3).

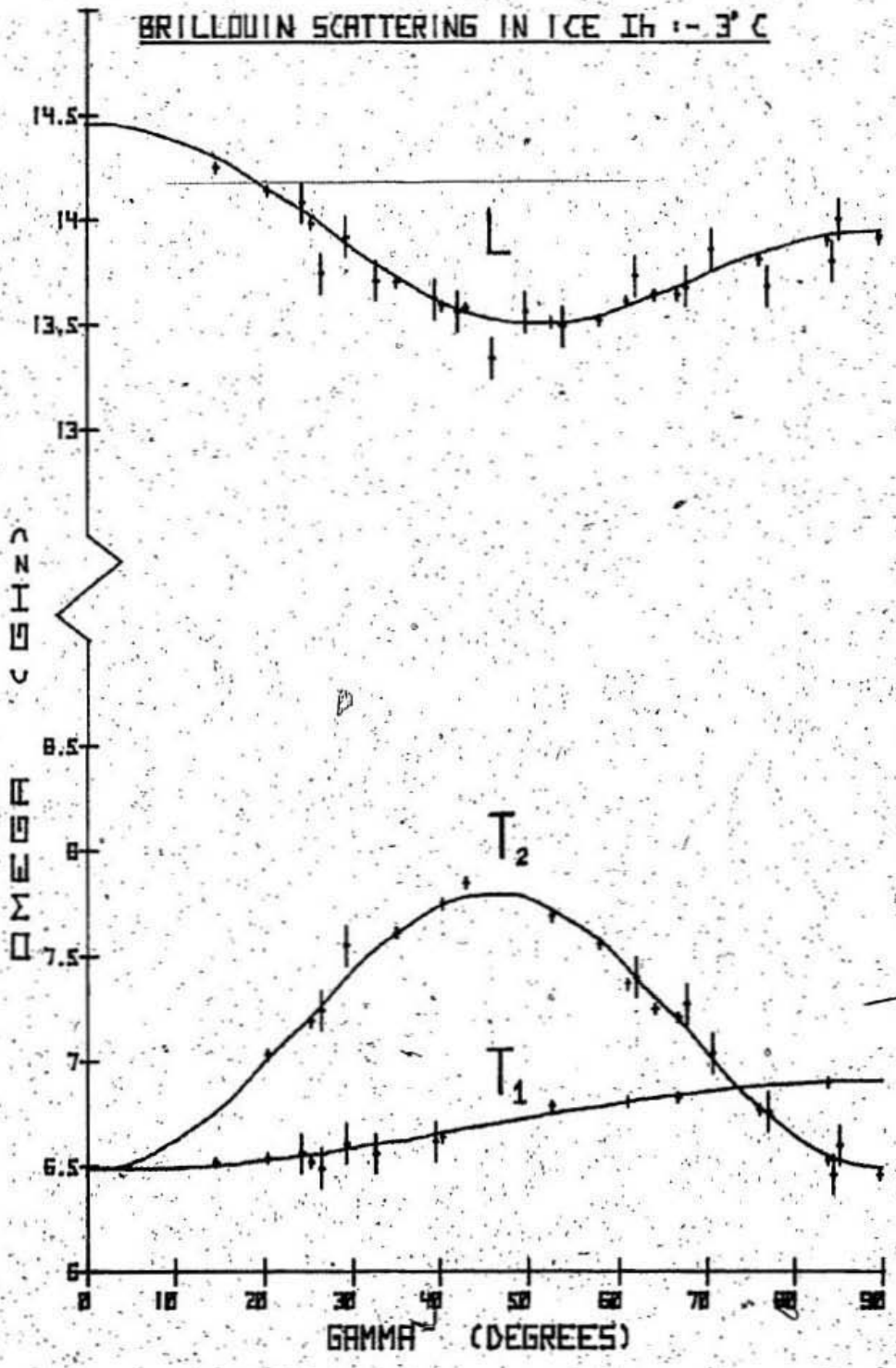
BRILLOUIN SCATTERING IN ICE Ih :- 3° C
14.5
14
13.5
13
8.5
8
7.5
7
6.5
6
OMEGA (GHz)
L
T2
T1
0
10
20
30
40
50
60
70
80
90
GAMMA (DEGREES)

Fig. 3.3

CHAPTER 4

THE ELASTIC CONSTANTS OF NATURALLY OCCURRING ICE SAMPLES

4.1 Selection of Samples

The three types of naturally occurring ice samples chosen for detailed study represent three widely differing environments of ice formation. These environments, glacial, fresh water lake and ocean, yield a near maximum range in water purity and crystal growth conditions, thereby facilitating likely observation of any variations in elastic properties among natural ice samples.

The glacial ice sample was taken from the Mendenhall Glacier in Alaska. The Mendenhall is a temperate glacier providing ideal conditions for the growth and subsequent annealing of large unflawed ice monocrystals.[2] For this reason, samples of Mendenhall ice have been used in a wide range of ice physical property investigations, continuing with the present work. Prolonged annealing at the freezing point has reduced impurity concentrations in meltwater from monocrystals of Mendenhall ice to levels resembling those in distilled water.[75] Hence, crystal quality and age are the principal factors distinguishing Mendenhall ice from the artificial ice samples used in the Brillouin experiment described in the previous chapter. A second type of glacial ice, that from an iceberg, was selected for use in a few measurements (results noted in Sec. 6.1) but was not subject to detailed study.

Ice crystal growth conditions in the fresh water lake environment are considerably more complex than those existing in a temperate glacier. Rapid temperature changes lead to variable and high freezing rates and large thermal gradients. Thus, crystal grain size is irregular and often small, that is with linear dimensions less than one centimetre. Crystals are probably not well annealed as temperatures near the freezing point may persist for only a very short time. Large values of stress in the ice sheet covering a lake can disrupt ice crystals and crystal growth may be modified by dissolved gaseous and solid impurities in the water. These impurities are likely dispersed throughout the ice crystals since the migration of impurity ions is inhibited at temperatures significantly below the freezing point. The Brillouin experiment on lake ice was undertaken to determine whether the non-ideal crystal growth conditions in the fresh water lake environment modified the elastic properties of lake ice relative to those of glacial ice.

The high concentration of dissolved impurities in ocean water give rise to ice crystal growth conditions very different from those present in any fresh water environment. Since several types of impurity ions are present in concentrations far exceeding those which may be dispersed uniformly within the ice crystals, the freezing process is accompanied by the expulsion of these ions to regions which have not solidified. The resulting substance is heterogenous, consisting of regions of ice interspersed with air bubbles and liquid inclusions containing concentrated dissolved, and at lower temperatures precipitated, impurities. A Brillouin spectroscopic determination of the elastic moduli of local, apparently homogeneous,

regions in a sea ice sample was undertaken to facilitate reliable future analysis of the elastic properties of sea ice in terms of the elastic properties of an ice matrix and a distribution of gaseous and liquid inclusions.

Samples of Mendenhall ice were provided by the Cold Regions Research and Engineering Laboratory (CRREL) of Hanover, New Hampshire. The samples were collected in the summer of 1965 and stored at -35°C until September 1979, whereupon they were shipped by air to St. John's in an insulated box containing several kilograms of broken ice for thermal ballast. Although the maximum temperature of the samples in transit was not determined, their dry surfaces at the time of arrival indicated that this temperature was below 0°C. Pending their use in the Brillouin experiment the samples were stored for one month in a chest freezer at approximately -25°C.

A lake ice sample was obtained from Paddy's Pond, near St. John's, for use in the Brillouin experiments. The sample was taken from the 40 cm thick ice cover near the middle of the lake using an ice auger and saw to cut a 10 cm by 13 cm by 40 cm deep rectangular block. Following collection in late February 1979, the sample was stored, pending its use in the Brillouin experiment, for five months in a chest freezer at approximately -25°C.

A sample of sea ice collected from the Weddell Sea (73° 56' S, 42° 46' W) in the Antarctic was provided by CRREL. The sample was the bottom 14.3 cm of a 1.5 m core drilled in what was characterized as first-year columnar sea ice, sampled at the end of the first summer.[76] The temperature of the sample at the time of collection was around -2° to -3°C. Following collection in

mid-February 1980, the sample was stored at -17.8°C for about two months while in transit to CRREL and subsequently was stored at -28.9°C for about three months prior to being shipped to St. John's. The method of shipment was similar to that used for the Mendenhall ice except that the transit time, nearing 24 hours, was somewhat longer. Nevertheless, ice chips used for thermal ballast adjacent to the sample did not fuse, indicating that the sample temperature upon arrival was less than 0°C. While awaiting its use in the Brillouin experiment, the sample was held for one week at approximately -25°C in a chest freezer.

4.2 Sample Preparation and Description.

Small irregular samples with volume less than .5 cm^3 and no linear dimension greater than 1 cm were utilized in the Brillouin spectroscopic determinations of the elastic moduli of the three types of natural ice. A hammer and very sharp steel chisel were used to chip the working samples from the much larger bulk samples. Two or three sharp blows were generally required to extract one sample. The first of these separated the sample from the bulk and the second or third reduced the sample dimensions to those allowing the sample to be accommodated by the Brillouin scattering apparatus. While all methods of extracting a small sample of natural ice could possibly modify the properties of the sample, the method used in the present instance appears to minimize this risk. No change in the temperature of the sample occurs, and plastic deformation is avoided by applying stress over a very short time interval. Propagation of hairline fractures through portions of a sample sometimes occurred, but when these were noted in subsequent visual inspections,

samples were discarded.

Each natural ice chip was immersed in liquid Freon 114 ($C_2 Cl_2 F_4$) and visually inspected through crossed polaroid filters before being mounted for Brillouin spectroscopy. Freon 114 is immiscible with water, has a boiling point of 4°C and has a refractive index matching that of ice. Its use thus made possible detailed visual inspection of samples with highly irregular surfaces. Furthermore, evaporation from samples wet with Freon 114 kept their surfaces from reaching the melting point during brief periods of handling in room temperature air. Cracks, bubbles, solid inclusions, other optical imperfections and crystal grain boundaries were noted in the course of the visual inspections. Accordingly, only those samples of optimal optical quality were selected for use in the Brillouin experiments.

The bulk samples and consequently the selected working samples of Mendenhall ice were monocrystalline and completely free of observable optical imperfections. In contrast, the bulk sample of lake ice contained air bubbles dispersed throughout its volume. However, these were not uniformly distributed but were concentrated in horizontal layers, presumably corresponding to intervals of rapid freezing. The working sample was chipped from a layer of minimum bubble density about 4 cm from the bottom of the bulk sample and included no visible air bubbles. The sample appeared clear and of good optical quality, although some flaws were present as evidenced by occasional bright scattering from points along the path of the focused laser beam used in Brillouin spectroscopy. The sample was bicrystalline, with a flat grain boundary clearly visible through

crossed polaroids and dividing the volume of the sample in the approximate ratio 1:3. The grain boundary was invisible in ordinary light and did not appear to scatter laser radiation. Its presence was neglected in the Brillouin scattering measurements by choosing the scattering volume to lie in the larger monocrystal, a few millimetres from the grain boundary. Each of several chips extracted from the ice near the selected sample were found to be bicrystalline or polycrystalline. This indicated that crystal grains in the region from which the sample was taken had linear dimensions averaging 1 cm or less.

The bulk-sample of sea ice contained a high density of tiny air bubbles and other optical flaws making it translucent even when viewed in sections only 0.5 cm thick. In observation through crossed polaroid filters, most samples chipped from the bulk appeared polycrystalline with grains of millimetre dimensions but in some cases, including that of the samples used for Brillouin spectroscopy, the observations were ambiguous. Brine inclusions could not be visually identified in the chip samples but were nevertheless likely present. Fig. 4.1 shows a thin section cut from the sea ice core just below the point where the sample used in the present work was extracted.

4.3 Apparatus for Housing Natural Samples

The apparatus for the Brillouin spectroscopic determination of the elastic moduli of natural ice samples consisted of the optical setup described in Chapter 3 together with a specially designed sample housing and cooling system. The sample housing was built to accommodate small ice chips of arbitrary shape thereby minimizing the need for sample preparation. As well, the housing provided a

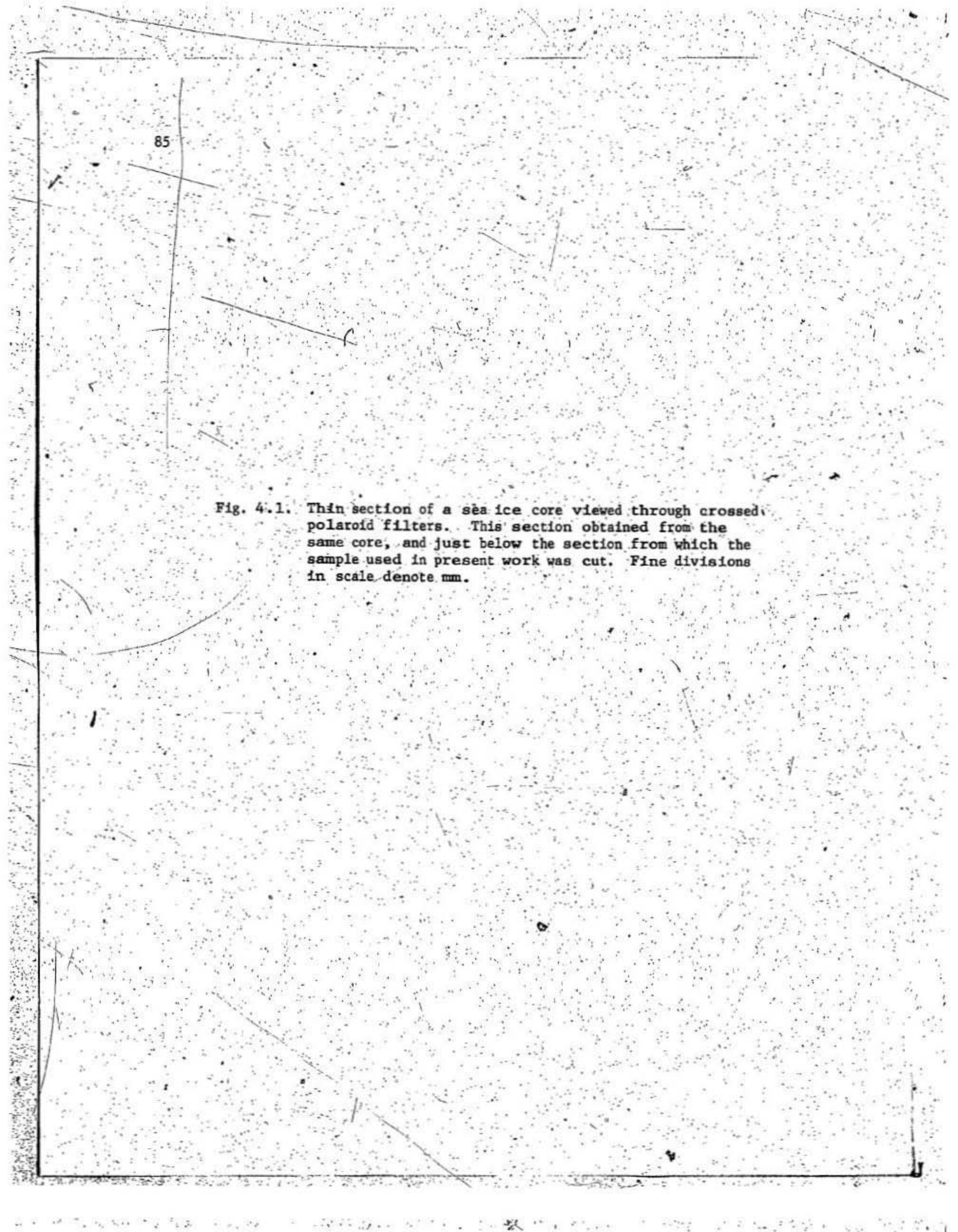

Fig. 4.1. Thin section of a sea ice core viewed through crossed polaroid filters. This section obtained from the same core, and just below the section from which the sample used in present work was cut. Fine divisions in scale denote mm.

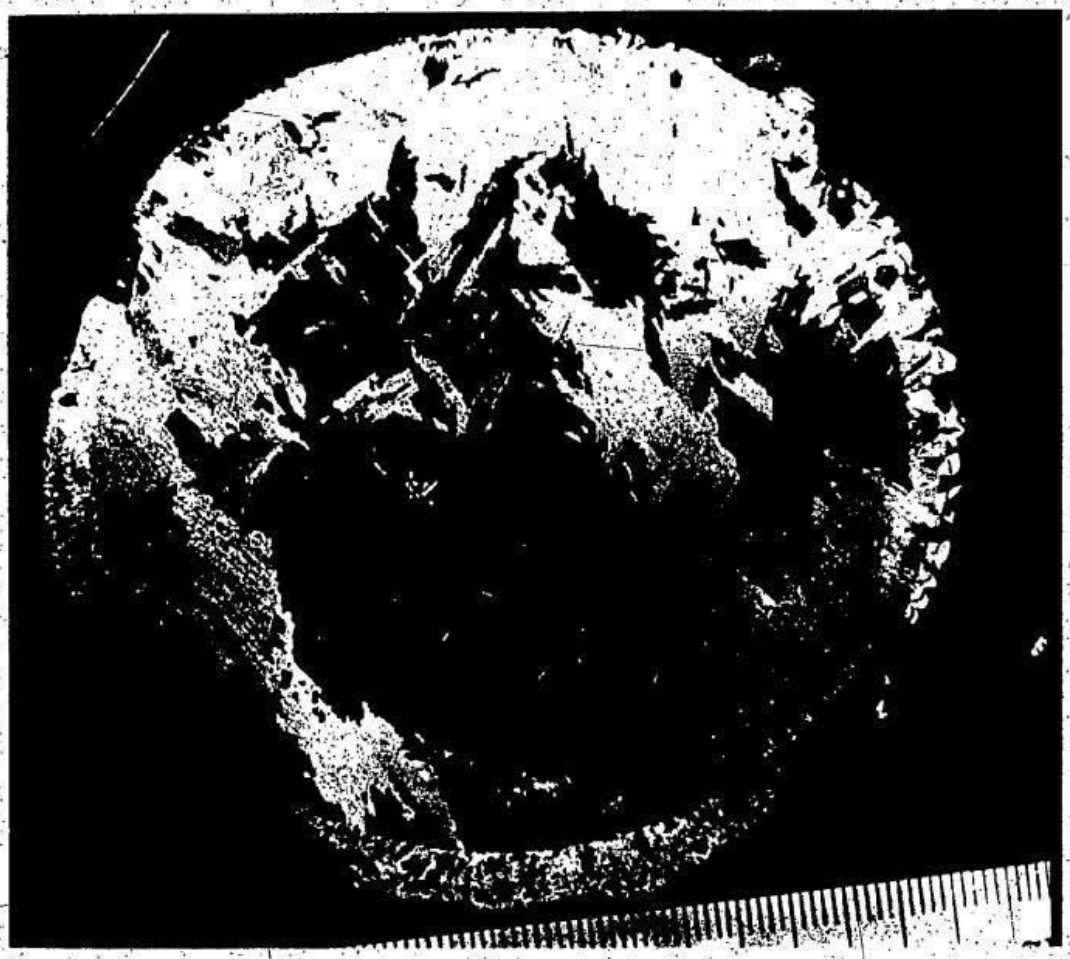

Fig. 4.1

high degree of flexibility in positioning ice samples relative to the Brillouin scattering optics. This flexibility was essential in order to avoid optical flaws in the path of the incident or scattered laser radiation and to select specific scattering volumes within heterogeneous samples.

The principal features of the sample housing are illustrated in Fig. 4.2. Cooling and temperature control were provided by three thermoelectric modules joining the copper heat sink surrounding the sample cell to the water-cooled copper outer enclosure. The pair of modules adjacent to the outer enclosure provided most of the cooling power. The copper plate separating the two layers of modules was thus maintained at a temperature near the desired temperature of the sample and small corrections, either positive or negative, were made with the module adjacent to the sample cell.

The temperature of the sample was monitored by a thermistor embedded in epoxy attached to the heat sink. Calibration of the thermistor was based on the melting points of seven liquids: cyclohexane, benzene, water, aniline, ethylene glycol, quinoline and carbon tetrachloride, arranged in order of decreasing melting points. With the cooling system in its normal operating mode, each liquid was first frozen and then melted to the extent that the solid-liquid boundary touched the bottoms of the steel wires used for holding ice samples. The thermistor reading was noted and assumed to correspond to the temperature of a sample, were it to be suspended in the liquid. The calibration was estimated to be accurate to within $0.5^{\circ}C$.

The cooling system provided good temperature stability over multi-hour time intervals without the aid of thermostatic control.

Fig. 4.2. Sample housing and cooling system for Brillouin spectroscopy in natural ice samples. A - ice sample; B - indium coated steel wires; C - Spectrosil optical cell; D - copper cell enclosure and heat sink; E - teflon stopper; F - coil spring; G - 6.35 mm hex bolt; H - 1 mm o.d. stainless steel tube; I - thermoelectric module for temperature control; J - thermoelectric modules for cooling; K - copper plate; L - semi-rounded brass plate; M - O ring seal; N - brass cover; O - copper cylindrical outer housing; P - dry N_2 input and output; Q - cooling water pipe.

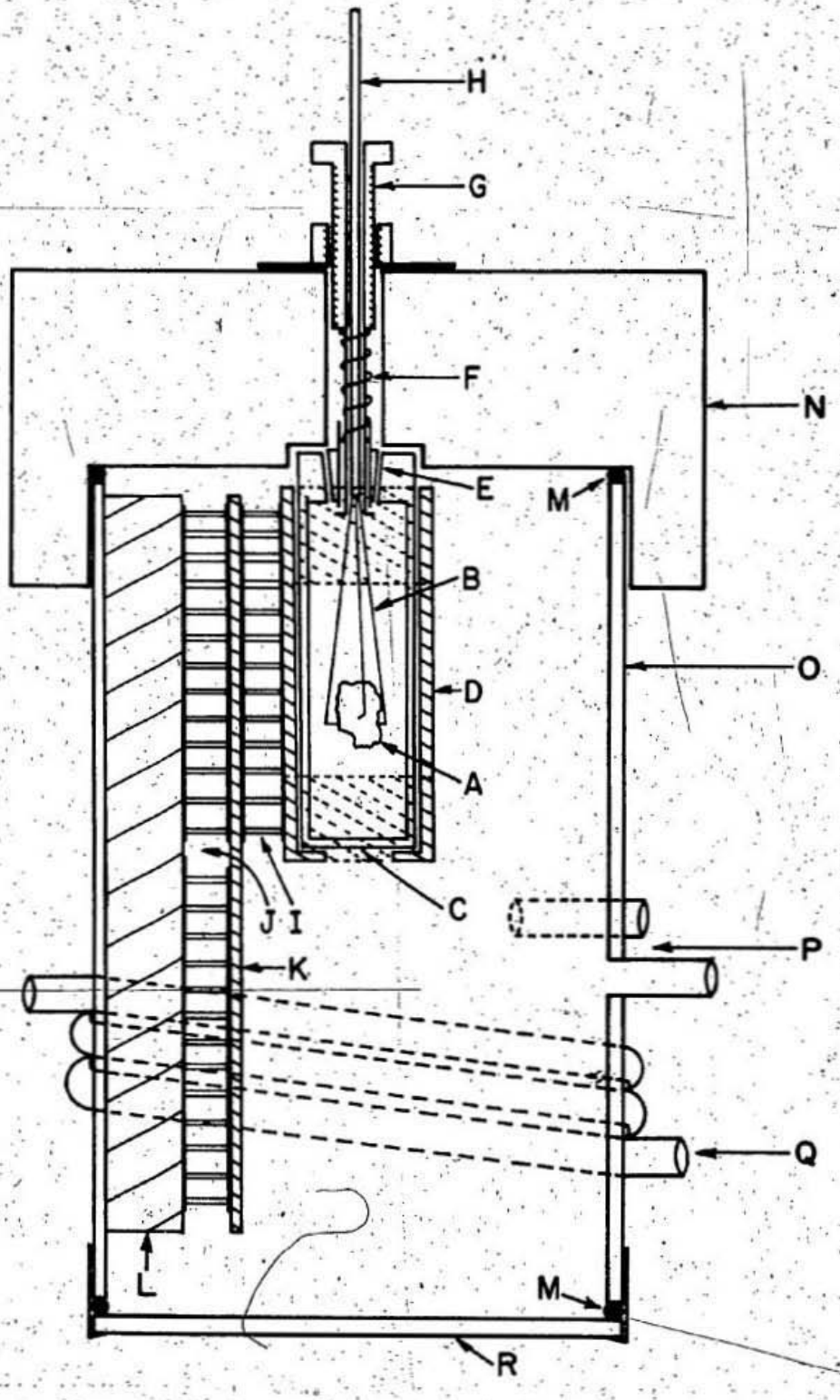

Fig. 4.2

Fluctuations in sample temperature were due almost entirely to changes in the temperature of the cooling water and seldom exceeded 0.5° over 24 hours. Manual adjustments to the current supplying the inner thermoelectric module compensated for temperature drift and maintained the sample temperature within a range of $\pm 0.2^{\circ}$ during spectral accumulation.

Thermal contact between the ice chip suspended in the sample cell and the cell walls was provided by the liquid in which the sample was immersed. The appropriate immersion liquid was selected on the basis of several required physical properties. These included optical transparency, minimal absorption or scattering of x-rays, immiscibility with water, a refractive index matching that of ice and a liquid range at atmospheric pressure which included the desired sample temperature. The liquid, 1,2-dichlorotetrafluoroethane (Freon 114), met all requirements with the exception of x-ray transparency and hence was used in some of the work on sea ice where Laue diffraction photographs were not required. In all other work, a blended hydrocarbon-fluorocarbon mixture was used for sample immersion. The liquids, 2,2-dimethylpropane (neopentane) and perfluoromethylcyclohexane had refractive indices of 1.348^{77} (Sodium D line, $6^{\circ}C$) and 1.285^{77} (Sodium D line, $17^{\circ}C$) and matched the refractive index of ice, 1.309 (Sodium D line, $0^{\circ}C$) when blended in the ratio 5:8 respectively.

The ice sample and surrounding liquid were housed in a precision rectangular optical cell fabricated from Spectrosil to permit x-ray transmission through the cell walls. The internal cell dimensions were 1 cm x 1 cm x 3.2 cm. The top of the cell was

sealed by a tapered teflon stopper which in turn was penetrated by three concentric stainless steel tubes (see Fig. 4.2). All gaps were filled with Apiezon grease to minimize evaporation of the immersion liquid. The higher volatility of neopentane relative to perfluoromethylcyclohexane led to a change in the concentration ratio of the two liquids and hence to a change in refractive index if significant evaporation were allowed to occur. Gradual evaporation resulting from an imperfect seal at the top of the cell sometimes necessitated changing the immersion liquid at weekly intervals.

The assembly at the top of the cell permitted rapid insertion of the ice into the cell and subsequent raising and lowering of the sample and rotation of the sample by measured amounts about a vertical axis. The thin indium-coated steel wires holding the sample applied minimal stress to the ice and did not significantly obstruct optical access. The wires were made to grip or release the sample by translating the innermost stainless steel tube relative to the adjacent concentric tube.

Thermal contact between the outer cell walls and the adjacent copper enclosure was maintained with heat sink compound while all other thermal connections were soldered. The outer housing was made relatively airtight but was not designed to withstand atmospheric pressure and hence was not evacuated. Moisture accumulation on the internal cold surfaces was prevented by a continuous flow of vaporized liquid nitrogen through the enclosure at the rate of about .5 litres per minute. This precaution was necessitated by the tendency of precipitated moisture to rapidly cloud the optical surfaces of the sample cell and to induce electrolytic corrosion of the

thermoelectric modules. A quartz bottom plate allowed the incident laser beam to enter the enclosure, while scattered light exited through a 1.7 cm diameter hole drilled in the side of the copper outer housing. This hole, and a 1 cm diameter x-ray access hole drilled on the opposite side of the cylindrical housing, were covered with Mylar sheets to yield an airtight seal while providing high optical and x-ray transparency.

The outer housing was suspended on a steel rod anchored to the laboratory bench by way of an x - y translation stage. The translation stage was used to make small measured adjustments to the position of the sample relative to the detecting optics. The adjustments lay in the plane normal to the direction of the scattered light received by the detecting optics and had a range limited only by the dimensions of the sample. Unmeasured coarse adjustments to the position of the sample along the direction of the scattered light were made by sliding the x - y translation stage along the optical track to which it was attached. It was thereby possible to choose an arbitrary scattering volume within an ice sample. This capability was useful in the lake ice experiment and essential in the work on sea ice.

4.4 Optical Alignment

Optical alignment of the sample cell was necessary in order to ensure knowledge of the Brillouin scattering geometry. The bottom of the cell was made perpendicular to the incident laser beam using the reflection of the beam from the cell bottom to indicate alignment. Similarly, reflection of a He-Ne laser beam travelling along

the axis of the detecting optics indicated perpendicular alignment of the side walls of the cell.

In order to maximize the intensity of observed Brillouin scattering, the incident laser beam was positioned so as to precisely intersect the axis of the detecting optics. The positioning was carried out by first translating the sample housing to a point where the incident beam missed the ice sample suspended in the cell and travelled instead through the surrounding fluid. The beam was then clearly visible to the eye due to relatively intense Rayleigh scattering by the fluid. Next, the beam was translated in the plane normal to the axis of the detecting optics until the longitudinal components in the Brillouin spectrum of the liquid reached maximum intensity. The sample housing was then translated back to a point where the observed scattering volume lay within the ice sample. The advantage in using the Brillouin spectrum of the liquid to indicate precise positioning of the incident beam resulted from the better than 10 to 1 ratio in the intensity of the longitudinal Brillouin component in the liquid relative to that in ice. As well, a weak or nonexistent Brillouin spectrum in optically flawed natural ice did not necessarily indicate improper positioning of the incident beam but rather was often due to obstruction of the incident or scattered light.

Two components were added to the optical system described in Chapter 3 to improve the capability of the system for resolving Brillouin spectra in optically flawed samples. Firstly, a 1 mm diameter aperture was placed on the axis of the detecting optics about 2 cm from the sample. This mask reduced the amount of stray

light, scattered by flaws in the sample, reaching the detector and eliminated the appearance of spurious spectral components occasionally caused by very bright scattering centres slightly off axis. Secondly, a 2 mm thick parallel sided glass plate was sometimes inserted in the path of the scattered light, adjacent to the sample housing. The plate was aligned perpendicular to the scattered light and then rotated about an axis normal to the plane of scattering thereby translating the region of observation along the path of the incident light. An optical flaw obstructing the incident beam generally caused a momentary surge in the intensity of scattered light reaching the detector as the plate was gradually rotated through the orientation at which the flaw and the region of observation coincided. Accordingly, the scattering volume was chosen to lie below any optical flaws in the path of the incident beam. With the exception of those points noted above, the optical system, optical alignment procedure and general method for obtaining spectral data did not change appreciably between the Brillouin experiment on natural ice and the experiment on artificial ice discussed in the previous chapter.

4.5 Glacial Ice

(i) X-ray data

Both the Mendenhall ice samples and the lake ice sample from Paddy's Pond were of sufficiently good optical and crystallographic quality to allow Brillouin data acquisition and analysis to be carried out using methods quite similar to those used in the experiment on artificial ice. In particular, x-ray orientations could be determined for monocrystals of both types of ice and these were subsequently

correlated with high-resolution Brillouin spectra. The spectra were typically obtained in time intervals of the order of a few hours and showed the longitudinal and usually one or both transverse Brillouin components. The resulting frequency shift data were analyzed to yield the elastic constants using the procedures outlined in the previous chapter.

Laue photographs from the samples of Mendenhall ice and Paddy's Pond ice are shown in Fig. 4.3. The large uniform oval spots in the Mendenhall ice photograph are typical of an unstrained monocrystal. The Laue photograph from Paddy's Pond ice shows spots of slightly less regular shape and as well shows a few small spots formed by the x-ray beam grazing an adjacent crystal grain. The photographs shown were readily analyzed using the techniques of Chapter 2 to yield crystal orientation and are typical of the series of Laue photographs taken to facilitate analysis of the Brillouin data. Exposure times of about one hour were needed to obtain good resolution of the Laue spots. Attenuation of the x-ray beam by the walls of the sample cell and by the fluorocarbon component of the sample immersion liquid necessitated the lengthy exposure times.

(ii) Temperature

A uniform sample temperature of $-16^{\circ}C$ was chosen for the Brillouin spectroscopic measurements of the elastic moduli of each of the three types of natural ice. This temperature was the same as that used by Jona and Scherrer[26] in their determination of ice elastic moduli and lay within the range of temperatures investigated by Dantl[35] and by Bass et al.[28] As well, $-16^{\circ}C$ lies within the range of those temperatures most frequently associated with the occurrence

Fig. 4.3. Laue x-ray diffraction photographs from natural ice samples. A – Monocrystalline ice chip from Mendenhall Glacier; B – Predominantly monocrystalline ice chip from Paddy's Pond; C, D – Polycrystalline chips of Antarctic sea ice. Small, irregular or smeared spots indicate disruption of constituent monocrystals; E, F, G – Bicrystalline ice chip from Arnold's Cove Brook. X-ray beam through upper monocrystal only (E). X-ray beam through grain boundary (F). X-ray beam through lower monocrystal predominantly (G). No disruption of monocrystals in the region near boundary is indicated; H – Polycrystalline chip of bubbly ice from iceberg. Disruption of constituent monocrystals is indicated.

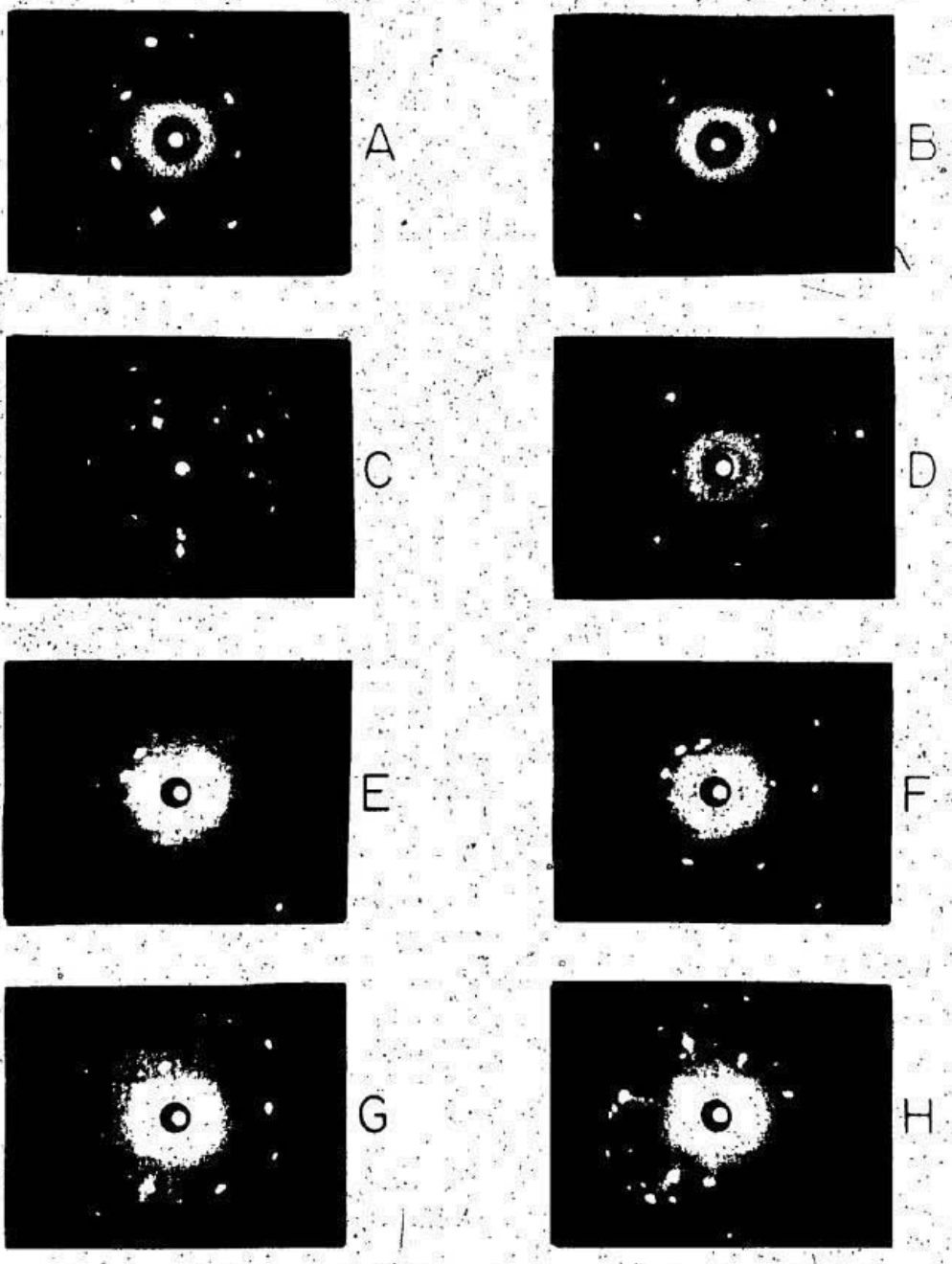

Fig. 4.3

of ice in the natural environment. At temperatures nearer the melting point the properties of natural ice-samples could be expected to show increasing time dependence due to such processes as crystal annealing and the migration of impurities. Local property modification resulting from the warming of ice by optical absorption along the path of the incident laser beam would also increase in likelihood as the sample temperature approached 0°C. These considerations warranted maintenance of the temperature of the samples used in the present investigation at a point well below freezing, particularly in the case of sea ice. The elastic moduli determined for the natural ice samples at -16°C can be corrected to correspond to a range of temperatures using Dantl's[35] temperature correction coefficients. This procedure has been used in Chapter 6 to compare the measurements in artificial ice at -3°C with those in natural ice at -16°C. The uncertainty in sample temperature in the present instance was estimated to be ±.5° due mainly to uncertainty in thermistor calibration.

(iii) Brillouin Spectra

A typical Brillouin spectrum from a sample of Mendenhall ice is shown in Fig. 4.4. The unshifted central component is about 150 times as intense as the longitudinal Brillouin component. This ratio, about average for the Mendenhall ice, was somewhat smaller than the analogous ratio usually obtained in Brillouin spectra from artificial ice. Most of the unshifted light reaching the detector was due to reflection from surfaces within the sample housing. The larger size of the sample cell along with its rectangular shape probably accounted for the relatively low intensity of stray scattering. The 200 mW

Fig. 4.4. Representative Brillouin spectrum from Mendenhall ice at -16°C. The correspondence of Brillouin components with unshifted components (note inter-order overlap) is as indicated in Fig. 3.2. See text for further description of spectrum.

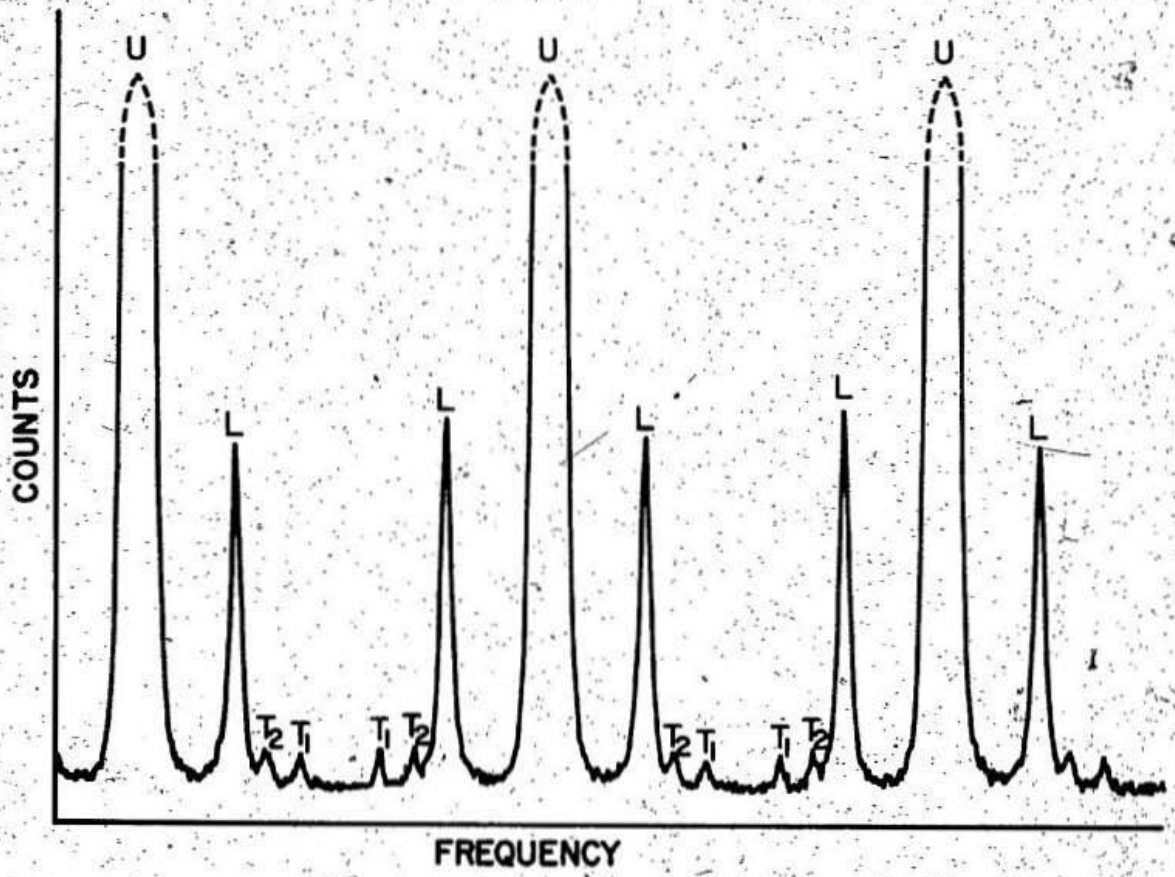

Fig. 4.4

incident laser beam was completely invisible within the ice sample and was reflected almost imperceptibly by the boundary between the sample and surrounding liquid indicating good refractive index matching.

The separation of the plates in the Fabry-Perot interferometer was left unchanged throughout all phases of the present work. Hence the free spectral range remained at 11.101 GHz. The linewidths of the longitudinal and transverse Brillouin components did not differ significantly in the Mendenhall ice from those measured in the artificial ice samples. The instrumental linewidth in the spectrum illustrated in Fig. 4.4 is about 0.25 GHz while the longitudinal and transverse components had approximate linewidths of 0.35 GHz and 0.25 GHz, respectively. A 100 Å interference filter centred at the laser frequency was placed in the path of the scattered light to block the very broad and relatively intense Raman component in the Mendenhall ice spectra. The remaining flat background had an intensity per unit frequency averaging about 25% of that due to Brillouin scattering at the peak of the longitudinal components.

A total of 18 Brillouin spectra were obtained from two crystals of Mendenhall ice. No effort was made to mount the crystals at any particular crystallographic orientation. The mounting of the first crystal resulted in its c axis making an angle, θ, of 78° with the direction of the incident laser beam and subsequent rotation about the vertical axis permitted by the apparatus yielded a good distribution in values of the angle γ (see Sec. 3.3). This first crystal yielded five Brillouin spectra during the seven-day period it was mounted in the apparatus. It was then removed to allow replacement

of the partially evaporated immersion liquid and was replaced by a second crystal with its c axis making an angle of about 77° with the incident beam direction. After yielding three Brillouin spectra this crystal was remounted with $\theta \approx 68°$. The second crystal was housed in the apparatus for a total of 30 days. The Brillouin spectra showed no evidence of any change in elastic properties occurring over this period.

The excellent optical quality of the Mendenhall ice facilitated observation of at least one transverse component in all but one of 18 Brillouin spectra. In 10 of the spectra, both transverse components were observed. Including the longitudinal components, a total of 45 Brillouin frequency shift measurements were obtained. These appear in Table 4.1. The estimated standard deviation in the frequency shift measurements was ±.040 GHz.

(iv) Elastic Constants

Elastic constants were least-squares fitted to the data in Table 4.1 using the FORTRAN program referred to in Chapter 3. The resulting frequency shift (sound velocity) vs. γ curves are shown in Fig. 4.5. Before calculating the elastic constants, it was necessary to specify values for the density, ρ, and refractive index, n, of Mendenhall ice at -16°C. Precise measurements of the density of 11 apparently perfect monocrystalline samples of Mendenhall ice were made by Butkovich[43] at temperatures near -4°C. These values, corrected to correspond to a temperature of -3.5°C, yielded an average density of 917.18 kg/m^3. The linear thermal expansion coefficients of several types of ice were measured by Butkovich[73] and averaged to yield an equation for the expansion coefficient over the temperature range 0°C

TABLE 4.1

BRILLOUIN SPECTROSCOPIC DATA FOR MENDENHALL ICE, -16°C

Euler Angles (deg.) ϕ	θ	ψ	γ(deg.)	Brillouin Frequency Shifts (GHz) L	T_1	T_2
1st Crystal:						
216.7	78.0	129.8	65.9	13.77	6.91	7.30
186.4	79.2	130.1	56.1	13.62	6.83	-
235.8	77.3	129.8	76.6	13.91	-	6.86
259.8	76.9	129.1	87.8	13.99	-	6.50
4.0	77.5	125.3	32.7	13.82	6.62	7.54
2nd Crystal:						
132.4	79.2	240.7	70.3	13.85	-	6.94
200.7	77.9	243.1	60.1	13.76	6.91	-
297.8	74.2	239.0	59.4	13.69	-	7.52
125.6	112.5	271.8	49.4	13.61	6.78	7.79
178.4	113.3	273.9	21.7	14.26	6.61	7.16
132.5	115.3	272.4	42.8	13.67	-	-
191.8	112.1	273.9	24.9	14.19	6.60	7.24
211.7	111.2	273.3	35.3	13.89	6.69	7.67
218.4	110.9	273.1	39.7	13.78	6.74	7.82
71.4	110.5	264.4	87.9	14.05	-	6.53
52.6	109.9	262.9	80.6	13.99	6.97	6.74
227.0	110.7	267.2	45.5	13.63	6.77	7.86
201.6	111.8	266.6	29.2	14.03	6.62	7.44

Fig. 4.5. Brillouin frequency shift versus γ for Mendenhall ice at -16°C. Heights of vertical bars indicate standard deviation. Curves identified as in Fig. 3.3.

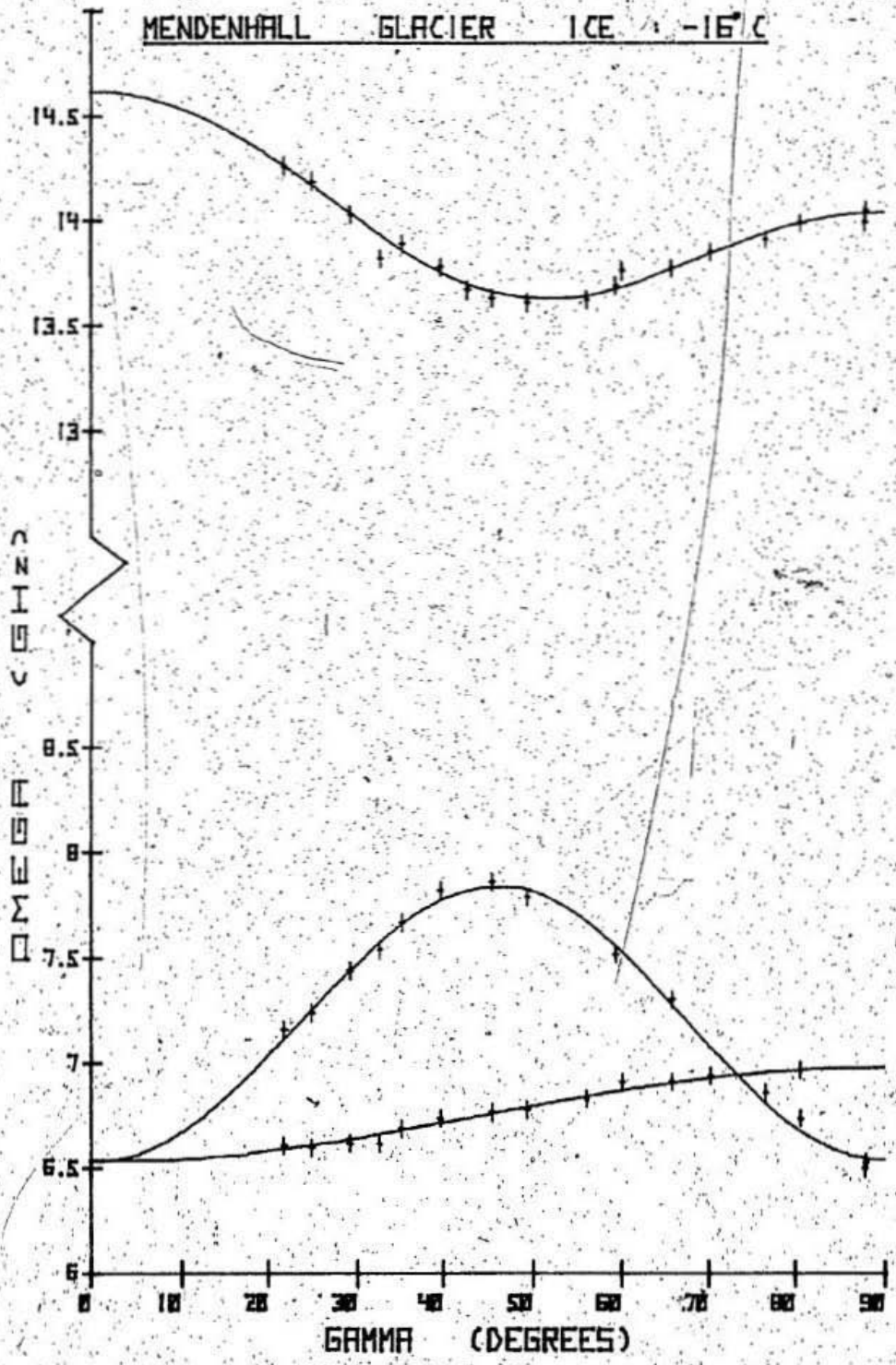
MENDENHALL GLACIER ICE : -16° C
14.5
14
13.5
13
8.5
8
7.5
7
6.5
6
OMEGA (RAD/SEC)
0
10
20
30
40
50
60
70
80
90
GAMMA (DEGREES)

Fig. 4.5

to -30°C. This equation was used to produce the following expression for the temperature dependence of the density of ice.

$$\rho^{-1} = \rho_o^{-1} [1 + 1.576 \times 10^{-4} T - 2.778 \times 10^{-7} T^2 + 8.850 \times 10^{-9} T^3 - 1.778 \times 10^{-10} T^4] \quad (4\text{-}1)$$

In equation (4-1), ρ denotes density, ρ_o denotes the density at 0°C and T is the temperature in degrees Celsius. Accordingly, the value quoted above for the density of Mendenhall ice at -3.5°C was found to correspond to a density of 919.10 kg/m^3 at -16°C.

The uncertainty in density determination for individual samples of Mendenhall ice was estimated by Butkovich[43] to be ±.021 kg/m^3. However, the empirical standard deviation in the density measurements from the 11 apparently perfect monocrystals was ±.056 kg/m^3 indicating a small but measurable difference in density among the samples. The maximum standard deviation in values of the linear thermal expansion coefficient given by the expression from Butkovich[43] leading to equation (4-1) is ±1.5%. Hence an uncertainty of ±.03 kg/m^3 in the calculated density of Mendenhall ice at -16°C results from the application of equation (4-1) in correcting the density from -3.5°C. A final contribution to the error in the density results from uncertainty of ±.5°C in the temperature of the ice sample. This gives rise to an uncertainty of ±.08 kg/m^3 in density. Combining the four statistically independent error terms noted above yields a value of 919.10 ±0.10 kg/m^3 for the density of the Mendenhall ice samples used in the present determination of elastic moduli.

The value for the refractive index of ice at -3° stated in Chapter 3 was n = 1.312 ± .001. This value, when corrected using the

Lorentz-Lorenz[78] relation, for the increase in density which occurs upon cooling becomes $n = 1.3127 \pm .001$ for ice at $-16^{\circ}C$. Values for the remaining parameters in the Brillouin equation, $\lambda = 5.145 \times 10^{-7}$ m, $\alpha = 90^{\circ} \pm 0.2^{\circ}$ are taken from the previous chapter.

The elastic moduli determined for Mendenhall ice at $-16 \pm 0.5^{\circ}C$ are given below:

$$\left.\begin{aligned} c_{11} &= 139.13 \pm .22\% \\ c_{12} &= 70.26 \pm .74\% \\ c_{13} &= 58.01 \pm .52\% \\ c_{33} &= 150.59 \pm .32\% \\ c_{44} &= 30.11 \pm .46\% \end{aligned}\right\} \times (10^{8} \pm .38\%) N/m^{2}$$

The error terms associated with the individual elastic constants were determined empirically, by the methods referred to in Chapter 3, while the systematic error, common to all five elastic constants was calculated from the uncertainties in ρ, n and α indicated above. The systematic error was primarily due to uncertainty in α.

4.6 Lake Ice

(i) Brillouin spectra

The Brillouin spectra from the lake ice sample from Paddy's Pond did not differ significantly from the Mendenhall ice spectra in terms of linewidths or relative intensities of the various spectral components. Although the optical quality of the lake ice sample was inferior to that of glacial ice, the optical flaws which appeared as bright pinpoints of light along the path of the incident laser beam could invariably be avoided by appropriate sample positioning. Those

flaws in the ice which were large enough to be visible without magnification were seen to be tiny air bubbles or particles of embedded foreign solid material.

A total of 14 Brillouin spectra were obtained from a single bicrystalline sample of lake ice. In all cases, the scattering volume was chosen to lie at least 1 mm from the grain boundary in the larger of the two fused monocrystals, this being the first monocrystal traversed by the incident laser beam. The determination of elastic moduli was consequently based entirely on data from a single small monocrystal thereby ensuring that possible variations in elastic properties over the extent of the bulk sample of lake ice did not affect the measurements.

The sample was mounted with the c axis of the larger monocrystal making an angle of 75° with the direction of the incident laser beam. In the course of obtaining the Brillouin spectra, the sample was rotated so as to yield values of γ ranging from 28.5° to 89.9°. This range was sufficient to allow determination of the elastic constants without remounting the sample. All but two of the 14 Brillouin spectra showed at least one transverse component while three of the spectra showed both transverse components. A total of 29 Brillouin frequency shift measurements were obtained from the lake ice sample. The estimated standard deviation in the individual frequency shift measurements was ±.044 GHz. The measurements appear in Table 4.2.

(ii) Elastic constants

Elastic constants were fitted to the data in Table 4.2 to yield the least squares frequency shift vs. γ curves shown in Fig. 4.6.

TABLE 4.2

BRILLOUIN SPECTROSCOPIC DATA FOR LAKE ICE (PADDY'S POND), -16°C

Euler Angles (deg.)			γ(deg.)	Brillouin Frequency Shdfts (GHz)		
φ	θ	ψ		L	T_1	T_2
72.6	106.2	251.7	89.7	13.94	-	-
60.6	105.3	251.4	81.5	13.93	-	6.68
7.7	102.9	251.0	58.3	13.60	6.82	-
178.7	106.6	254.3	28.5	14.00	6.61	-
126.4	106.4	251.1	53.0	13.57	-	-
101.0	103.9	249.1	72.5	13.87	-	6.74
112.5	105.0	249.3	63.6	13.74	-	7.35
124.2	104.9	249.9	55.5	13.65	-	7.68
135.9	105.9	250.5	47.0	13.62	6.82	-
148.0	104.9	250.4	40.4	13.72	6.78	-
156.2	105.2	251.5	35.9	13.81	6.72	7.82
167.1	104.8	251.3	32.1	13.89	6.66	7.65
179.7	104.5	252.3	30.5	13.99	6.66	7.57
74.7	104.7	247.8	89.9	14.04	-	6.52

Fig. 4.6. Brillouin frequency shift versus γ for lake ice at -16°C. Heights of vertical bars indicate standard deviation. Curves identified as in Fig. 3.3.

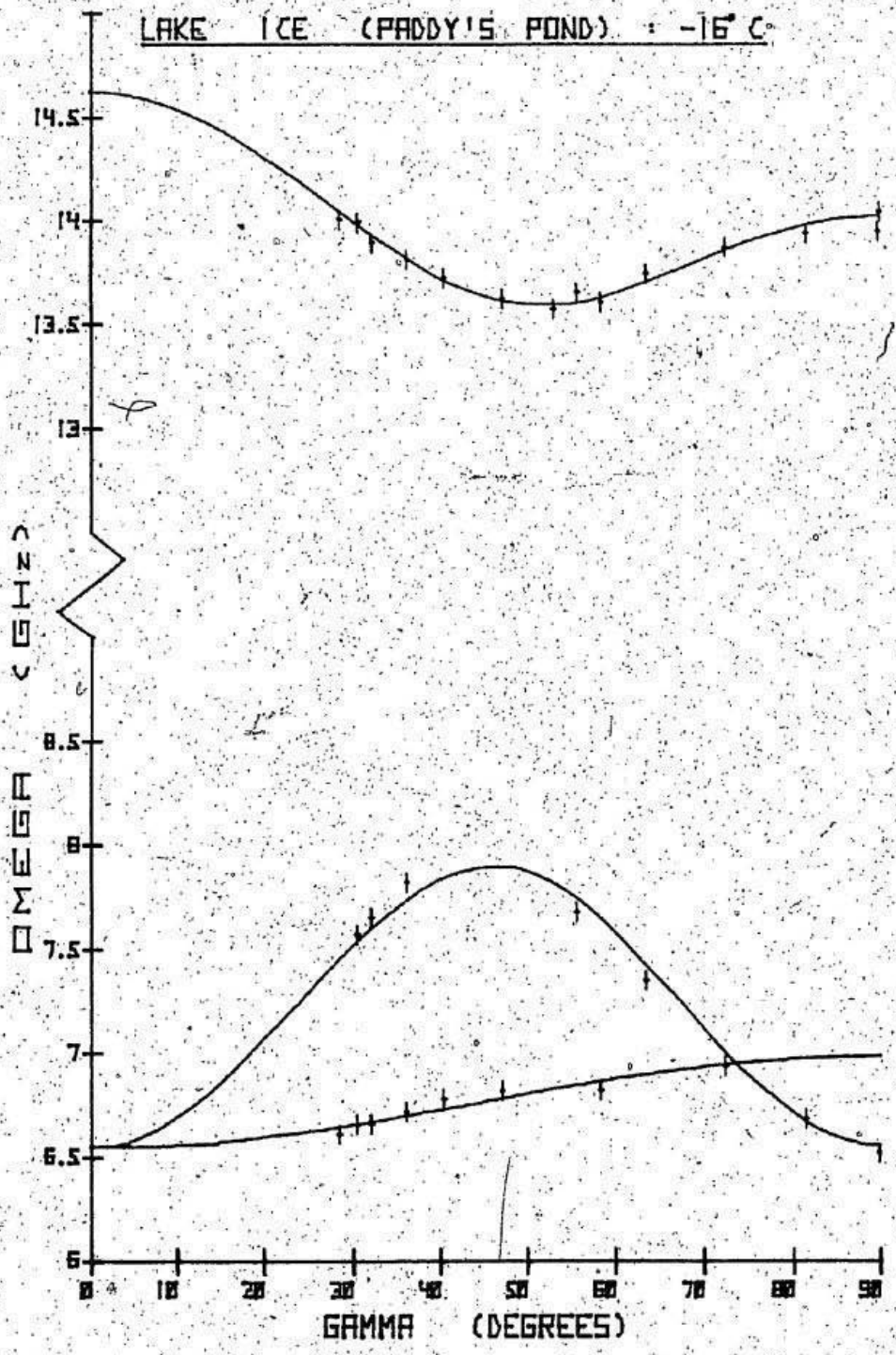
LAKE ICE (PADDY'S POND) : -16° C
14.5
14
13.5
13
8.5
8
7.5
7
6.5
6
OMEGA (GHz)
0
10
20
30
40
50
60
70
80
90
GAMMA (DEGREES)

Fig. 4.6

With the exception of the density, the multiplicative parameters in the Brillouin equation, along with their uncertainties, were set equal to those values used in the determination of elastic constants for Mendenhall ice. The density was calculated from the value used for artificial ice at $-3^{\circ}C$ since an accurate measurement of the microscopic density of lake ice could not be obtained. The density value therefore reflected results of several measurement techniques applied to a variety of types of ice and included an appropriately large uncertainty. The previously quoted density of ice at $-3^{\circ}C$, 917.5 ± 1.5 kg/m^3, was corrected to correspond to $-16^{\circ}C$ via equation (4-1). Accordingly, the density of lake ice at $-16 \pm .5^{\circ}C$, neglecting the insignificant uncertainty in temperature and thermal expansion coefficient, was taken to be 919.5 ± 1.5 kg/m^3.

The elastic moduli determined for lake ice at $-16 \pm .5^{\circ}C$ are given below. The error has been divided into its nonsystematic and systematic components.

$$\left.\begin{aligned} c_{11} &= 138.76 \pm .28\% \\ c_{12} &= 69.79 \pm 1.33\% \\ c_{13} &= 56.57 \pm .76\% \\ c_{33} &= 150.71 \pm .47\% \\ c_{44} &= 30.24 \pm .73\% \end{aligned}\right\} \times (10^{8} \pm .41\%)\,N/m^2$$

Because of the good agreement between the values quoted above and those quoted for Mendenhall ice and for artificial ice (see Chapter 6), an intended second determination of the elastic moduli of lake ice, utilizing a different sample, was not carried out.

4.7 Sea Ice

(i) Optical quality

The very poor optical and crystallographic quality of the sea ice sample necessitated substantial changes in the procedures for the acquisition and analysis of Brillouin data. X-ray orientations could not be obtained for any of the various crystallites comprising the polycrystalline sample. The incident laser beam did not on average travel more than 0.5 mm through the sample before striking a major optical flaw. Similarly, optical flaws frequently obstructed light emanating from the scattering volume. The incident beam was completely diffused within the sample giving rise to very intense parasitic scattering which often obscured the Brillouin components. Nevertheless, by careful positioning of the sample with respect to the incident beam and the axis of the detecting optics it was possible to obtain Brillouin spectra of sufficiently high resolution to allow determination of the elastic constants. The methods of Sec. 2.2 were essential in facilitating analysis of the Brillouin data.

Laue photographs from two samples of sea ice used in the Brillouin measurements are shown in Fig. 4.3. The numerous small, irregular and smeared spots indicate a fine grained polycrystalline texture with considerable disruption of the constituent monocrystals. Diffraction spots of size comparable to the spot formed by the undeflected x-ray beam suggest that a few crystallites of multimillimetre dimensions are present in the samples. The Laue photographs could not be interpreted to yield crystal orientation.

Before a Brillouin spectrum could be obtained from the sea ice sample a suitably clear region for the scattering volume had to

be located. No Brillouin spectrum whatsoever was observed if the path of either the incident or scattered light was obstructed by an optical flaw. The first step in finding an appropriate scattering volume consisted of translating the sample in the plane normal to the incident laser beam until visual inspection showed that the beam was penetrating at least a few millimetres into the sample before striking a major optical flaw. The first major flaw in the path of the beam was in most cases readily noted by the brilliance with which it scattered the incident light.

After finding a sufficiently clear path for the incident beam, the optical detection system was used to monitor the intensity of light scattered at the laser frequency as the height of the region of observation in the sample was varied. At first the height of the sample was coarsely adjusted using the x-y translation stage supporting the sample housing. Starting with the region of observation in the immersion liquid below the sample, the sample was gradually lowered until a sharp rise (usually by a factor between 10 and 1000) in the intensity of light reaching the detector indicated that an optical flaw in the ice coincided with the scattering volume. The sample was then raised slightly and a 2 mm thick parallel sided glass plate was inserted in the path of the scattered light. Rotation of this plate yielded precise adjustments in the height of the region of observation (see Sec. 4.4) and consequently facilitated a detailed check for even minor optical flaws along the path of the incident beam.

When the path of the incident beam between the point of entry into the ice sample and the region of observation appeared

entirely free of optical flaws, spectral accumulation was commenced. In many cases, no Brillouin components were observed due to obstruction of the path of the scattered light emerging from the sample. About 15 minutes of spectral accumulation were needed to verify the existence or nonexistence of longitudinal Brillouin components in the spectrum of the observed scattered light. If no components appeared, the height of the region of observation was varied slightly and a new check was made. After repeating this step several times, if necessary, the sample was rotated a few degrees and more checks for observable Brillouin scattering were carried out. In many instances, none of the above methods were successful and it was necessary to reposition the sample relative to the incident beam and return to the beginning of the entire procedure.

(ii) Brillouin spectra

An example of a Brillouin spectrum from sea ice is shown in Fig. 4.7. The unshifted central component is about 2,500 times as intense as the longitudinal Brillouin component. This ratio, about typical for sea ice, was ten times greater than that obtained in Brillouin spectra from any other type of ice, reflecting the poor optical quality of the sample. The background count midway between adjacent unshifted components had an intensity per unit frequency about 130% of that due to Brillouin scattering at the peak of the longitudinal components. This count was due to stray scattered light leaking into the detection system, Raman scattering in ice and to the finite contrast of the triple-passed Fabry-Perot interferometer. The wings of the central component gave rise to a

Fig. 4.7. Representative Brillouin spectrum from sea ice. Spectrum recorded prior to changing interferometer from 3 pass to 5 pass mode of operation. The correspondence of Brillouin components with unshifted components (note inter-order overlap) is as indicated in Fig. 3.2. See text for further description of spectrum.

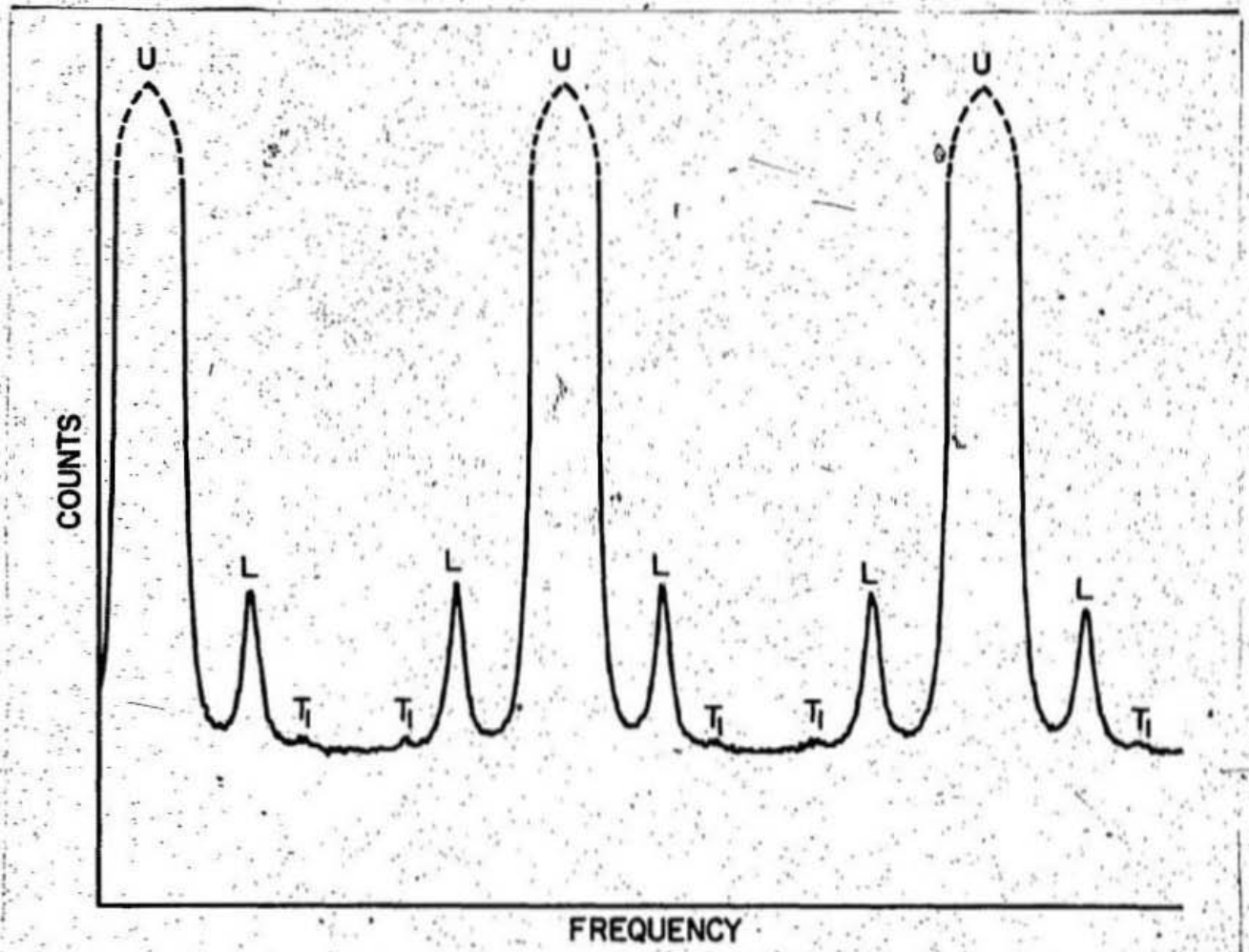

Fig. 4.7

significant curvature in the background spectrum in the neighbourhood of the Brillouin components, often making accurate frequency shift measurements difficult.

In most Brillouin spectra from sea ice, the linewidths of the spectral components were similar to those observed in Mendenhall ice and in artificial ice. In some cases, however, the longitudinal components were noticeably broadened. This effect was probably due to minor optical flaws in the region of scattering which diffused either the incident beam or the cone of scattered light capable of being received by the detecting optics. In either case, light scattered through an increased range of angles would reach the detecting optics giving rise (according to the Brillouin equation) to broadened components. Those spectra showing significantly broadened longitudinal components invariably possessed much lower than normal ratios of the intensity of the Brillouin peaks relative to the intensity of the unshifted scattered light. The instrumental and longitudinal linewidths in the spectrum shown in Fig. 4.7 are 0.26 GHz and 0.43 GHz, respectively.

A total of 23 Brillouin spectra of sea ice were obtained from two samples. The first sample mounted in the apparatus yielded one spectrum before being replaced due to excessive difficulty in obtaining subsequent spectra. Six spectra similar to that shown in Fig. 4.7 were then obtained from the second sample. For these spectra, the optical setup remained unchanged from the setup used for Mendenhall ice except that the 100 Å interference filter was removed from the path of the scattered light. Since a significant portion of the background originated from sources other than Raman scattering and

hence lay within the bandpass of the filter, the background reduction was not sufficient to compensate for the overall loss of scattered light intensity due to imperfect transmission.

The lengthy accumulation times (usually exceeding 24 hours) accompanied by poor resolution in the first seven spectra necessitated changes in both the optical setup and the data acquisition technique. To improve contrast and hence reduce background count in the subsequent spectra, the Fabry-Perot interferometer was switched from the three pass to the five pass mode of operation. Although this reduced the intensity of scattered light reaching the detector, it had the desirable effect of almost eliminating curvature from the background spectrum in the region usually occupied by the transverse Brillouin components. (Unless at least one transverse component was present, a Brillouin spectrum from sea ice could not be included in the analysis leading to the determination of the elastic constants.) In the three pass mode, background curvature often completely obscured the transverse components or made measurement of their frequency shifts very uncertain. As a result, spectra which in some cases represented more than 24 hours of accumulation time, had to be rejected.

The segmented time base feature of the DAS system was used to reduce the time required to obtain a suitable signal to noise ratio in the transverse components. The dwell time over a region of channels centred 3.26 GHz from the adjacent unshifted component, and having a width of 3.77 GHz, was increased by a factor of 30. This region invariably included a longitudinal Brillouin component and one or both transverse components, if resolvable.

Two problems necessitated special precautions in using the segmented time base. Firstly, the linear relation between multichannel analyzer channel number and the physical separation of the Fabry-Perot interferometer plates could be broken discontinuously at the beginning and at the end of the slowly scanned ramp segment. This effect was due presumably to a problem in the DAS electronics or to a variation in the response of the high voltage amplifier driving the piezoelectric elements in the Fabry-Perot interferometer. The effect resulted in a displacement of up to ten channels (0.3 GHz) in the position of peaks located within the slowly scanned region.

A second problem resulted from a slight consistent nonlinearity in the relation between channel number and Fabry-Perot plate separation. The effect of this nonlinearity was approximately cancelled out when frequency shift measurements of upshifted and downshifted Brillouin components in the same spectral order were averaged together. This averaging was not possible when components were resolved only once within an order. Hence, a systematic error in frequency shift measurements could result when measurements were made only within a short, asymmetrically positioned region of enhanced resolution as described above.

A Brillouin spectrum of sea ice demonstrating the effect of five pass operation of the interferometer and including a slowly scanned ramp segment is shown in Fig. 4.8. All sea ice spectra with the exception of the first seven were of this form. Ratios of the intensities of the spectral components were similar to those given for the spectrum shown in Fig. 4.7. About 80% of the total accumulation time was spent on the slowly scanned region of the spectrum.

Fig. 4.8. Representative Brillouin spectrum from sea ice. Spectrum recorded with interferometer in 5-pass mode of operation. Raised section was scanned 30 times more slowly than remaining portion of spectrum (see text for further description). The correspondence of Brillouin components with unshifted components (note inter-order overlap) is as indicated in Fig. 3.2.

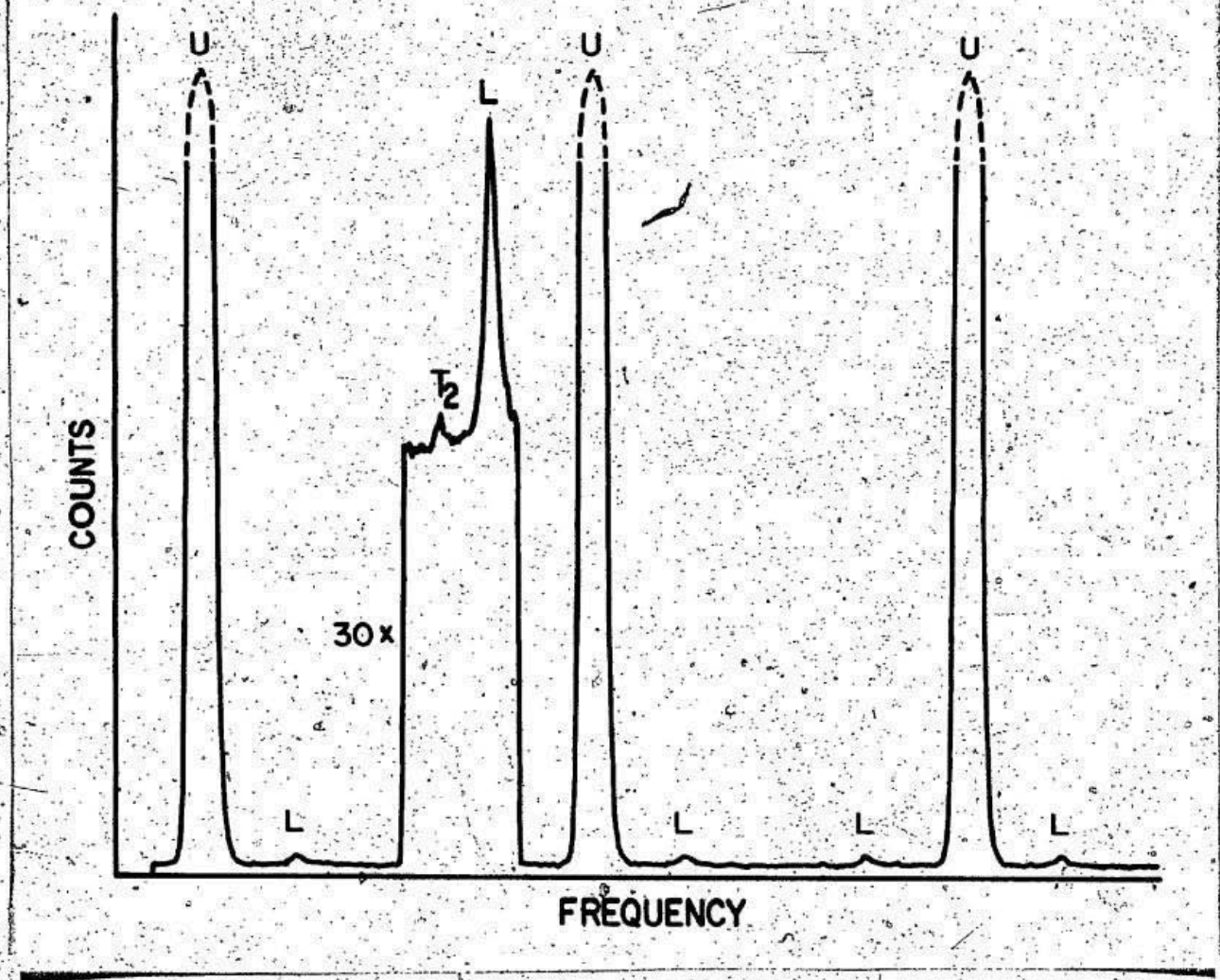

Fig. 4.8

Use of the segmented time base feature reduced by a factor of seven the time required to get a given signal strength for components lying within the region.

Frequency shift measurements from spectra incorporating the segmented time base feature were made in a manner which eliminated the two potential sources of systematic error mentioned previously. The frequency shift of the longitudinal Brillouin component was averaged from two measurements made in the order not including the slowly scanned region. The frequency shifts of the transverse components were then determined from the relative frequency separation of the longitudinal and transverse components appearing in the region of enhanced resolution. Hence the absolute positions of components within the slowly scanned region were not used. The uncertainty in transverse frequency shift measurements included both an uncertainty in relative frequency shift along with the uncertainty in absolute frequency shift of the longitudinal component. The error in relative frequency shift was typically small due to good resolution of the transverse components and the very high signal to noise ratio of the longitudinal component in the slowly scanned region. The overall error in frequency shift measurements was estimated to be ±1 channel or ±.03 GHz.

(iii) Elastic constants

Table 4.3 shows the data obtained from the 23 Brillouin spectra from sea ice. The table also shows simulated values for the angle γ determined from the Brillouin data along with frequency shift data converted to the format required for analysis via the computer

TABLE 4.3

BRILLOUIN SPECTROSCOPIC DATA FOR SEA ICE, -16°C

Brillouin Frequency Shifts (GHz)			$2\rho V^2 (10^8 N/m^2)$			
L	T_1	T_2	L^2	$T1^2$	$T2^2$	γ(deg.)
1st Crystal:						
14.006	-	6.651	277.09	-	60.86	76.7
2nd Crystal:						
13.775	6.913	-	268.02	67.50	-	59.4
13.592	6.758	-	260.95	64.51	-	47.3
13.893	6.910	-	272.63	67.44	-	65.3
13.952	6.904	-	274.95	67.33	-	68.2
13.867	6.619	7.522	271.61	61.88	79.92	32.3
13.539	6.771	-	258.92	64.76	-	47.5
13.663	6.760	-	263.68	64.55	-	46.2
13.747	6.756	-	266.93	64.47	-	38.7
13.804	6.658	7.667	269.15	62.61	83.03	35.5
13.927	6.955	-	273.97	68.33	-	67.1
14.068	6.976	-	279.55	68.74	-	74.5
13.663	6.840	-	263.68	66.08	-	50.8
13.981	6.942	-	276.10	68.07	-	69.8
14.013	6.691	7.367	277.36	63.24	76.66	27.0
13.945	-	6.759	274.68	-	64.53	72.4
14.035	6.942	-	278.36	68.07	-	72.5
13.927	-	6.991	273.97	-	69.03	69.1
13.709	6.764	7.843	265.46	64.62	86.89	42.2
13.618	6.837	-	261.95	66.03	-	48.8
14.028	-	6.831	277.96	-	65.91	73.5
13.981	-	6.867	276.10	-	66.61	71.9
13.916	-	7.079	273.54	-	70.78	67.8

program referred to in Chapter 2. The quantities L^2, $T1^2$ and $T2^2$ are squared frequency shift data incorporating the linear coefficients in the Brillouin equation. Their units match those of the elastic constants. Values for L^2, $T1^2$ and $T2^2$ are calculated by multiplying the squares at the respective Brillouin frequency shifts, Ω_L, Ω_{T1} and Ω_{T2} by $\rho\lambda^2/2n^2\sin^2(\alpha/2)$. These values were then substituted directly for X and Y defined as in equations (2-20) or (2-24) and hence were used in evaluating the sum squared error term, χ^2, defined in equations (2-25) and (2-27).

The 50 Brillouin frequency shift measurements indicated in Table 4.3 yielded 19 pairs and four triples of acoustic velocity measurements of the form described in Section 2.2. Each triple was broken down into three pairs which were individually weighted at 2/3 for inclusion in the determination of the elastic constants. All other pairs were given unit weight. The elastic constants were then calculated using the methods of Sec. 2.2.

Accurate values could not be obtained for either the density or the refractive index of sea ice. Hence the values were set equal to those used in the analysis of the Brillouin data from lake ice. The uncertainties in these values, along with the uncertainty in the scattering angle, which combined to total .4% in the case of lake ice, were neglected in the analysis of the sea ice data. The principal reasons for neglecting the systematic error included the difficulty in estimating its value and the fact that it was likely negligible when compared with the errors in the individual elastic constants.

The elastic constants determined for local, apparently homogeneous regions of ice within a sea ice sample are given below:

$$\left.\begin{aligned} c_{11} &= 142.7 \pm 4.8\% \\ c_{12} &= 73.2 \pm 6.9\% \\ c_{13} &= 59.5 \pm 2.5\% \\ c_{33} &= 147.4 \pm 1.4\% \\ c_{44} &= 29.8 \pm 1.7\% \end{aligned}\right\} \times 10^8 \text{ N/m}^2$$

The quoted uncertainties were calculated numerically since an analytic determination of the propagation of error through the transformations given in Sec. 2.2 was inherently complex and lay outside the scope of the present work.

The numerical error calculation was based on 25 computer simulated repetitions of the process of determining the elastic constants. In each repetition, a normally distributed random number with mean zero and standard deviation ± .03 GHz was added to each of the 50 frequency shift measurements listed in Table 4.3. The uncertainty in an individual elastic constant was then taken to be the square root of the empirical second moment about the mean of the set of 25 determinations of that elastic constant. The numerical error analysis not only yielded estimates for the standard deviations, but also yielded further information on the probability distributions of the values for the elastic constants. In particular, a significant statistical bias in the estimates for each of three of the elastic constants was noted. The mean of the set of 25 determinations of c_{11} was 6% higher than the least squares value for c_{11}. Similarly, the mean for c_{12} was 8% high, the mean for c_{33} was 2% low, while the means for c_{13} and c_{44} were not significantly biased.

The above results imply that the transformations used in calculating the elastic constants translate unbiased error in sound velocity measurements into biased expectation values for the final results. More specifically, the values determined for c_{11} and c_{12} are likely to be high, the value determined for c_{33} is likely to be low while the expected values of c_{13} and c_{44} are likely unbiased. These observations should be noted when comparing the elastic constants determined for sea ice with those determined for the fresh water ice samples where knowledge of crystal orientation obviated the need for application of the methods of Sec. 2.2. While the method of analysis of the fresh water ice data may also have induced bias in the expectation values for the elastic constants, the effect would undoubtedly be much less severe than in the present instance. It was not considered practical to duplicate the above described error analysis for the fresh water ice data due to the slowness of execution of the required least squares fit routine and the consequent utilization of very large amounts of computer time.

Fig. 4.9 shows the Brillouin frequency shift vs. γ curves specified by the elastic constants determined for sea ice. To facilitate plotting of the experimental data in the same format used for the fresh water ice samples, simulated values for γ were assigned to each frequency shift measurement. The γ values were calculated by equation (2-15) from pairs of acoustic velocities satisfying equation (2-20) or equation (2-24). The pairs were determined from the experimental data by choosing points along the curves specified by (2-20) or (2-24) having minimum distance from the measured velocity pairs.

Fig. 4.9. Brillouin frequency shift versus synthesized γ values for sea ice at -16°C. Heights of vertical bars indicate standard deviation. Curves identified as in Fig. 3.3.

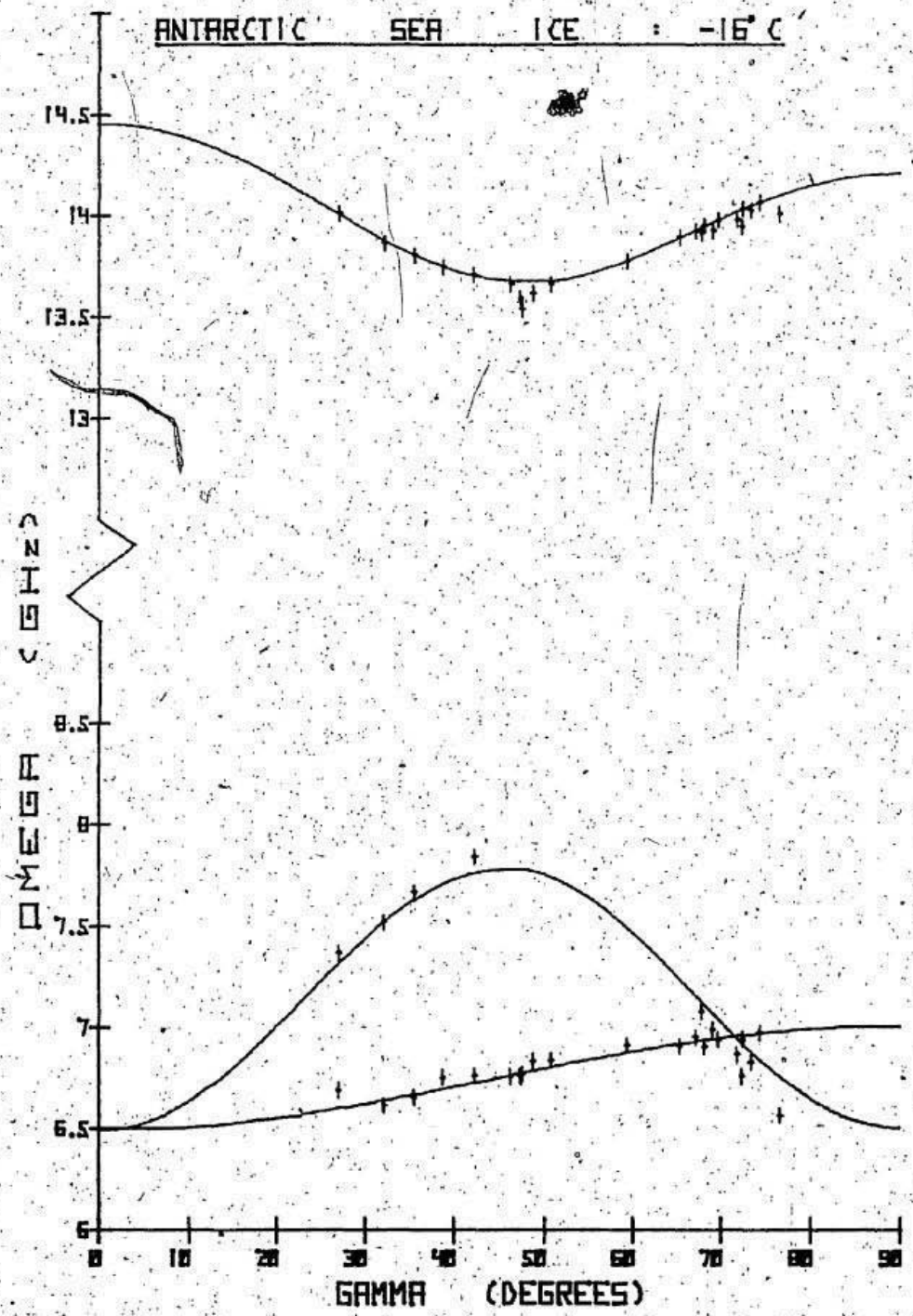
ANTARCTIC SEA ICE : -16° C
14.5
14
13.5
13
8.5
8
7.5
7
6.5
6
OMEGA (GHz)
0
10
20
30
40
50
60
70
80
90
GAMMA (DEGREES)

Fig. 4.9

The distribution of the data over values of the angle γ was fairly good, especially in view of the fact that prior knowledge of crystal orientation could not be used as a guide in selecting desirable angles of rotation of the sample about the vertical axis of the sample housing. The γ values obtained were to a large extent random, but some selection was achieved by rejecting Brillouin spectra which appeared, after a short period of accumulation, to be duplicating existing data. As well, in come cases γ could be varied in a controlled manner over a range as wide as 20^{o} by turning the sample by small amounts about the vertical axis. So long as the scattering volume remained within one crystallite, γ varied continuously with the angle of rotation.

(iv) Inclusions and grain boundaries

Limitations on the duration of the Brillouin experiment on sea ice made it impractical to extend the objectives beyond obtaining values for the elastic constants in local homogeneous regions. Hence no special effort was made to observe Brillouin scattering from brine inclusions or from crystal grain boundaries.

The Brillouin frequency shift for the longitudinal acoustic mode in water was about 50% of the free spectral range of the interferometer. The relatively intense Brillouin component from water would thus lie in a region of minimum background and would probably be observed on a Brillouin spectrum from sea ice if a brine inclusion were to inadvertently coincide with the scattering volume. No such component was observed in any of the 23 Brillouin spectra obtained.

Aside from the possibility that brine inclusions were very few or nonexistent within the sample, two explanations appear

reasonable. Firstly, brine inclusions might cause dispersal of the incident beam to the extent that no Brillouin spectrum whatsoever would be observable. Secondly, the inclusions might absorb some portion of the incident laser radiation. Since brine cells are in precise equilibrium with the surrounding ice, slight warming accompanied by a thermal gradient could lead both to enlargement of the cells and to their migration in the direction of increasing temperature. Hence, a brine cell might be expected to migrate along the incident beam, towards the beam source, since the light behind the inclusion would be diffused and therefore less able to induce significant heating by absorption.

Evidence suggesting the occurrence of the above phenomenon was provided in many instances by spectra which, after accumulating for a few minutes or hours, suddenly showed very large increases in the intensity of the unshifted component. This increase in stray scattering was attributed to the appearance of an optical flaw within the scattering volume. When the volume of observed scattering was moved a fraction of a millimetre lower, towards the point at which the beam entered the sample, normal levels of unshifted scattering resumed. However, in several instances the high levels of stray scattering reappeared after a few hours, necessitating further lowering of the region of observation.

The incident laser power used in obtaining the Brillouin spectra of sea ice was 100 mW. A lower laser power level or a defocusing of the incident beam might have eliminated the effect described above and permitted observation of Brillouin scattering from brine inclusions. However, the resultant increase in required

accumulation time along with problems stemming from insufficient light for the Fabry-Perot stabilization system made such changes impractical. The laser power used in the work with glacial ice and lake ice was 200 mW. In no case was this power level observed to induce any optical flaws in the samples.

Crystal grain boundaries undoubtedly existed near the scattering volumes corresponding to several of the Brillouin spectra from sea ice. If a grain boundary were to traverse the scattering volume, broadened or twinned longitudinal components would result in most cases. Furthermore, the peak intensity of the longitudinal component relative to the background would be reduced and an asymmetry in the upshifted relative to the downshifted components could appear (see Chapter 5). Each of the above noted effects, including asymmetry, was observed from time to time in Brillouin spectra from sea ice. In these cases spectral accumulation was terminated and data was not used in the determination of the elastic constants.

CHAPTER 5

BRILLOUIN SPECTROSCOPIC STUDIES OF A CRYSTAL GRAIN BOUNDARY REGION IN NATURAL ICE*

5.1 Introductory Remarks

The grain boundary studies reported here were not initially foreseen as comprising part of the overall objectives of the present work, but rather were undertaken when an unexpected feature was observed in a Brillouin spectrum emanating from the boundary region in a bicrystalline ice sample. The primary aim of the subsequent investigation was to substantiate the anomalous character of the initial observations and to provide experimental details of the phenomenon which might assist in a future comprehensive theoretical or experimental analysis. Unlike the work discussed in the previous chapters, determination of elastic constants was not an objective of the grain boundary studies.

5.2 Physical and Crystallographic Description of Bicrystalline Sample

The ice sample used in the grain boundary experiment was taken from a 5 kg bulk sample of polycrystalline river ice from Arnold's Cove Brook on the Isthmus of Avalon about 150 km from St. John's, Newfoundland. The bulk sample was chopped from the 30 cm thick ice cover near the centre of the brook about 0.5 km from its

---

*A synopsis of this chapter has been published.[79]

mouth. An approximate half metre tidal variation in the depth of the brook occurred at the point where the sample was collected. The temperature at the time of collection was about -20°C and the sample was not exposed to temperatures higher than -16°C at any time prior to completion of the Brillouin experiments. Extensive massive fractures in the ice cover near the point at which the sample was collected along with frequent audible cracking indicated high stress in the surrounding ice. The stress likely resulted from the strong current beneath the ice, combined with the restraining effect of numerous large protruding boulders in the stream bed. The results of a water analysis of a 1 litre filtered sample of meltwater from the bulk ice sample are shown in Table 5.1.

Several chip samples extracted from the bulk sample of river ice showed polycrystalline grain structure when visually inspected through crossed polaroid filters and showed disruption of the individual grains when checked by Laue x-ray photography. Air bubbles and small particulate inclusions were present in some samples, but those samples extracted from near the bottom (ice-water interface) of the bulk sample were of excellent optical quality. The ~0.5g sample selected for Brillouin spectroscopy was among those taken from near the bottom of the bulk sample and possessed no visible optical flaws. Inspection of the selected sample through crossed polaroid filters showed two crystal grains, each comprising about 50% of the sample volume. The boundary between the grains appeared perfectly flat and uniform.

When mounting the sample for Brillouin spectroscopy, care was taken to ensure that the boundary was as nearly as possible normal

TABLE 5.1

ANALYSIS OF MELTWATER FROM BULK ICE SAMPLE FROM ARNOLD'S COVE BROOK

Conductivity		8.64×10^{-3} $(\Omega m)^{-1}$
pH		6.88
Impurity Concentrations in ppm by Weight	Na^+	13.19
	Cl^-	20
	Ca^{++}	1.13
	SO_4^{--}	5
	Mg^{++}	.80
	Mn	.01
	Fe	.14
	K^+	.60
	NH_4^+	.051
	F^-	.01
	NO_3^-	.005

to the axis of rotation of the sample housing and hence, to the incident laser beam. The original intention of this alignment was to reduce the range of sample positions at which the x-ray beam used for Laue photography would traverse both crystal grains. However, as the Brillouin experiment proceeded, it became apparent that the principal advantage of the horizontal boundary lay in the ease with which the region of observation could be moved across the boundary by adjusting the height of the sample. The exact orientation of the boundary in the mounted sample could not be determined without apparatus and techniques beyond those required for the regular course of the Brillouin experiments. Hence, based only on the observations through crossed polaroid filters, its normal was estimated to make an angle of $0^{\circ} \pm 15^{\circ}$ with the incident laser beam. The high uncertainty was due to the small linear dimensions of the boundary as well as to ambiguity resulting from the dependence of visual observations on sample orientation and position relative to the eye.

Laue x-ray diffraction photographs were taken to determine the orientation of the two crystal grains comprising the sample and to look for evidence of disruption of the grains or of the ice at the grain boundary. Three of the photographs are shown in Fig. 4.3. No evidence of disruption either in the crystal grains or at the grain boundary was present. This contrasted with three other chips from the bulk sample, each of which showed grain disruption.

Precise orientations for both monocrystals in the bicrystalline ice sample were calculated from Laue photographs taken at three different orientations of the bicrystal. The different orientations were obtained by rotating the sample about the vertical axis of the

sample housing. At each orientation, a series of Brillouin spectra and associated Laue photographs was taken, with each spectrum/photograph corresponding to a different height of the scattering volume (or x-ray beam) relative to the grain boundary. Photographs taken with the incident x-ray beam entirely above or below the boundary served to identify those Laue spots corresponding to crystal planes of the upper or lower monocrystals respectively. A photograph taken with the grain boundary approximately bisecting the cross-section of the incident beam was then interpreted using the methods of Chapter 2 to yield simultaneous orientations for both the upper and lower monocrystals.

Table 5.2 lists the Euler angles for both the upper and lower monocrystals at each of the three orientations of the bicrystal. Values for the angles γ between the c axes of the respective monocrystals and the propagation direction of phonons giving rise to observable Brillouin scattering are also listed. The values shown for the longitudinal Brillouin frequency shifts were calculated from the γ values using elastic constants which were taken to be the arithmetic means of the respective elastic constants quoted in Sec. 5.4 and Sec. 6.2 for artificial ice, Mendenhall ice, lake ice and sea ice at $-16^{\circ}C$. Density, refractive index and scattering angle were each assumed to match values quoted in Sec. 4.6 in connection with the analysis of the lake ice data. The above assumptions were substantiated by subsequent analysis of the Brillouin spectra (see following section).

The angles of rotation of the bicrystal were selected, based on the initial x-ray determination of the orientations of the

TABLE 5.2

ORIENTATIONS OF UPPER AND LOWER MONOCRYSTALLINE COMPONENTS OF BICRYSTALLINE ICE SAMPLE AND CORRESPONDING LONGITUDINAL BRILLOUIN FREQUENCY SHIFTS, Ω

Spectrum Series #		1	2	3
Upper Crystal Euler angles	ϕ_u	87.14°	23.37°	198.42°
	θ_u	19.07°	14.65°	14.32°
	ψ_u	337.53°	325.23°	350.24°
	γ_u	47.17°	31.97°	58.72°
	Ω_u (GHz)	13.619	13.930	13.654
Lower Crystal Euler angles	ϕ_l	239.04°	163.64°	5.01°
	θ_l	71.13°	76.17°	74.97°
	ψ_l	77.99°	78.66°	71.53°
	γ_l	83.37°	60.67°	30.27°
	Ω_l (GHz)	14.012	13.680	13.981

Note: Subscripts u and l denote the upper and lower monocrystals respectively.

monocrystals in the mounted sample, to yield a near maximum difference in frequency shift between the observed longitudinal Brillouin components from the upper and the lower monocrystals. Hence, phonons giving rise to observed Brillouin scattering at each of the three bicrystal orientations underwent substantial changes in velocity upon crossing the boundary. The distinct difference in frequency shift aided in establishing the location of the region of observation relative to the boundary and simplified the decomposition of Brillouin spectra from the boundary region. Fig. 5.1 shows the γ values and corresponding calculated Brillouin frequency shifts of the longitudinal component in the upper and lower monocrystals at each of the three sample orientations.

The relative orientation of the two monocrystals was determined four times from four independent sets of Laue data. Three of the determinations utilized the orientational data given in Table 5.2 while the fourth determination was based on Laue data not correlated with Brillouin spectra and hence not tabulated. The relative orientation was calculated from the lab-to-crystal rotation matrices, R, as defined in equation (2-6), for the upper and lower monocrystals. The relative rotation matrix, R_{rel}, is given by

$$R_{rel} = R_l R_u^{\dagger} \tag{5-1}$$

where R_u and R_l denote the lab-to-crystal rotation matrices for the upper and lower monocrystals respectively. The matrix R_{rel} defined by (5-1) transforms a fixed vector expressed in the coordinates of the upper crystal frame of reference into coordinates referred to the lower crystal frame of reference. Euler angles can be used to

Fig. 5.1. Frequency shift versus γ for longitudinal Brillouin component in ice at -16°C. Curve determined by mean elastic constants quoted in text (Sec. 5.4). Symbols mark γ values and corresponding longitudinal Brillouin frequency shifts in upper and lower monocrystals comprising bicrystalline sample. Spectrum series numbers 1, 2 and 3 refer to orientations of the bicrystal (see Table 5.2) while u and l refer to scattering in the upper and lower monocrystals respectively.

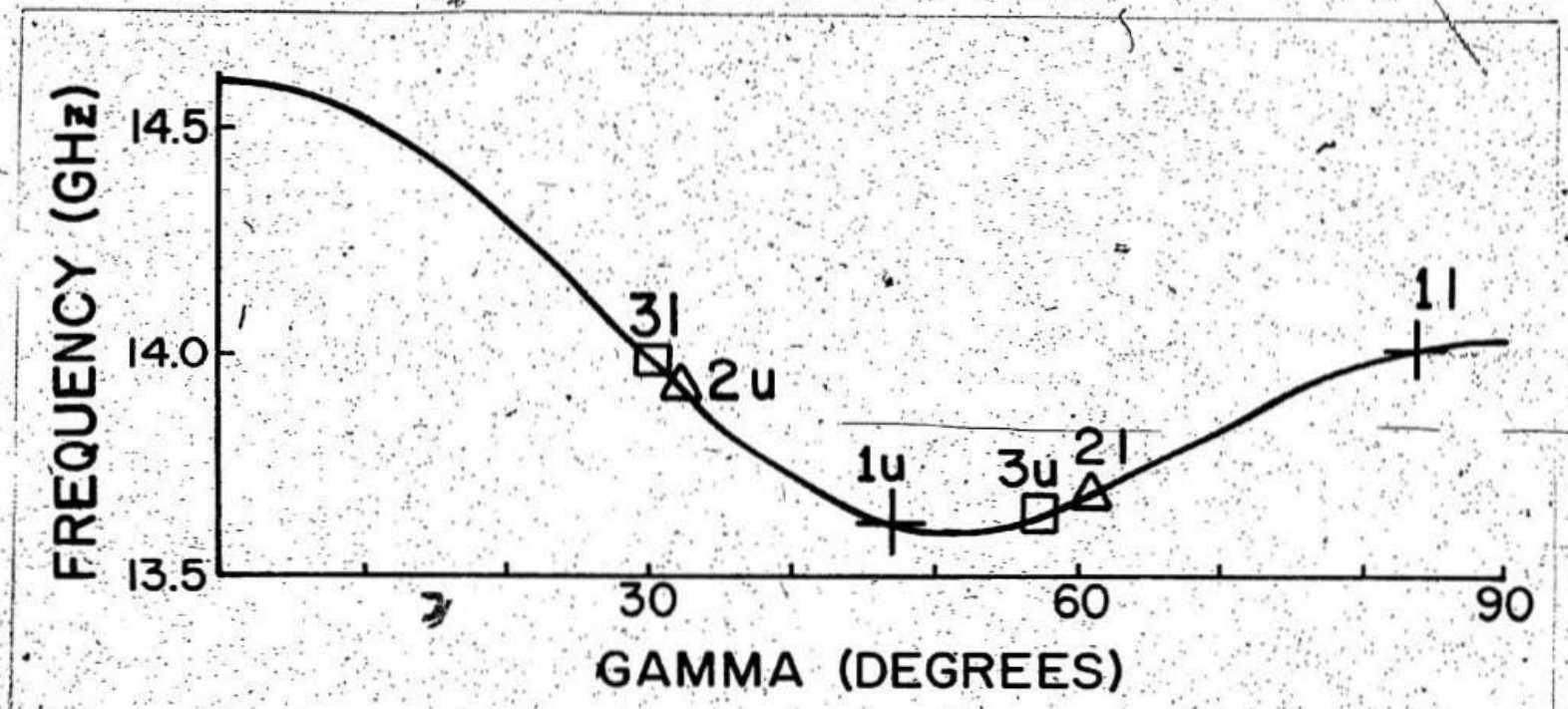
FREQUENCY (GHz)
14.5
14.0
13.5
30
60
90
GAMMA (DEGREES)
3l
2u
1u
3u
2l
1l

Fig. 5.1

parameterize R_{rel} according to the same formulation by which the individual lab-to-crystal rotation matrices for the monocrystals are parameterized.

Accordingly, the Euler angles specifying the four determinations of R_{rel} are given in Table 5.3. The small scatter in the Euler angle values indicates an uncertainty of less than $.5^{o}$ in the determination of crystal orientation. Calculations using the mean Euler angles, specifying R_{rel} show that the basal planes of the two monocrystals are approximately perpendicular, making an angle of 88.2^{o} with one another. Similarly, the $(\bar{1}\,2\,0)$ plane of the upper crystal makes an angle of 4.0^{o} with the basal plane of the lower crystal while the basal plane of the upper crystal makes an angle of 2.7^{o} with the $(2\,\bar{1}\,0)$ plane of the lower crystal. If the latter two angles were both 0^{o}, the two monocrystals would possess parallel low order crystallographic planes. This could be interpreted as indicating twinning, that is, crystal growth at a preferred relative orientation.[80] Setting the two angles equal to 0^{o} yields a relative rotation matrix specified by the Euler angles $\phi = 180^{o}$, $\theta = 90^{o}$ and $\psi = 70.9^{o}$. While these values differ from the corresponding average values given in Table 5.3 by an amount in excess of probable uncertainty, their proximity suggests that some degree of preferential orientation of the monocrystals was induced during growth of the sample.

Since the orientation of the plane of the grain boundary could not be determined precisely, correlation of the boundary with particular crystallographic planes is highly uncertain. However, coincidence of the boundary plane with the basal plane of the upper crystal or the nearly parallel $(2\,\bar{1}\,0)$ plane of the lower crystal is

TABLE 5.3

FOUR DETERMINATIONS OF EULER ANGLES SPECIFYING RELATIVE ROTATION MATRIX FOR BICRYSTALLINE SAMPLE

Determination #		1	2	3	4	Mean
Euler Angles*	ϕ	176.0	176.4	176.8	176.5	176.4
	θ	88.1	87.6	88.9	88.2	88.2
	ψ	69.1	69.4	68.2	69.0	68.9

a plausible assumption. The normals to these crystallographic planes made angles in the neighbourhood of 15° with the vertical and hence lay within the region of uncertainty in the boundary orientation. A careful visual check to test the above assumption was planned upon conclusion of the Brillouin experiments but failure of the sample cooling system and subsequent melting of the sample made this impossible.

5.3 Dimensions of Region of Observation

The optical system used for the Brillouin spectroscopic grain boundary studies was identical to that used in the work on lake ice (Sec. 4.4) in all respects except for the glass plate used to control the level of the region of observation in the sample. The 2 mm thick glass plate was replaced with a microscope cover slip having a measured thickness of .24 mm and a refractive index of 1.52. This thin plate was rotated by measured amounts to yield precise adjustments in the height of the region of observation relative to the crystal grain boundary.

The finite-sized region of observation in the sample was defined by the focal spot of the lens (focal length = 40 cm) used to collimate the scattered light incident on the interferometer. Since all apertures in the collecting optics were circular, the region of observation could be assumed to be of circular cross-section if the dimensions of the illuminated region in the sample exceeded the diameter of the focal spot of the collimating lens. Translation of the incident beam during spectral accumulation indicated that the beam width was approximately .3 mm. This value exceeded that estimated below for the diameter of the region of observation.

Three Brillouin spectra from the grain boundary region were used in estimating the diameter of the region of observation. The ratio of the intensity of the component attributed to longitudinal Brillouin scattering in the upper crystal to the analogous scattering intensity from the lower crystal was assumed proportional to the area ratio of the portions of the region of observation lying above and below the boundary respectively. Hence, three area ratios were estimated from the three Brillouin spectra. These area ratios were then correlated with the relative heights of the region of observation as determined from the angles of rotation of the thin glass plate in the path of the scattered light. The resultant estimate for the diameter of the region of observation was .21 mm. The validity of the calculations depended (a) on the grain boundary having negligible width relative to .21 mm and (b) on the longitudinal Brillouin components having a fundamental intensity which did not vary with proximity to the boundary. The former assumption is substantiated by data presented in the following sections while the latter is less definite but appears to be in reasonable agreement with observations.

5.4 Brillouin Spectra

(i) Adjustments and calibration

The initial three Brillouin spectra obtained from the bi-crystalline river ice sample did not include the grain boundary within their regions of observation. The spectra had appearances closely resembling those of the Mendenhall ice spectra or the lake ice spectra. Measured frequency shifts, when correlated with crystal

orientation, lay within experimental uncertainty of the Ω vs. γ curves specified by the elastic constants determined for glacial ice or lake ice or for artificial ice corrected to $-16^{\circ}C$ (see Chapter 6 regarding similarity of elastic properties of the various types of ice). Hence, rather than undertake a complete determination of the elastic moduli of the river ice sample, the elastic properties were assumed to be specified by the average of the four previous Brillouin determinations of the elastic moduli of ice. Accordingly, from data quoted in Table 6.3 (Sec. 6.2) the elastic constants of monocrystalline river ice were taken to be:

$$\left.\begin{aligned} c_{11} &= 139.29 \\ c_{12} &= 70.82 \\ c_{13} &= 57.65 \\ c_{33} &= 150.10 \\ c_{44} &= 30.14 \end{aligned}\right\} \times 10^{8}\ N/m^{2}$$

The fourth Brillouin spectrum of the bicrystalline sample was obtained from a region of observation roughly centred on the grain boundary. The bicrystal was at the orientation indicated for spectrum series 1 in Table 5.2. Since Brillouin scattering by longitudinal phonons propagating in the upper monocrystal was observed simultaneously with Brillouin scattering by longitudinal phonons in the lower monocrystal, the resultant spectral components were twinned (see Fig. 5.2). The frequency shift difference between the respective upper and lower crystal longitudinal components was anticipated from the data in Table 5.2 to be 0.393 GHz. This corresponded to a separation of 14 channels between the peaks of the adjacent twinned longitudinal

components in the three order Brillouin spectrum with the same inter-order spacing as for glacial ice and lake ice.

While the expected separation between the twinned longitudinal Brillouin components was observed in the pair lying to the right of the adjacent unshifted component and corresponding to upshifted Brillouin scattering, the downshifted components lying to the left of the central peak appeared too closely spaced. The difference in apparent relative spacing between the upshifted and downshifted pairs of longitudinal Brillouin components gave rise to an unexpected but clearly observable shift asymmetry in the Brillouin spectrum.

To improve resolution of the twinned longitudinal components and thereby make the asymmetry more visible, the scanning range of the Fabry-Perot interferometer plates was reduced by lowering the amplitude of the ramp waveform used to drive the piezoelectric elements. In this way, a two order Brillouin spectrum was recorded with one order of the unshifted component occurring near each end of the range of 1024 channels forming the horizontal base of the multichannel analyzer display. The resulting spectrum showed features identical to those observed in the three order spectrum but the components were distributed over twice as many channels and thus could be resolved in more detail. The difference in separation of the upshifted and downshifted longitudinal component pairs was distinct, with the more widely spaced upshifted pair appearing on the left-hand side of the spectrum.

A further reduction in ramp amplitude was required in order to expand the spectrum sufficiently to facilitate the decomposition and detailed analysis of the twinned longitudinal Brillouin

components. Accordingly, the scanning range of the interferometer plates was reduced to yield a single order spectrum with components distributed over 3.8 times as many channels as was the case for the original three order spectra. Further expansion was not possible if both upshifted and downshifted longitudinal components were to be observed on the spectrum simultaneously. Thus, the ramp amplitude was not readjusted throughout the remainder of the experiment. The more widely spaced upshifted longitudinal component pair occurred on the right-hand side of the single order spectrum since the unshifted component was approximately centred in the range of channels. This contrasted with the two order spectrum and ruled out the possibility that nonlinearity in the scanning of the interferometer plates might be responsible for the observed asymmetry.

The usual multiple-order Brillouin spectrum incorporates its own frequency standard since the number of channels separating adjacent orders of the unshifted component corresponds to a known frequency range (i.e., the free spectral range), but no analogous standard exists in single order spectra. A frequency standard for the single order grain boundary spectra was thus established by using Brillouin frequency shifts as references. At each of the three previously indicated orientations of the bicrystal, Brillouin spectra were recorded with the region of observation lying first in the upper monocrystal, at least 1 mm above the grain boundary and then in the lower monocrystal at least 1 mm below the boundary. The reference frequency shifts for the longitudinal components were taken from Table 5.2. Due to slight nonlinearity in the relationship between MCA channel number and physical separation of the interferometer

plates, separate frequency standards were calculated for the upshifted and downshifted Brillouin components. On the left-hand (downshift) side of the spectrum, 1 GHz was found to correspond to 131.69 ± .17 channels, based on six Brillouin spectra. Similarly, an average from the six spectra indicated that 1 GHz corresponded to 130.45 ± .29 channels on the right-hand (upshift) side of the spectrum. The small scatter in the determinations showed that scattering angle and ramp amplitude, while possibly varying slightly from spectrum to spectrum, were very nearly constant throughout the experiment. As well, the dependence of longitudinal Brillouin frequency shift on orientation was seen to be accurately specified by the assumed elastic constants.

(ii) Observations

Three Brillouin spectra from the grain boundary region of the bicrystalline ice sample are shown in Fig. 5.2. The method by which these and other spectra associated with the grain boundary experiment were transferred from the DAS memory for storage, analysis and graphical reproduction is discussed in Sec. 5.5. The three spectra correspond to the three bicrystal orientations listed in Table 5.2 and illustrate both the difference in apparent separation between the upshifted and downshifted longitudinal component pairs and the dependence of this asymmetry on crystal orientation. In particular, it should be noted that at orientation numbers 1 and 3, the upshifted pair ~~is~~ more widely spaced while the downshifted pair is more widely spaced at orientation number 2. With the exception of the bicrystal orientation and the angle of the tilted glass plate which controlled the height of the region of observation, no changes in the optical

Fig. 5.2. Series of spectra showing effect of changes in orientation of ice bicrystal on observed asymmetry in longitudinal component pairs. At series 2 orientation, downshifted (left hand side of spectrum) longitudinal lines show greater frequency shift difference while upshifted lines are more widely spaced at series 1 and series 3 orientations. Only height of region of observation and bicrystal orientation differ among the three spectra. Reference lines u and l show frequency shifts of components, measured far from the boundary in the upper and lower monocrystals, respectively. Central component located at channel 549. 1 channel = .00763 GHz.

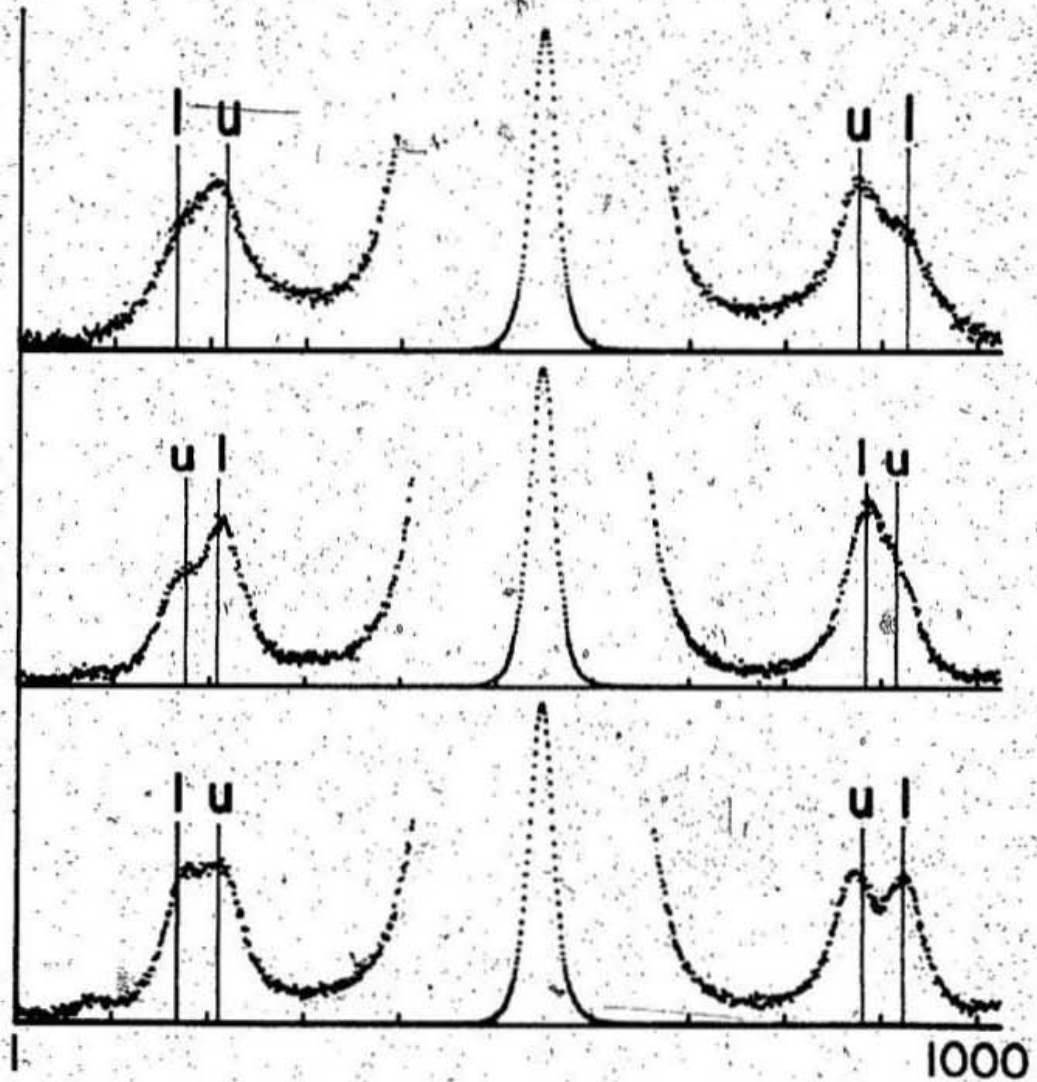
SERIES 1
γ_u = 47.2°
γ_l = 83.4°
SERIES 2
γ_u = 32.0°
γ_l = 60.7°
SERIES 3
γ_u = 58.7°
γ_l = 30.3°
l u
u l
1
1000
FREQUENCY (CHANNELS)

Fig. 5.2

system or any other component of the experimental setup were made between recordings of the three spectra. The orientational dependence of the asymmetry in the boundary spectra along with the dependence of the asymmetry on the proximity of the region of observation to the boundary (to be discussed following) provide definite evidence that the effect is not instrumental.

Fig. 5.3 shows a series of six Brillouin spectra recorded with the bicrystal at orientation number 3. The two reference spectra obtained with the region of observation far from the boundary show symmetrically matched upshifted and downshifted longitudinal Brillouin components. In contrast, the four spectra from the boundary region show distinctly wider spacing between the longitudinal components on the upshifted side of the spectrum. The individual components associated with longitudinal sound propagating in the upper and lower monocrystals are seen to maintain their identities in the boundary region spectra. This indicates that the merging of acoustic properties from those of one monocrystal into those of the other takes place on a scale which is small compared to the diameter of the region of observation.

The Brillouin spectra shown in Fig. 5.3 were underlain by a flat background component due primarily to Raman scattering and having an intensity per unit frequency about twice that due to Brillouin scattering at the peak of the longitudinal components. This ratio was roughly maintained in the spectra emanating from the boundary region when the effect of the split region of observation was taken into consideration. Thus, it appeared that no major changes in the fundamental intensity of Brillouin scattering were

Fig. 5.3: Brillouin spectra obtained with the ice bicrystal at orientation No. 3 and with the region of observation at six different heights relative to the grain boundary. Schematic diagrams at left show heights. Diameter of region of observation (circle) is .21 mm. Distance from centre of region to boundary centre (in mm) is indicated by number to right of diagram. Reference spectra No.'s 1 and 6, obtained relatively far from the boundary in the upper and lower monocrystals respectively. Central component located at channel 549. 1 channel = .00763 GHz.

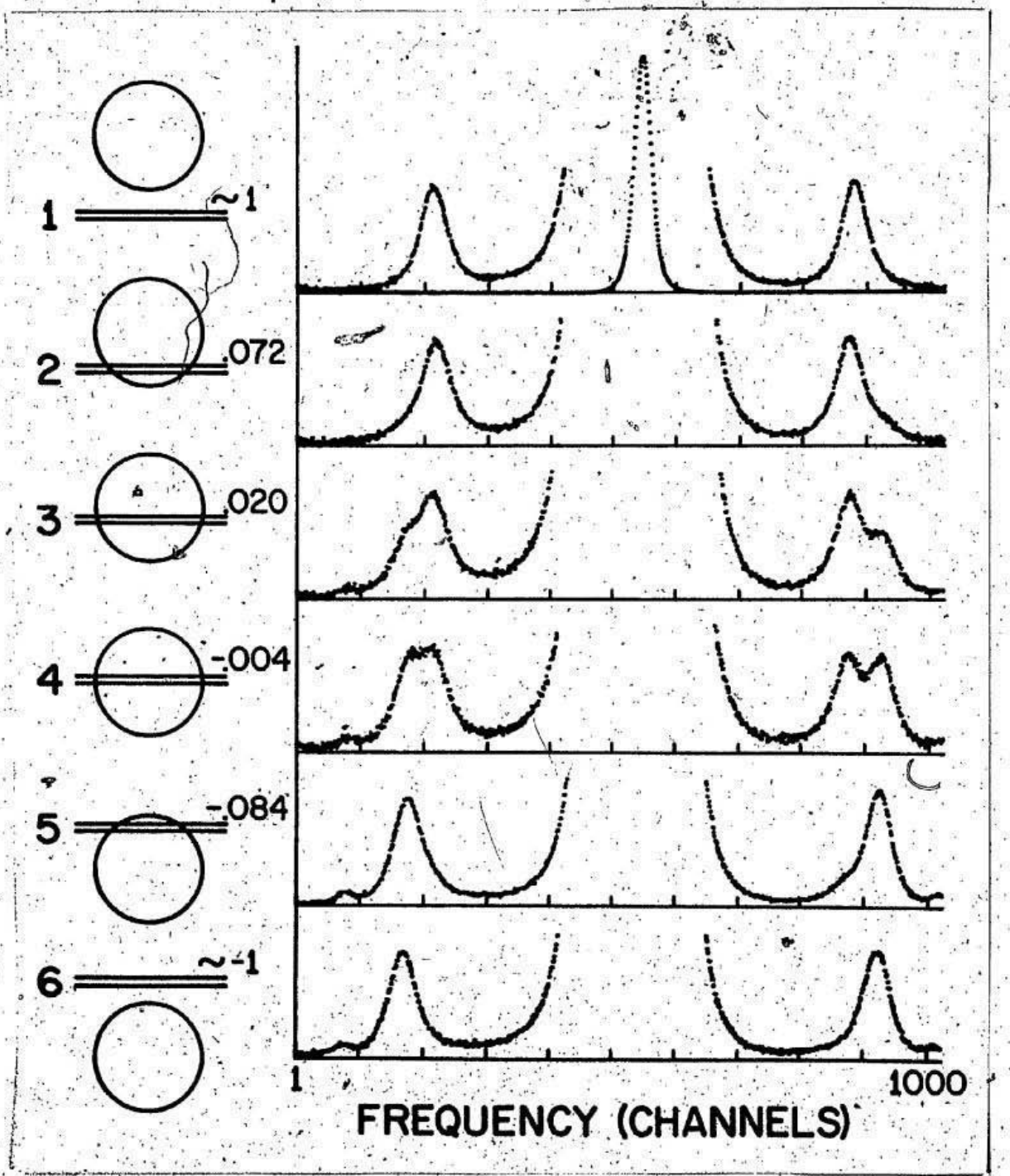

Fig. 5.3

associated with proximity to the grain boundary.

A slight asymmetry in the wings of the upshifted component was visible in all of the Brillouin spectra obtained from the river ice sample. This asymmetry also occurred in the spectra from other types of ice and appeared to result from slight imperfections in the alignment of the various components of the collecting optics and from asymmetry of scattering volume illumination. No alignment procedure was sufficiently precise to completely eliminate the asymmetry. However, its consistent effect of slightly raising the background on the downshift side of the central component did not significantly impede interpretation of the Brillouin spectra.

5.5 Analysis

A total of 15 very high resolution Brillouin spectra of the type illustrated in Fig. 5.2 and Fig. 5.3 were obtained from the bicrystalline river ice sample at three orientations. These spectra, with accumulation times ranging between one and six days possessed sufficiently high signal to noise ratios to permit decomposition and detailed analysis of the merged longitudinal Brillouin components. To facilitate this analysis the spectral data were transferred in digital form from the MCA of the DAS unit to an HP 9825 electronic calculator (microcomputer). Since no interface between the machines was available, the required 15,360 MCA channel count values for the 15 spectra were transferred manually with the aid of a dictaphone or telephone. Once transferred, the data were stored on magnetic tape for future analysis and graphical reproduction via the plotter associated with the 9825 system.

Compositions of spectra stored on the HP 9825 calculator were used both to compare boundary region spectra with equivalent spectra obtained far from the boundary and to investigate the potential effect of shrinking the region of observation in the grain boundary spectra. Two series of composed spectra corresponding to bicrystal orientation numbers 2 and 3 are shown in Fig. 5.4 and Fig. 5.5 respectively. The first spectrum in each series is a composite of the two spectra obtained with regions of observation in the upper and lower monocrystals at least 1 mm from the grain boundary. Each of these composite spectra illustrates the expected appearance of a Brillouin spectrum having a region of observation that, while centred on the grain boundary, was so large that any localized effects associated with the boundary were negligible. No significant asymmetry in the paired longitudinal components is visible in either of these spectra.

The composite spectra from the boundary region illustrated in Fig. 5.5 show asymmetry which tends to increase as the effective region of observation is localized in the neighbourhood of the grain boundary. A very substantially reduced diameter for the region of observation might yield a spectrum resembling that shown as number 4 in the series. This composite spectrum indicates the effect of eliminating the component of light scattered by portions of the upper and lower monocrystals lying far from the boundary. The spectrum was formed by subtracting the far-from-boundary composite spectrum number 1 from the near-boundary spectrum number 3. Before subtraction the spectra were normalized such that no portion of the resultant composite spectrum dipped below the baseline determined by the

Fig. 5.4. Composite spectra formed from linear combinations of Brillouin spectra in series 2. Unshaded portions of schematic diagrams at left show regions of observation. Two spectra recorded with regions of observation far from the grain boundary are composed to yield spectrum 1. Two spectra recorded with regions of observation overlapping the grain boundary are composed to yield spectrum 2. Spectrum 1 is subtracted from spectrum 2 to yield spectrum 3 thereby simulating the effect of physical reduction of the size of the region of observation (see text). Reference lines u and l show frequency shifts of longitudinal Brillouin components, far from the boundary, in the upper and lower monocrystals respectively.

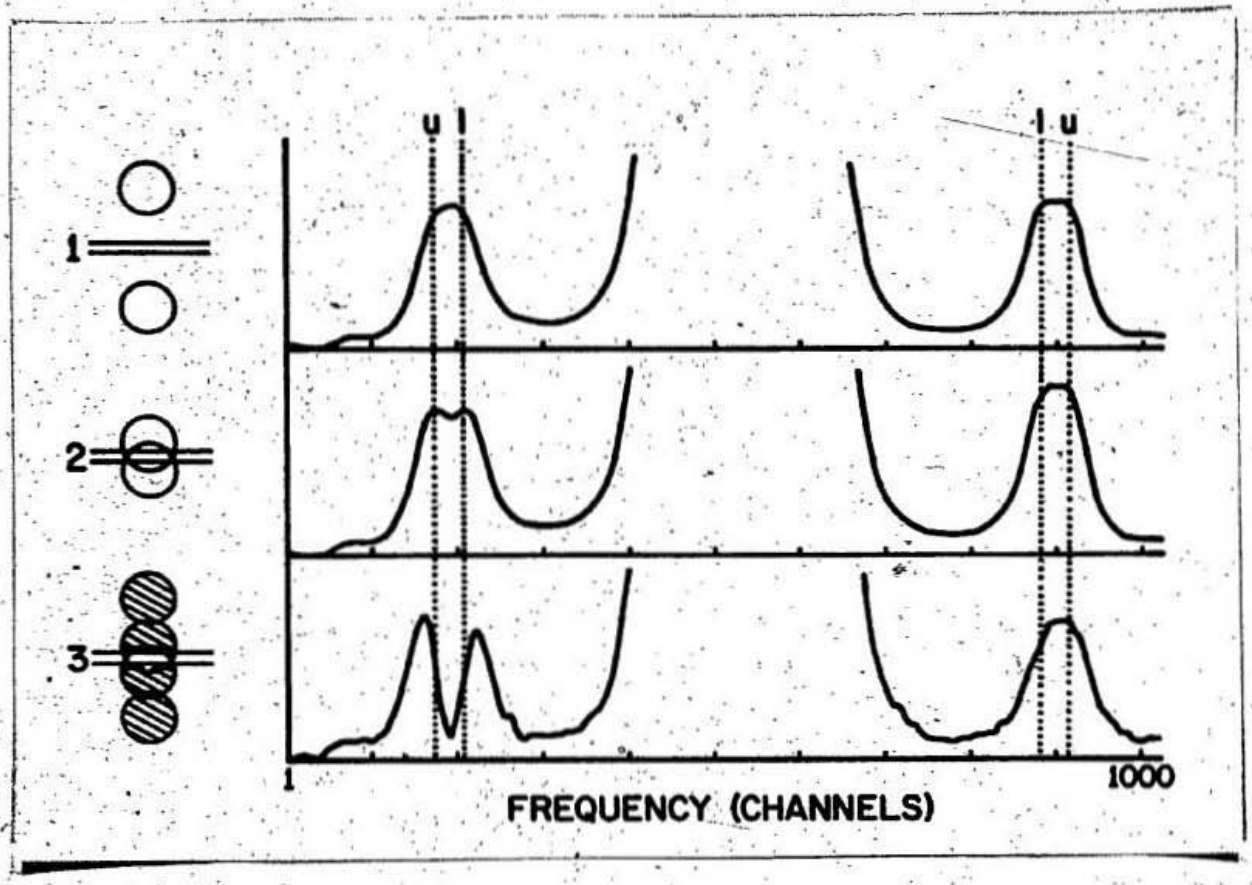

Fig. 5.4

Fig. 5.5. Composite spectra (analogous to those illustrated in Fig. 5.4) formed from linear combinations of Brillouin spectra in series 3 (see Fig. 5.3). Unshaded portions of schematic diagrams at left show regions of observation. 1 and 6 (Fig. 5.3) yields 1 (Fig. 5.5). 2 and 5 (Fig. 5.3) yields 2 (Fig. 5.5). 4 Fig. (5.3) is 3 (Fig. 5.5.). 3 minus 1 (Fig. 5.5) yields 4 (Fig. 5.5). Reference lines u and l show frequency shifts of longitudinal Brillouin components, far from the boundary in the upper and lower monocrystals respectively.

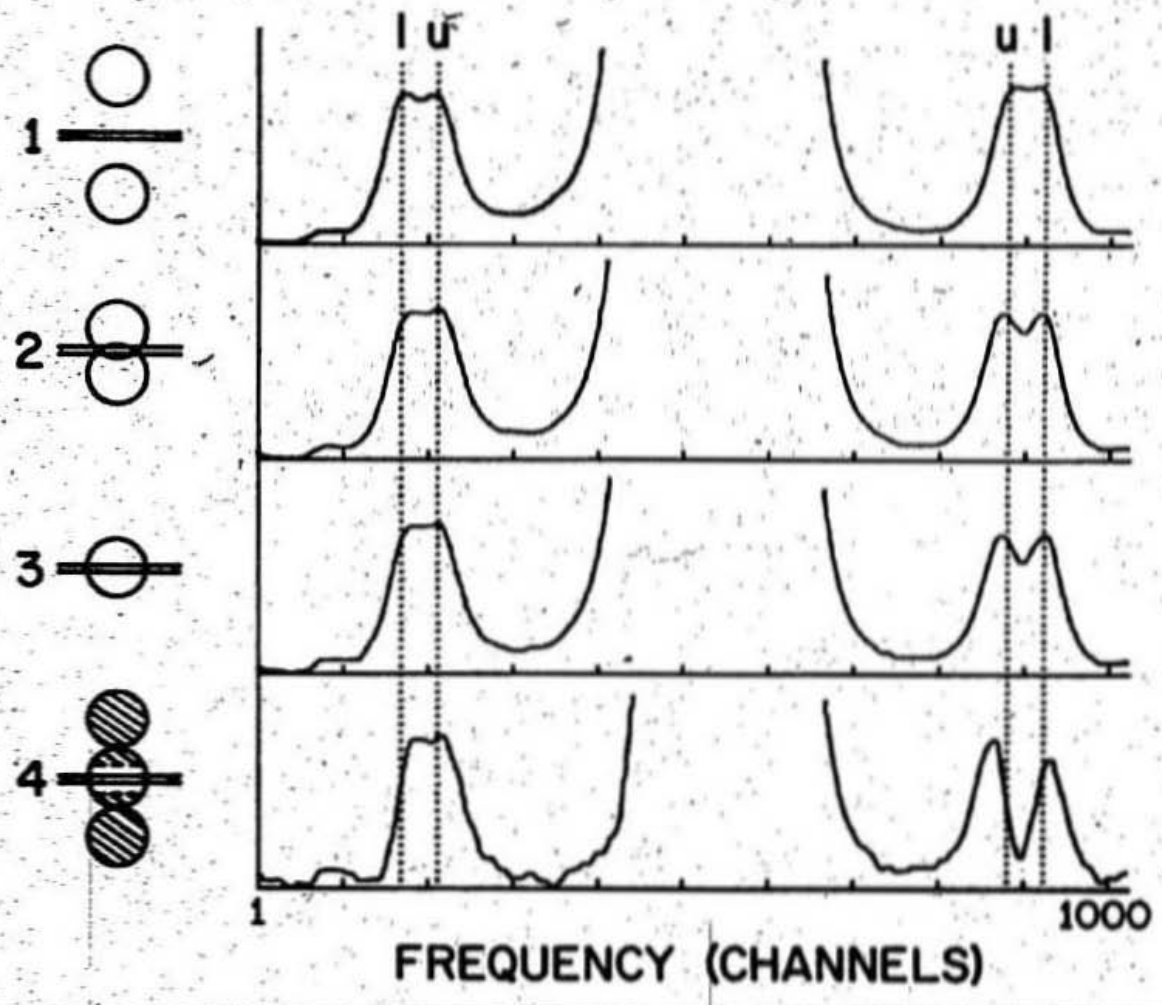

Fig. 5.5

background count.

Comparison of the spectra shown in Fig. 5.4 with those shown in Fig. 5.5 indicates the striking dependence of the observed asymmetry on crystal orientation. Both series of spectra suggest that the effect giving rise to the asymmetry is localized within a region near the boundary which is small but not negligible in thickness when compared with the .21 mm diameter of the region of observation. In contrast, the boundary itself, being defined as a region of intermediate acoustic properties, is negligible in thickness compared to .21 mm.

To further substantiate the above conclusions and to more completely analyze the spectral features accounting for the observed asymmetry, the spectra were decomposed into individual components associated with scattering in one or the other of the two monocrystals. The decomposition was carried out through synthesis of the individual spectral components using the five parameter lineshape function given below:

$$I = I_p\{1 + 4(F_p-F)^2(2^{1/L}-1) \,/\, [H + A(F_p-F)]^2\}^{-L} \qquad (5\text{-}2)$$

In equation (5-2), I denotes intensity, I_p is peak intensity, F is frequency, F_p is peak frequency, H is full width at half peak intensity, L is an exponent to account for multiple passing of the interferometer and A is a small coefficient giving a linear dependence of half width on frequency. Equation (5-2) is basically an exponentiated Lorentzian function. While the instrumental function for a single pass Fabry-Perot is approximately Lorentzian and that for three passes is approximately Lorentzian to the third power, the

principal justification for using equation (5-2) was that it worked well in modelling both the Brillouin and unshifted spectral components. As well, it explicitly included the physically meaningful parameters I_p, F_p and H. The parameters L and A carried less intuitive significance but were found essential in making the lineshape function flexible enough to yield good fits. The value of L lay between 2.4 and 2.7 for the unshifted components and lay between .85 and 2.0 for the longitudinal Brillouin components. The parameter A, used to break symmetry of the lineshapes about F_p, had magnitude less than .2 in all cases.

Brillouin spectra were synthesized as sums of lineshape functions of the form 5.2 plus an added flat background term. The syntheses of all 15 grain boundary spectra were carried out on a graphics terminal connected to the PDP 11/70 computer system. The method of trial and error was used in fitting the synthesized spectra, with the criterion for a good fit being overlap of the plotted summed lineshape functions with the plotted raw spectra data. A sum squared error term was evaluated with each trial and was used as a guide in optimizing some of the parameters. However, an overall minimum in sum squared error did not specify a useful fit due to the nearly 1000 to 1 ratio by which the height of the unshifted component typically exceeded the heights of the longitudinal Brillouin components. Because of this high ratio, a small error in fitting the unshifted component, particularly in the wings, tended to obliterate the longitudinal components.

The first step in the trial and error fitting procedure was to fit the central component with a lineshape function having least

squares value for I_p and F_p and having values for H, L and A which yielded good overlap in the wings extending beyond the 0.2%-of-peak-intensity points. The lineshape parameters for the central component were then held constant while functions were fitted to each individual longitudinal or transverse Brillouin component present on the spectrum. The components were fitted one at a time, usually in sequence from left to right across the spectrum. This sequential fitting procedure was then repeated several times until a good overall fit was obtained. In almost every case, the final fit lay entirely within the scatter in the experimental data over all regions of the spectrum excluding that portion of the unshifted component lying above the 0.2%-of-peak-intensity points. The slight but nevertheless significant error in fitting the unshifted component could not be avoided without increasing the number of parameters in the lineshape function. An example of a synthesized Brillouin spectrum, plotted simultaneouly with the corresponding raw data, is shown in Fig. 5.6.

The time required to complete each trial and error fit was about two hours. The total time required to fit all 15 spectra did not appear to justify construction and programming of a spectrum fitting algorithm utilizing nonlinear least squares methods combined with a set of appropriate constraints to ensure that all parameters remained within physically meaningful bounds. While such an algorithm would have the advantage of treating all spectra in an a priori identical manner, it is questionable whether any significant improvement in the reliability of the spectral decompositions would be obtained. However, in view of the nature of the methods used for spectral synthesis in the present instance, the resultant derived data are appropriately used only in qualitative analysis of the Brillouin

Fig. 5.6. Spectrum showing typical quality of spectral synthesis by trial and error technique described in text. Solid line is sum of seven lineshape functions of the form (equation (5-2)). Dots show raw data from spectrum recorded near grain boundary at bicrystal orientation No. 3 (spectrum No. 5, Fig. 5.3).

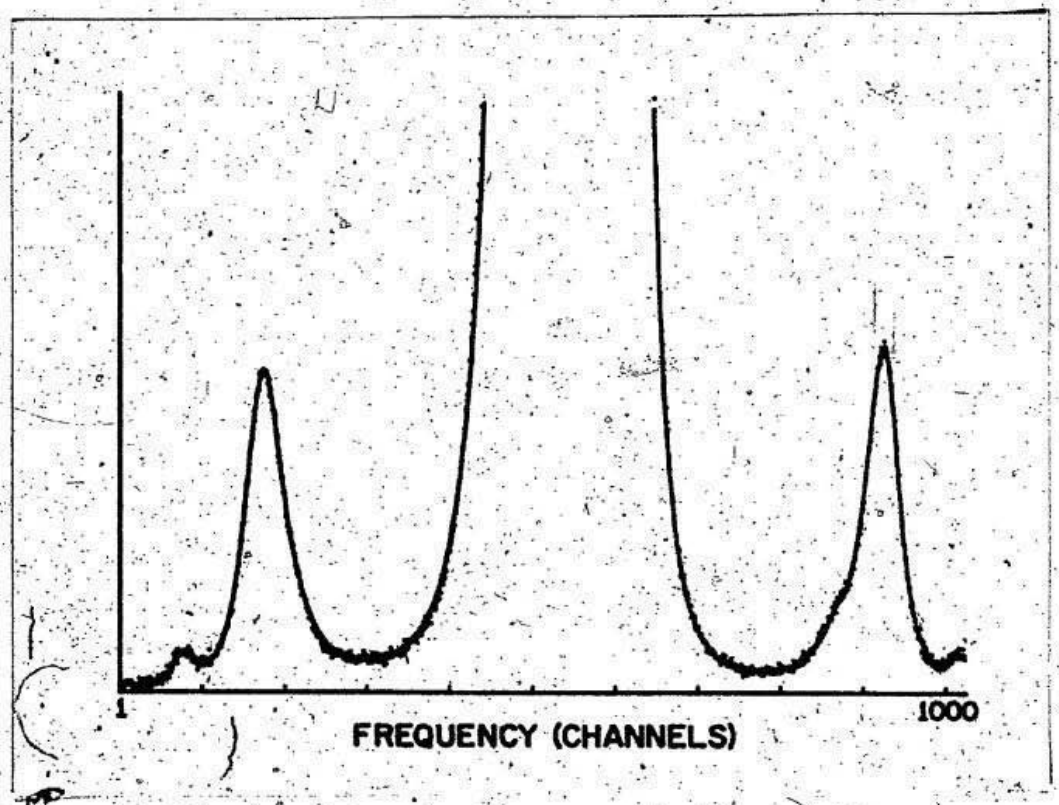

Fig. 5.6

spectra obtained from the crystal grain boundary region.

5.6 Discussion and Conclusions

An immediate application of the process of spectral decomposition lies in the mathematical reduction of the size of the region of observation. Fig. 5.7 shows a Brillouin spectrum synthesized from components fitted to the two slightly off-centred boundary region spectra designated by numbers 2 and 5 in Fig. 5.3. The lineshape functions corresponding to the dominant longitudinal components in the two boundary region spectra have been deleted in forming Fig. 5.7 thus yielding a composite spectrum showing Brillouin scattering from only those portions of the regions of observation lying nearest the boundary.

The general similarity between Fig. 5.7 and the spectrum numbered 4 in Fig. 5.5 substantiates conclusions previously drawn regarding the thinness of the boundary and the localized nature of the effect causing the observed asymmetry. The two spectra, while both corresponding to bicrystal orientation number 3, are composed from independent sets of measured spectral data and represent different methods of effectively shrinking the region of observation. The close agreement in indicated frequency shift deviations of the longitudinal Brillouin components in the two composite spectra suggests that a physical reduction in the size of the region of observation would yield equivalent results. No attempt was made to experimentally verify this conjecture since major modifications of the optical setup would have been required.

The synthesis and resultant decomposition of the Brillouin spectra from the grain boundary region showed that effects associated

Fig. 5.7. Synthesized spectrum composed from lineshape functions used in fitting spectrum No. 2 (Fig. 5.3) and spectrum No. 5 (Fig. 5.3). Functions corresponding to dominant longitudinal components have been deleted from the composed spectrum thereby simulating reduced physical size of the region of observation (indicated by unshaded portion of schematic diagram at right). Note similarity between this spectrum and the composite spectrum 4 in Fig. 5.5. Also, see text.

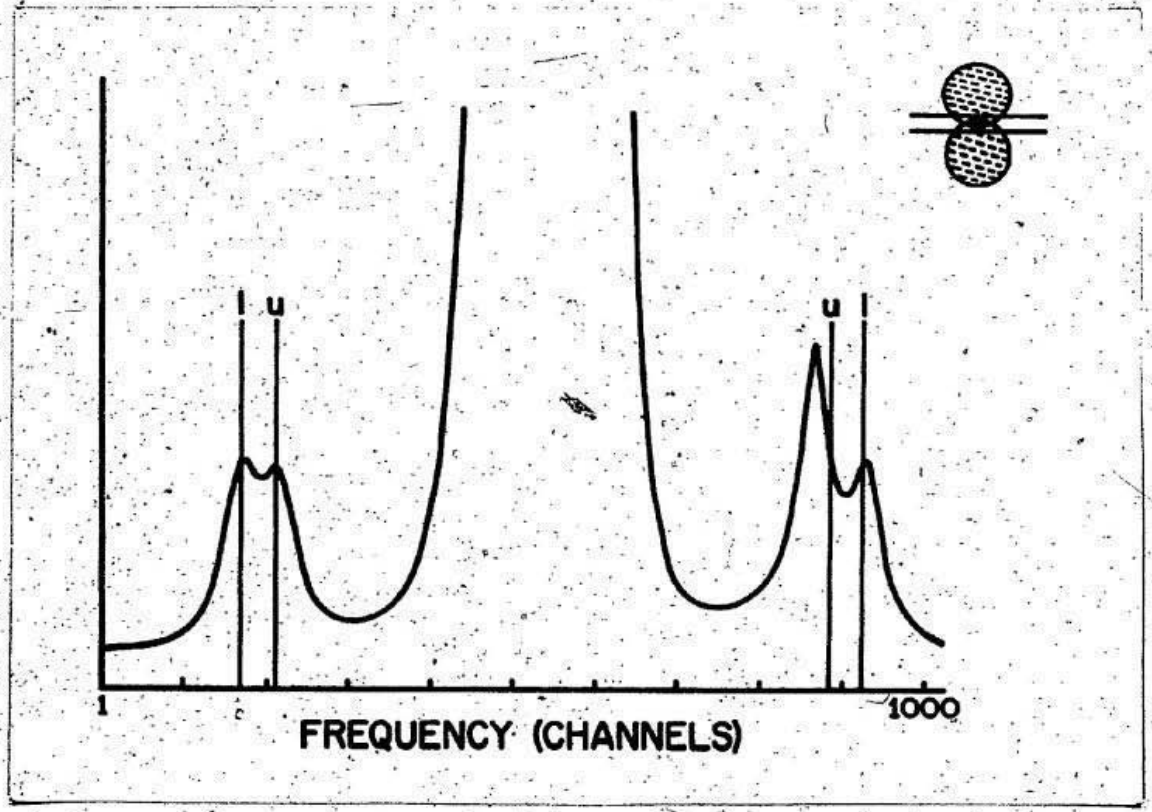

Fig. 5.7

with proximity to the boundary modified the peak frequencies of the observed longitudinal components. Alternative explanations for the modified appearance of the boundary region spectra, in particular, changes in the widths or intensities of components or the superposition of a third component on the longitudinal component pairs, were found inconsistent with observations.

The primary evidence for the above conclusion came from attempts to synthesize the various grain boundary spectra without changing the parameters, F_p, for the merged longitudinal components from those values appropriate for spectra with regions of observation lying far from the boundary. In all cases, no combination of values for the remaining four parameters in equation (5-2) yielded good fits to the longitudinal component pairs. Furthermore, no improvement was obtained by introducing a third component assumed to correspond to some intermediate acoustic velocity. However, when F_p was taken as a variable parameter, good fits were obtained with values for I_p, H, L and A corresponding reasonably well with those values used in synthesizing spectra obtained far from the grain boundary.

Fig. 5.8 gives a synopsis of the longitudinal frequency shift data for the near-boundary and far-from-boundary Brillouin spectra at each of the three bicrystal orientations. The indicated frequency shifts were determined from the values of the parameter F_p used in fitting the longitudinal components on the various spectra. The near-boundary frequency shifts were specified by fits to observed spectra with regions of observation approximately centred on the boundary. Since these regions of observation were probably wider than the thin local region characterized by a maximum perturbation

Fig. 5.8. Synopsis of longitudinal Brillouin frequency shift data obtained in ice crystal grain boundary studies at -16°C. Tall lines show frequency shift for scattering far from the grain boundary while short lines indicate frequency shifts observed in near boundary spectra. u and l denote the upper and lower monocrystals respectively.

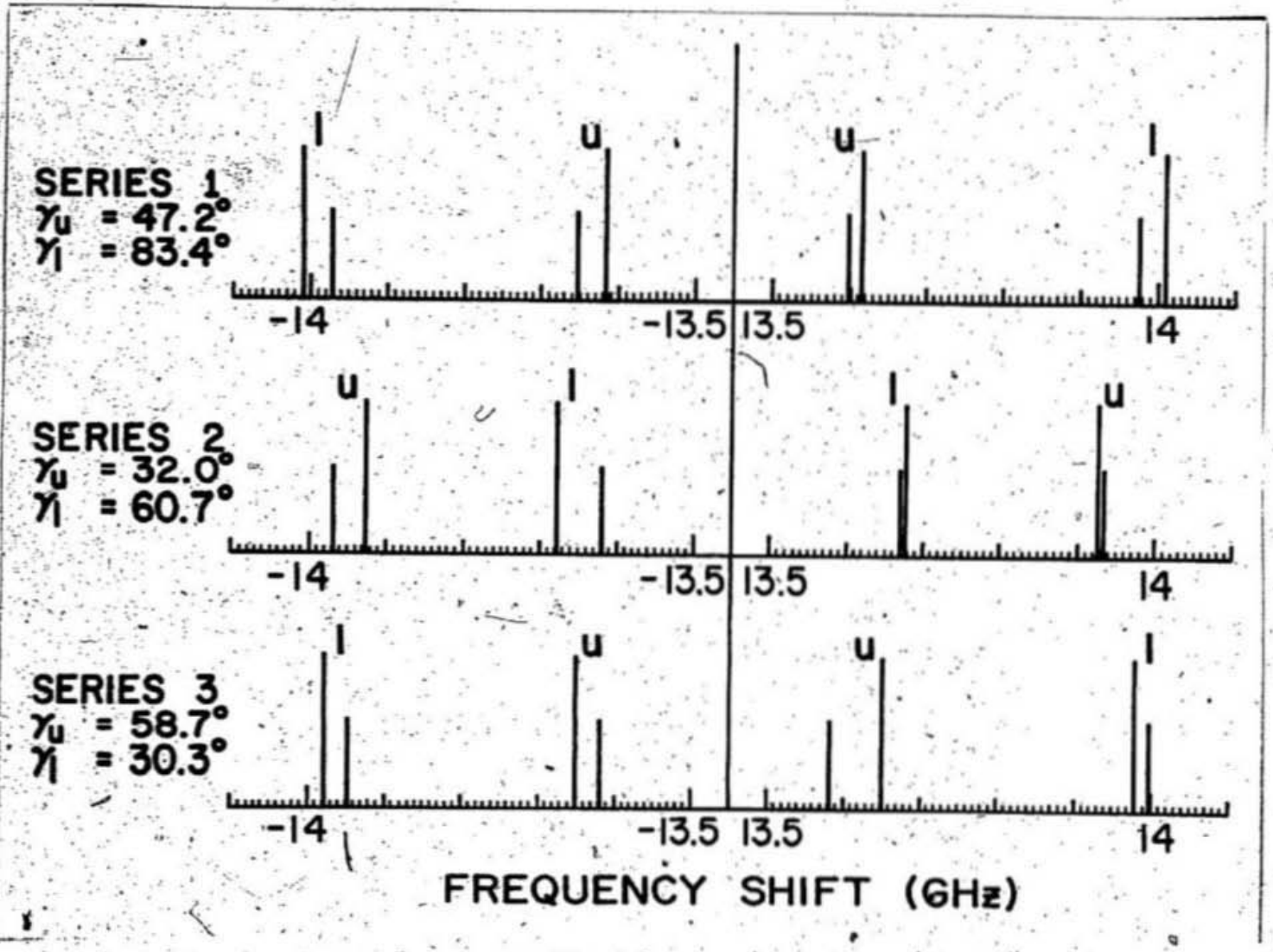
SERIES 1
γ_u = 47.2°
γ_l = 83.4°
SERIES 2
γ_u = 32.0°
γ_l = 60.7°
SERIES 3
γ_u = 58.7°
γ_l = 30.3°
l
u
-14
-13.5
13.5
14
FREQUENCY SHIFT (GHz)

Fig. 5.8

to the far-from-boundary frequency shifts, the deviations indicated in Fig. 5.8 represent minimum values. That is, a Brillouin spectrum emanating from a more highly localized region centred on the boundary could be expected to show equal or greater changes in longitudinal frequency shift relative to shifts measured far from the boundary. The principal purpose of Fig. 5.8 is to point out the direction of these changes.

No clear pattern is apparent in the data illustrated in Fig. 5.8. This suggests a fairly complex relationship between observed frequency shift deviations and the orientation of the two monocrystals relative to the geometry of the Brillouin scattering optics. As well, observations may have been affected by the orientation of the plane of the boundary although this orientation remained approximately constant since the boundary was nearly normal to the axis about which the sample was rotated.

A detailed analysis of the physical processes giving rise to the frequency shift deviations and consequent asymmetry in Brillouin spectra from the crystal grain boundary region lies outside the scope of the present work. No analogous Brillouin spectroscopic studies of the boundary region in bicrystalline samples of any substance have been reported in the literature. Furthermore, the theory of Brillouin scattering by bulk acoustic modes propagating in anisotropic media near a plane of steep gradient or discontinuity in elastic properties has not been published. Some work on Brillouin scattering from surface modes in transparent thin films[81,82] and in opaque media[83] has, however, been carried out. While the geometrics and techniques employed in these experiments differed greatly from

those described above, the methods of theoretical analysis[84,85,86] and the experimental observations may have some bearing on the interpretation of the present results.

The wavelength of the phonons yielding the observed longitudinal Brillouin scattering in ice is 2.77×10^{-7} m. This distance traverses about 500 unit cells and, if assumed to substantially exceed the thickness of the region of disrupted crystal structure associated with the grain boundary, would justify treatment of the boundary as a discontinuity or surface. Accordingly, interface modes of the type described by Stoneley[87,88] could be expected to propagate along the boundary and the interaction of these with the adjacent acoustic field in the bulk[84] might account for the observed frequency shift deviations in the Brillouin spectra.

The theoretical work of Fletcher[89] implies the existence of a quasi-liquid layer on the surface of an ice crystal. This layer is hypothesized to have thickness between 1×10^{-9} and 4×10^{-9} m at $-5^{\circ}C$ and to blend continuously into the crystal structure of the underlying ice. Higher temperatures or the presence of impurities would give rise to a thicker quasi-liquid surface layer while in pure ice at temperatures below $-10^{\circ}C$ the layer would have zero thickness. Experiments have suggested that an analogous liquid-like layer exists at the interface between ice and other materials and at ice crystal grain boundaries. Thermal contraction studies with a silicon strain gauge embedded on the surface of an ice single crystal indicated the presence of a viscous layer separating ice and silicon.[90] Evidence for a viscous water-like layer between grains in polycrystalline ice was provided by measurements of diffusion rates of radioactive

cesium through small polycrystalline samples.[91]

Based on published research to date, a reliable estimate regarding the presence, nature or thickness of a disrupted (liquid-like) boundary layer in the sample used in the present investigation is not possible. Clearly, such a layer could have a marked effect on the acoustic properties of the local region near the boundary. If the layer had thickness approaching 0.21 mm it would be directly observable by Brillouin spectroscopy with the optical setup described above. However, even taking into account the significant impurity concentration in the sample and the fact that impurities, when concentrated at the grain boundary, would enhance thickness of a disrupted layer, it remains probable that the boundary region was thinner than the region of observation by a few orders of magnitude. Nevertheless, a disrupted layer with thickness approaching or exceeding one acoustic wavelength appears entirely plausible and its potential existence must be taken into consideration in any attempt to interpret the above Brillouin spectroscopic observation (i.e., in terms of interactions between bulk and surface acoustic modes).

Few methods exist for directly observing or measuring the physical properties of ice crystal grain boundaries. With the exception of the x-ray diffraction topographic techniques used, for example, by Higashi,[80,92] most experiments have been based on measurements of bulk properties of bicrystalline or polycrystalline ice samples followed by inferences of crystal grain boundary properties. In view of the importance of grain boundaries in governing the mechanical properties, such as creep,[93] yielding or fracture of large naturally occurring ice masses, further means of direct

measurement of grain boundary properties appear highly desirable. It has been demonstrated above that a highly localized region of observation combined with a very short acoustic wavelength makes Brillouin spectroscopy useful for such direct measurements. It is hoped that full interpretation of the existing observations, followed by further Brillouin experiments will, in the near future, lead to a significant improvement in the understanding of the grain boundary region in ice.

CHAPTER 6

SYNOPSIS OF RESULTS AND DISCUSSION

6.1. The Brillouin Spectroscopic Measurements

The results of four independent determinations of the elastic moduli of ice by Brillouin spectroscopy have been quoted in Chapters 3 and 4. The ice samples utilized in these measurements represented widely varying environments of formation. Aside from the resultant variations in crystal quality and purity of the samples, all experimental parameters except the temperature were kept as nearly constant as possible. Hence, reliable conclusions regarding the dependence of the elastic properties of ice on the environment of formation can be drawn from the data obtained. The change in sample temperature from $-3^{\circ}C$ for the artificial ice measurements to $-16^{\circ}C$ for the measurements on natural ice may slightly increase uncertainty in comparing the respective sets of results. However, this uncertainty is not viewed as significant since detailed results regarding the temperature dependence of the elastic moduli of ice are quoted in the literature[28,30,35] and since the change in elastic properties over a $13^{\circ}C$ temperature range is relatively small.

The five elastic moduli determined for each of the four ice samples are listed, for purposes of comparison, in Table 6.1 along with corresponding values determined by several previous authors. The present results will be compared with those of previous authors in Sec. 6.3. The derived quantities appearing in Table 6.1 are

TABLE 6.1

MEASURMENTS OF THE ADIABATIC ELASTIC MODULI OF ICE Ih

	Artificial Ice	Glacial Ice	Lake Ice	Sea Ice	Artificial Ice	Artificial Ice	Artificial Ice (aged)	Artificial Ice	Artificial Ice	Lake Ice
Author	Present	Present	Present	Present	Jona & Scherrer[26]	Baan et al.[28]	Dantl[35]	Brockamp & Querfurth[30]	Proctor[32]	Bogordskii[29]
Method	Brillouin spectroscopy	Brillouin spectroscopy	Brillouin spectroscopy	Brillouin spectroscopy	Schaefer-Bergmann method	Resonant Bars and Plates	Ultrasonic Pulse	Ultrasonic Pulse	Ultrasonic Pulse	Ultrasonic Pulse
Measurement Temperature	-3°	-16°	-16°	-16°	-16°	-2° to -30°	-.7° to -140°	0° to -20°	-163° to -213°	-15°
Frequency	10 GHz	10 GHz	10 GHz	10 GHz	15 MHz	5kHz-50kHz	5MHz-190MHz	2 MHz, 12MHz	15 MHz	4 MHz
Elastic Moduli Corrected to -16° (see text) c_{11}	139.61±.61	139.13±.61	138.76±.68	142.7±6.8	138.5±.8	133±8	132.1±.4	137.5±.7	139.1	133.9±13
c_{12}	71.53±.46	70.26±.58	69.79±.97	73.2±5.1	70.7±1.2	63±8	67.0±1.3	67.7	68.6	68.0±7
c_{13}	57.65±.32	58.01±.37	56.57±.49	59.5±1.5	58.1±1.6	46±9	58.0±4.1	52.5	53.9	77.9±8
c_{33}	150.13±.69	150.59±.75	150.71±.93	147.4±2.0	149.9 ± .8	142±7	144.3 ± .6	149.9	149.8	168.6±17
c_{44}	30.21±.15	30.11±.18	30.24±.25	29.8± .5	31.9± .3	30.6±.15	28.9±.2	30.7	30.8	33.7±3
$2\rho(\bar{v})^2$	122.42	122.44	122.67	122.22	123.90	120.35	116.63	123.18	123.75	127.08
100 (1-d)	.071%	.088%	.276%	-.096%	1.27%	-1.65%	-4.89%	.69%	1.14%	3.73%
$d.c_{11}$	139.51	139.01	138.38	142.8	136.7	135	138.6	136.6	137.5	128.9
$d.c_{12}$	71.48	70.20	69.60	73.3	69.8	64	70.3	67.2	67.8	65.5
$d.c_{13}$	57.61	57.96	56.41	59.6	57.4	47	60.8	52.1	53.3	75.0
$d.c_{33}$	150.02	150.46	150.29	147.5	148.0	144	151.4	148.9	148.1	162.3
$d.c_{44}$	30.19	30.08	30.16	29.8	31.5	31.1	30.3	30.5	30.4	32.4

discussed in Sec. 6.2 and in Sec. 6.3. The elastic constants of artificial ice have been corrected to correspond to a temperature of -16° using the temperature correction equations of Dantl[35] which have been reproduced, for reference, in the following section.

The systematic and nonsystematic components of the uncertainties in the elastic constants have been combined in Table 6.1. While the systematic error component is common to all five elastic constants determined for an individual sample, random variation in this component occurs among the sets of measurements from each of the four samples. The systematic uncertainty was due primarily to uncertainty in the scattering angle, α (see Sec. 3.4) and, to a lesser extent, to uncertainty in the density, ρ. The scattering angle was readjusted between each of the four determinations of elastic moduli, thus randomizing error in its value. The density was also assumed to vary randomly from sample to sample, within the range specified by the quoted uncertainty (see Sec. 3.6 and Sec. 4.6).

Inspection of the data listed in Table 6.1 shows general agreement among the Brillouin spectroscopically determined elastic moduli of the four ice samples. Among the 30 pairs of elastic constants which may be selected for comparison, 21 show agreement within the quoted uncertainties, that is within one standard deviation, while no pair is separated by more than 2.3 standard deviations. The maximum discrepancy is found in comparing c_{13} for artificial ice with the corresponding value for lake ice.

It is thus concluded that no significant variation in the elastic moduli of local homogeneous regions in ice can be identified from the present results. In view of the wide range of conditions

under which the samples studied were formed, it is further concluded that any differences exceeding 1% in the elastic properties of arbitrary samples of natural ice are almost certainly attributable to factors other than variability in the moduli of local homogeneous regions of ice. Curves showing Ω (Brillouin frequency shift) vs. γ (angle relative to c axis), specified by the elastic constants determined for each of the four samples of ice, are shown in Fig. 6.1.

The tendency of the elastic moduli of ice to decrease with sample age, as noted by Dantl,[35] has not been demonstrated in the present measurements. Accumulation of Brillouin data from the artificial ice crystals was commenced only a few hours following freezing and was continued for up to six weeks. During such time periods, no appreciable change in the dependence of sound velocity on crystal orientation was noted. Furthermore, while samples of Mendenhall ice were presumably annealed at the freezing point for time periods greatly exceeding the eight months over which the samples of Dantl[35] were aged, the agreement of their elastic constants with those of the unaged artificial ice samples is excellent. Additional discussion of the present results as compared with those of Dantl[35] is included in Sec. 6.3.

The concentration of dissolved ionic solids in water at the time of freezing does not significantly affect the elastic properties of the resulting ice. This conclusion arises from comparison of the elastic moduli of sea ice with the moduli determined for the three types of fresh water ice. Clearly, the concentration of solid ionic impurities present at the time of freezing varies over several orders of magnitude between seawater and the doubly distilled water

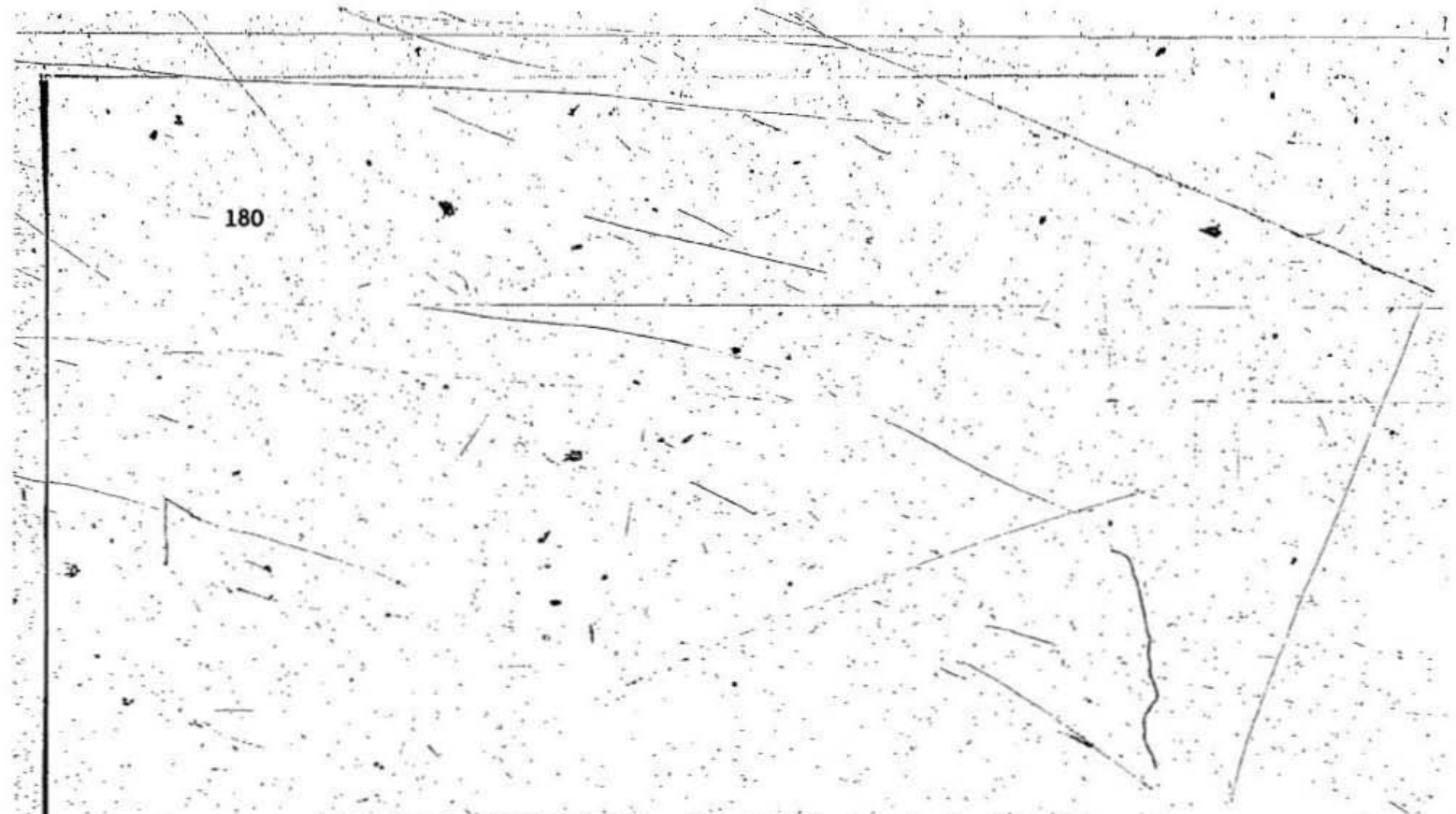

Fig. 6.1. Comparative plots of Brillouin frequency shift (Ω) versus propagation direction relative to c axis (γ) for sound waves in ice. A.I. - curves specified by elastic constants determined in present experiment for artificial ice; M.G.I. - Mendenhall glacier ice; L.I. - lake ice (from Paddy's Pond); S.I. - sea ice. Elastic constants are quoted in Table 6.1.

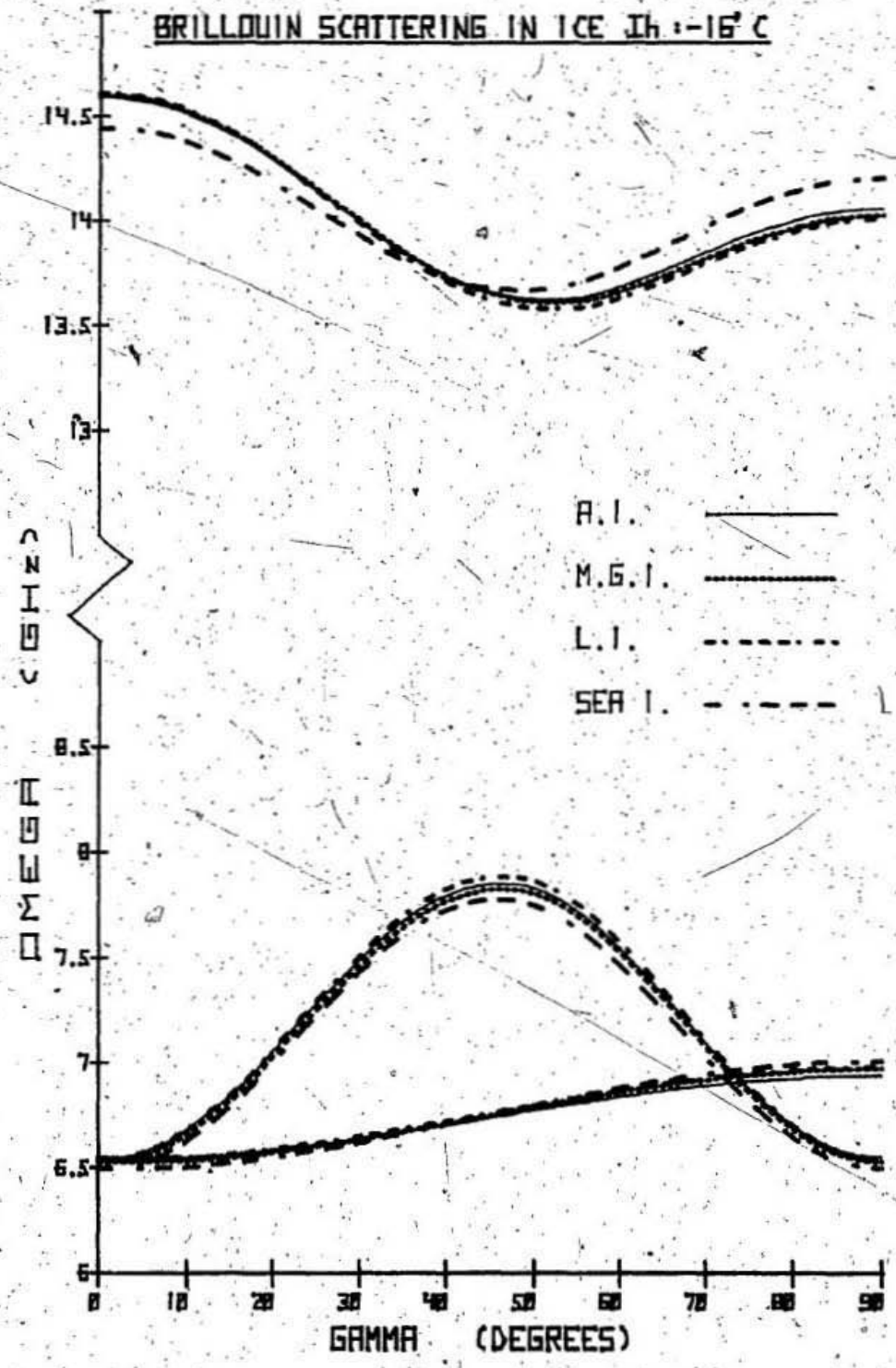
BRILLOUIN SCATTERING IN ICE Ih :-16° C
14.5
14
13.5
13
8.5
8
7.5
7
6.5
6
OMEGA (GHz)
A.I.
M.G.I.
L.I.
SEA I.
0
10
20
30
40
50
60
70
80
90
GAMMA (DEGREES)

Fig. 6.1

used in growing the artificial ice samples. The glacial ice and lake ice samples presumably include intermediate levels of dissolved impurities. The results of partial water analyses from the four samples are listed in Table 6.2.

Only the lake ice sample was sufficiently large to provide the 1 litre of meltwater required for a reasonably complete analysis. This analysis was carried out by the Memorial University of Newfoundland Water Analysis Facility. The total volumes of both the Mendenhall ice samples and the sea ice samples provided by CRREL were each less than 0.1 litre. Thus, these samples were not analyzed. The impurity concentrations for Mendenhall ice were taken from an analysis of melted monocrystalline Mendenhall samples reported by Higashi.[75] The indicated conductivity measurement for Mendenhall ice was quoted by Maeno[94] who also comments on large concentrations of atmospherit gases found dissolved in meltwater from Mendenhall crystals. The salinity, expressed in parts per thousand NaCl, of part of the core from which the sea ice sample was extracted, was measured by CRREL.

The lack of dependence of the elastic constants of ice on the impurity concentrations present at the time of freezing probably reflects the relatively low level of impurity ions actually dispersed within the ice crystals. The few ions which are dispersed uniformly (indicated by the Mendenhall ice analysis to have concentrations in the neighbourhood of 1 part in 10^6) apparently do not cause sufficient long range disruption of the crystal lattice to significantly modify the elastic properties. Alternatively, it may be possible that while these impurity levels do significantly modify the elastic properties of ice crystals, the levels actually

TABLE 6.2

ANALYSES OF MELTED ICE SAMPLES

Sample		Artificial Ice (before freezing)	Glacial Ice (meltwater)	Lake Ice (meltwater)	Sea Ice (meltwater)
Conductivity		$10^{-2}(\Omega m)^{-1}$	$10^{-4}(\Omega m)^{-1}$	$10^{-3}(\Omega m)^{-1}$	-
pH		5.90	-	5.00	-
Impurity Concentrations in ppm by Weight	Na^{+}	-	-	.60	2×10^{3}
	Cl^{-}	-	.2	6	3×10^{3}
	Ca^{++}	-	1	.11	-
	SO_4^{--}	-	.8	-	-
	Mg^{++}	-	.02	.03	-
	Mn	-	-	.01	-
	Fe	-	-	.03	-
	K^{+}	-	-	.07	-
	NH_4^{+}	-	-	.025	-
	F^{-}	-	-	.012	-
	NO_3^{-}	-	-	.005	-

incorporated in the crystal lattice were approximately equivalent in all four ice samples studied. These concentrations could in turn correspond to the equilibrium concentrations for uniformly dispersed foreign ions in annealed ice. A similar situation in all likelihood precludes any possibility of assessing the effect of dissolved atmospheric gases on the observed elastic properties of the four samples.

It is not clear whether or not higher concentrations of uniformly dispersed ionic impurities might exist in unannealed ice samples frozen rapidly from impure water. Clear monocrystalline ice samples incorporating up to 7 ppm HCl have been grown and studied.[60] The mechanism of incorporation of HCl at such concentrations was investigated but not determined. The polycrystalline bulk ice sample from Arnold's Cove Brook (see Chapter 5) included 20 ppm Cl^- and 13.2 ppm Na^+ (see Table 5.1) but nevertheless, excepting the presence of a few air bubbles, appeared uniformly transparent. As noted previously, the sample yielded sound velocity measurements matching those of artificial ice. A significant proportion of the included impurities in the sample may have been accommodated at crystal grain boundaries.

In summary, it has been concluded that the ion rejection process accompanying freezing and subsequent annealing of the natural ice samples studied in the present work has been relatively efficient. That is, it has reduced impurity concentrations to levels yielding insignificant or nonvarying distortion of the ice crystal lattice as evidenced by the uniformity in the elastic properties of the four samples. Unannealed samples, frozen rapidly

and maintained at temperatures well below freezing might possess higher dispersed impurity concentrations and hence show variations in elastic properties. Further theory and experimental work along these lines is necessary. Nevertheless, it appears that in assessing the microscopic elastic behaviour of most types of ice occurring in the natural environment, the presence of impurities in the water at the time of freezing can be disregarded. Of course, the bulk elastic properties will be strongly influenced by any air, brine or salt inclusions which may be present in a given sample. While a discussion of the potential effects of such inclusions lies outside the scope of the present work, the results obtained here are immediately applicable in one respect. That is, they establish a relatively precise and experimentally verified limit for the elastic properties of porous ice (sea ice) as the fractional volume of the pores approaches zero. Such a limit forms an important component of most elastic models for sea ice.[6,58]

The present Brillouin spectroscopic measurements indicate that disruption of ice crystals by strains exceeding the elastic limit does not give rise to significant volumes of ice possessing elastic properties differing from those of unstrained monocrystalline ice. Laue photographs from the sea ice sample (see Fig. 4.3) show disruption of the constituent monocrystals. If this disruption extended continuously over volumes comparable to the Brillouin scattering volume, then the effects of the resulting change in the local symmetry of the ice could be expected to appear in the Brillouin spectra. For example, if local strain had caused the complete destruction of the crystal lattice within the scattering volume, then

the observed sound velocities would be characteristic of an amorphous and hence isotropic medium. The sound velocities would then not necessarily satisfy the equations (2-20) and (2-24) with coefficients, S_i, appropriate for anisotropic hexagonal ice. No significant discrepancy was observed in the sound velocity data determined from any of the sea ice Brillouin spectra. As well, a Brillouin spectrum from a sample of bubbly iceberg ice (corresponding to Laue photograph H in Fig. 4.3 showed all three acoustic components having velocities satisfying equations (2-20) and (2-24) with the S_i set equal to those values quoted in the following section for monocrystalline ice. Substantial disruption of the constituent monocrystals in the polycrystalline iceberg ice sample is indicated by the smeared spots on the corresponding Laue photograph.

The fact that crystal disruption does not appear to affect the observed local elastic properties of ice is probably a consequence of annealing or recrystallization which occurs following disruption. Thus, when a large ice monocrystal is disrupted, it eventually becomes an aggregate of smaller undisrupted crystals. These small crystals have volumes apparently exceeding the Brillouin scattering volume (linear dimensions ~ 0.2 mm) and have elastic properties identical to those of large unstrained monocrystals. The above observations are not unexpected in view of the tendency of ice to recrystallize following disruptive strains, as noted in several previous experiments (for review and references, see Glen,[5] Chapter VI).

Since no significant variation was observed among the elastic properties of the four ice samples studied, the four sets of elastic constants were averaged to form a single set for use in calculating

the derived quantities discussed in the following section. Each elastic constant in the averaged set was taken to be the arithmetic mean of four values for that constant, obtained from the four types of ice and weighted by the reciprocal of their respective standard deviations. The weighted mean values thus form the best estimates for the elastic moduli of an arbitrary ice sample which can be obtained from the present data. The uncertainties in the mean values were determined assuming statistical independence of the uncertainties in the four respective measured values of the elastic constants. These uncertainties are applicable in assigning the quoted mean elastic constants to an arbitrary ice sample only if sample-to-sample variation in ice elastic moduli is assumed to be negligible. The weighted mean elastic moduli of ice, along with a number of derived quantities, are given in the following section.

6.2. Derived Elastic Parameters

While the elastic modulus tensor of a crystalline medium completely determines its elastic behaviour, quantities derived from the elastic moduli often possess more immediate physical significance than the tensor elements themselves. For instance, in engineering applications, the elastic properties of ice are often most appropriately discussed in terms of parameters such as bulk modulus, Young's modulus or polycrystalline averages for the various other quantities associated with isotropic elasticity theory. Derived quantities are also useful in comparing the elastic properties implied by one set of experimental results with those determined by some different method of measurement. Following is a determination of most of the commonly used elastic parameters, based on the weighted mean elastic constants

for natural or artificial ice at -16° as determined from the Brillouin spectroscopic data.

Table 6.3 lists the weighted mean elastic constants calculated from the four sets of Brillouin measurements, along with several quantities derived from these elastic constants. Uncertainties in the derived quantities have been calculated assuming statistical independence of the uncertainties in the five individual elastic constants. Strictly speaking, this assumption is not entirely valid since some degree of mutual interdependence of the uncertainties results from the manner in which the elastic constants are combined to form the sound velocity equations. However, this interdependence is very complex and is likely diminished substantially in the process of averaging the four sets of measurements.

Statistically precise error estimates for the derived quantities could be obtained numerically by repeatedly perturbing each element in all four sets of Brillouin frequency shift measurements by a normally distributed random variable of appropriate standard deviation. The desired derived quantity would then be calculated a large number of times and a quasi-empirical uncertainty estimated. All necessary data for this type of computation has been included in the previous chapters. The method involves extremely voluminous calculations and hence has not been used here.

Several of the derived parameters quoted in this section lack stated uncertainties. The probable errors can be determined from data included in this and the previous chapters. However, the required lengthy calculations are of limited value since those parameters without stated uncertainties are useful primarily for calculating further derived quantities. To avoid the possibility of generating

TABLE 6.3

ELASTIC PARAMETERS FOR ICE MONOCRYSTALS AT $-16^{\circ}C$

Property	Symbol	Value	Units
Dynamic elastic moduli	c_{11}	139.29±.41	$10^8 N/m^2$
	c_{12}	70.82±.39	$10^8 N/m^2$
	c_{13}	57.65±.23	$10^8 N/m^2$
	c_{33}	150.10±.46	$10^8 N/m^2$
	c_{44}	30.14±.11	$10^8 N/m^2$
Dynamic elastic compliances	s_{11}	103.18±.52	$10^{-12} m^2/N$
	s_{12}	-42.87±.45	$10^{-12} m^2/N$
	s_{13}	-23.16±.17	$10^{-12} m^2/N$
	s_{33}	84.41±.40	$10^{-12} m^2/N$
	s_{44}	331.79±1.21	$10^{-12} m^2/N$
Bulk modulus	K	88.99±.17	$10^8 N/m^2$
Compressibility	C	112.38±.21	$10^{-12} m^2/N$
Coefficients in expression for linear compressibility (see text)	β_1	37.14±.12	$10^{-12} m^2/N$
	β_2	.95±.31	$10^{-12} m^2/N$
Coefficients in expression for reciprocal of Young's modulus (see text)	e_1	103.176	$10^{-12} m^2/N$
	e_2	79.108	$10^{-12} m^2/N$
	e_3	97.871	$10^{-12} m^2/N$
Young's modulus at $\gamma = 0^{\circ}$	$E(\gamma=0^{\circ})$	118.46±.56	$10^8 N/m^2$
Young's modulus at $\gamma = 50.5^{\circ}$	$E(\gamma=50.5^{\circ})$	83.92	$10^8 N/m^2$
Young's modulus at $\gamma = 90^{\circ}$	$E(\gamma=90^{\circ})$	96.92±.49	$10^8 N/m^2$

TABLE 6.3 (Continued)

Property	Symbol	Value	Units
Coefficients in sound velocity equations, (2-15), (2-16), and (2-17)	k_1	169.43	$10^8 N/m^2$
	k_2	10.81	$10^8 N/m^2$
	k_3	109.15	$10^8 N/m^2$
	k_4	138.514897	$10^8 N/m^2$
	k_5	147.183748	$10^8 N/m^2$
	k_6	68.47	$10^8 N/m^2$
	k_7	8.19	$10^8 N/m^2$
Sound velocity integral (see text)	$2\rho(\bar{V})^2$	122.33359	$10^8 N/m^2$

unnecessary round-off error in subsequent calculations, such intermediate parameters have been quoted with several figures beyond those which are significant.

(i) Elastic compliance constants

The elastic compliance constants, s_{ij}, are the elements of the matrix which is the inverse of the 6 x 6 matrix $[c_{ij}]$. For media of hexagonal symmetry, the two matrices $[c_{ij}]$ and $[s_{ij}]$ are of identical form (see Nye[9] or Huntington[10] for details). Quantities such as Young's modulus, linear compressibility and bulk modulus are most simply expressed in terms of the compliance constants. As well, the compliance constants appear in the expression linking the adiabatic and isothermal elastic properties of a medium (to be discussed subsequently). The expressions below for the s_{ij} in terms of the c_{ij} have been adapted from Nye[9] and are appropriate for hexagonal media.

$$
\begin{aligned}
c &= [(c_{11}+c_{12})c_{33}-2c_{13}^2]^{\frac{1}{2}} \\
s_{11} &= (c_{11}c_{33}-c_{13}^2) \,/\, [c^2(c_{11}-c_{12})] \\
s_{12} &= (c_{13}^2-c_{12}c_{33}) \,/\, [c^2(c_{11}-c_{12})] \\
s_{13} &= -c_{13}/c^2 \\
s_{33} &= (c_{11}+c_{12}) \,/\, c^2 \\
s_{44} &= 1/c_{44}
\end{aligned}
\qquad (6\text{-}1)
$$

Values for the s_{ij} for ice, calculated via (6-1), appear in Table 6.3. The elastic constant c has value $157.77 \pm .45 \times 10^8$ N/m^2. It should be noted that the quoted uncertainties in the s_{ij} are definitely not statistically independent. Hence, properties

calculated from the s_{ij} must be written directly in terms of the c_{ij} for purposes of estimating the uncertainties.

(ii) Bulk modulus

The bulk modulus, K, is the ratio of applied hydrostatic pressure to resultant fractional decrease in volume. Its value in terms of the s_{ij} is readily determined directly from Hooke's law. The resulting expression can be written in terms of the c_{ij} via (6-1). The volume compressibility, C, is the reciprocal of the bulk modulus. The expressions appropriate for media at hexagonal symmetry are:

$$K^{-1} \equiv C = 3(s_{11}+s_{12}+s_{13}) + (s_{13}+s_{33}-s_{11}-s_{12})$$

$$K^{-1} = [3(c_{33}-c_{13}) + (c_{11}+c_{12}-c_{13}-c_{33})] \; / \; c^2 \qquad (6\text{-}2)$$

The value for the bulk modulus of ice at -16^{0}C, determined via (6-2) is given in Table 6.3. This value corresponds to the dynamic bulk modulus. The static (isothermal) bulk modulus will be quoted subsequently.

(iii) Linear compressibility

The linear compressibility, β, is the inverse ratio of applied hydrostatic pressure to resultant fractional decrease in length of a line having a specified orientation relative to crystal symmetry. In media of hexagonal symmetry, β depends on the angle γ between the specified direction and the hexagonal axis. Via Hookes law, the expression for β is found to be:

$$\beta = \beta_1 + \beta_2 \cos^2\gamma$$

where: $$\beta_1 = (s_{11}+s_{12}+s_{13}) = (c_{33}-c_{13}) / c^2 \qquad (6\text{-}3)$$

$$\beta_2 = (s_{13}+s_{33}-s_{11}-s_{12}) = (c_{11}+c_{12}-c_{13}-c_{33}) / c^2$$

Values for β_1 and β_2 are quoted in Table 6.3. The small value of β_2 relative to β_1 implies near isotropy in the linear compressibility of ice. The maximum variation of β with direction is 2.6%. Nevertheless, anisotropy beyond experimental uncertainty is noted.

Isotropy in β implies that the crystal lattice does not change shape under hydrostatic pressure. In ice, this would imply that the c/a ratio be independent of pressure. An x-ray crystallographic determination of the pressure dependence of c/a, analogous to the detailed temperature dependence studies of LaPlaca and Post,[72] has unfortunately not yet been carried out and reported in the literature. The model of ice used by Penny[14] in her theoretical determination of elastic moduli yielded the restriction $\beta_2 = 0$.

(iv) Young's modulus

Young's modulus, E, is the ratio of applied longitudinal stress to resultant longitudinal strain in the same direction. When static measurement techniques are employed, E is one of the most readily determined elastic parameters for either monocrystalline or isotropic samples. In monocrystalline media, E depends on the direction of applied stress relative to crystal geometry. The expression for E, derived from Hooke's law by Nye[9] for hexagonal media is:

$$E^{-1} = e_1 + e_2 \cos^2\gamma - e_3 \cos^4\gamma$$

where $e_1 = s_{11} = (c_{11}\, c_{33} - c_{13}^2) \,/\, [c^2(c_{11} - c_{12}]$

$e_2 = s_{44} - 2s_{11} + 2s_{13}$

$= [(c_{11}+c_{12})c_{33} - 2(c_{13}+c_{44})c_{13}] \,/\, (c^2 c_{44}) - 2e_1$

$e_3 = 2s_{13} + s_{44} - s_{11} - s_{33} = e_1 + e_2 - (c_{11}+c_{12}) \,/\, c^2$ (6-4)

Values for e_1, e_2 and e_3 for ice at -16° are quoted in Table 6.3. An absolute maximum in Young's modulus versus direction occurs at $\gamma = 0^\circ$ (stress applied along c axis) while a local maximum occurs at $\gamma = 90^\circ$. An absolute minimum in E occurs at $\gamma = 50.526^\circ$. The values for the extrema in Young's modulus are listed in Table 6.3. The maximum variation of E with direction in ice is about 34%.

(v) Sound Velocities in particular crystallographic Directions

The group velocity for sound propagation in an arbitrary direction in ice at -16°C can be determined through equations (2-15), (2-16) and (2-17) using the coefficients k_i, listed in Table 6.3 and the value for the density, $\rho = 919.5$ kg/m^3, quoted in Chapter 4. A mean value for the k_i and hence for the elastic constants was calculated from the integral over γ of the sum of the square roots of the right hand sides of the three sound velocity equations. The resultant value, denoted $2\rho(\overline{V})^2$, derived from the weighted mean elastic constants of ice at -16°, is given in Table 6.3. This value is used in Sec. 6.3 when comparing the results of the present experiment with results quoted in the literature. Further discussion of the significance of this derived quantity, along with its explicit defining relation are given in Sec. 6.3.

Table 6.4 shows the velocities of acoustic modes in ice at -16°C in several specific directions. An absolute maximum in V_L, equal to $(c_{33}/\rho)^{\frac{1}{2}}$ occurs at $\gamma = 0^{\circ}$. A local maximum in V_L, equal to $(c_{11}/\rho)^{\frac{1}{2}}$ occurs at $\gamma = 90^{\circ}$ while an absolute minimum in V_L occurs at $\gamma = 50.825^{\circ}$. The velocities of the transverse modes have equal values, given by $(c_{44}/\rho)^{\frac{1}{2}}$, at $\gamma = 0^{\circ}$ as required by cylindrical isotropy. The direction, $\gamma = 0^{\circ}$, also corresponds to an absolute minimum in the velocity of the T_1 mode which, in turn, increases monotonically in $\cos^2\gamma$ to a value given by $(c_{66}/\rho)^{\frac{1}{2}}$ at $\gamma = 90^{\circ}$. In hexagonal media, $c_{66} = (c_{11}-c_{12})/2$. The T_2 mode has an absolute maximum in velocity at $\gamma = 45.765^{\circ}$. This velocity, listed in Table 6.4, is the upper limit for the velocity of shear waves in ice. At $\gamma = 90^{\circ}$ the T_2 mode, having a polarization vector lying in the basal plane, propagates with velocity, $(c_{44}/\rho)^{\frac{1}{2}}$, equal to the transverse mode velocity at $\gamma = 0^{\circ}$.

Inspection of the curves shown in Fig. 6.1 shows that the two transverse mode velocities have equal values near $\gamma = 70^{\circ}$. The common velocity and corresponding angle can be determined by solving the quadratic equation (2-20), with X = Y. The resulting expression is:

$$V_{T1} = V_{T2} = \{[c_{11}-c_{12}-(c_{11}+c_{12}) \;/\; (S_3-S_5-1)] \;/\; (2\rho)\}^{\frac{1}{2}} \tag{6-5}$$

$$\text{when} \quad \cos^2\gamma = (c_{11}+c_{12}) \;/\; [(c_{11}-c_{12}-2c_{44})(S_3-S_5-1)]$$

The S_i are defined by equations (2-22) and have values, determined from the weighted mean elastic constants of ice at -16°, given below:

TABLE 6.4

SOUND VELOCITIES IN MONOCRYSTALLINE ICE, $-16^{\circ}C$

Mode	Direction (γ)	Velocity
Longitudinal	0°	4040.3 m/sec
Longitudinal	90°	3892.1 m/sec
Longitudinal	50.825°	3771.1 m/sec
Transverse (T_1,T_2)	0°	1810.5 m/sec
Transverse (T_1)	90°	1929.6 m/sec
Transverse (T_2)	90°	1810.5 m/sec
Transverse (T_2)	45.765°	2173.8 m/sec
Transverse (T_1,T_2)	73.488°	1920.2 m/sec

$$S_1 = 1298106.956 \times 10^{16}\ N^2/m^4$$

$$S_2 = 41197.97590 \times 10^{8}\ N/m^2$$

$$S_3 = 321.2202200 \qquad (6\text{-}6)$$

$$S_4 = 519.6074237 \times 10^{8}\ N/m^2$$

$$S_5 = 2.639804640$$

Values for the common transverse mode velocity and the corresponding direction of propagation are given in Table 6.4. By coincidence, the indicated value for γ differs by just over 0.5° from the angle between the c axis and the normals to crystallographic planes of the form {111}. Thus, shear wave velocity measurements in the direction normal to the plane (111) would be very nearly independent of polarization.

(vi) Elastic properties of isotropic polycrystalline ice

The elastic properties of homogeneous polycrystalline ice (no inclusions) are a complex function of the monocrystalline elastic constants and the sizes, shapes and orientations of the grains comprising the polycrystalline sample. Hence it is possible only to estimate the elastic parameters appropriate for polycrystalline ice. If grain orientation is approximately random and a sample includes a large number of grains, then the bulk elastic properties should show near isotropy. The elastic properties can then be expressed in terms of the parameters used in conventional isotropic elasticity theory. Estimation of the elastic parameters for isotropic polycrystalline ice from monocrystalline elastic constants requires an averaging procedure which in turn must be based on an assumed distribution of

grain shapes sizes and orientations.

Two elastic parameters completely determine the elastic behaviour of an isotropic medium. In dealing with polycrystalline ice, one of these is conveniently taken to be the bulk modulus, K, since the very near isotropy in the linear compressibility of ice assures that monocrystalline and polycrystalline values of K will not differ appreciably, regardless of grain structure. For purposes of the present analysis, the second elastic parameter has been chosen to be $\rho(\overline{V}_L)^2$ where $\overline{V}_L$ is the velocity of the longitudinal acoustic mode in polycrystalline ice. Clearly, $\overline{V}_L$ depends on grain structure, but its value must lie within the limits appropriate for monocrystalline ice. That is, 3771.1 m/sec $\leq \overline{V}_L \leq$ 4030.3 m/sec for homogeneous ice at -16°.

An estimate for $\overline{V}_L$ can be obtained from the monocrystalline elastic constants via the integral given below:

$$\overline{V}_L = \frac{1}{4\pi}\int V_L(\theta,\phi)d\Omega \qquad (6\text{-}7)$$

Equation (6-7) results from assuming that refractive effects at crystal grain boundaries are negligible and that a sound wave traversing a polycrystalline sample travels equal infinitesimal distances in monocrystals with orientations specified by polar coordinates θ,ϕ distributed uniformly over all solid angle, Ω. Cylindrical isotropy of the monocrystals allows the integral (6-7) to be reduced to,

$$\overline{V}_L = \int_0^{\frac{\pi}{2}} V_L(\gamma)\sin\gamma d\gamma \qquad (6\text{-}8)$$

where $V_L(\gamma)$ is determined by equation (2-15). Equation (6-8) was evaluated numerically using Simpson's rule to yield $\overline{V}_L$ = 3844.94 m/sec for homogeneous ice at -16°.

Equations linking the various parameters of isotropic elasticity theory are given in numerous texts, for instance Landau and Lifshitz[8] or Nye[9] or Malvern.[18] The relations utilized below are taken from these sources. The Lamé constants, λ and u are related to the bulk modulus, K and $\rho(\overline{V}_L)^2$ in the manner indicated below:

$$K = \lambda + 2u/3$$
$$\rho(\overline{V}_L)^2 = \lambda + 2u \qquad (6\text{-}9)$$

Accordingly, the values for λ and u given in Table 6.5 for ice at -16^o were determined from the bulk modulus given in Table 6.3 and the elastic constant, $\rho(\overline{V}_L)^2 = 135.94 \times 10^8$ N/m^2, determined from the value of $\overline{V}_L$ quoted above. The remaining quantities listed in Table 6.5 were calculated using the equations given below:

$G = u$	Shear modulus	
$E = 9KG/(3K+G)$	Young's modulus	(6-10)
$\sigma = [(3K/G-2) / (3K/G+1)]/2$	Poisson's ratio	

The shear velocity in polycrystalline ice is given by $\overline{V}_T = (G/\rho)^{\frac{1}{2}}$ and, using G from Table 6.5, was found to have value, $\overline{V}_T = 1956.9$ m/sec.

The elastic parameters quoted in Table 6.5 are good estimates only so long as a sample of polycrystalline ice possesses a uniform random distribution of grain orientations. The applied analysis can be partially adapted to account for preferred grain orientation by including an appropriate statistical weighting factor, $p(\gamma)$, in the integrand in equation (6-8). The factor $p(\gamma)\sin\gamma d\gamma$ equals the

TABLE 6.5

POLYCRYSTALLINE (ISOTROPIC) AVERAGED ELASTIC PARAMETERS, $-16^{\circ}C$

Property	Symbol	Value	Units
Bulk modulus	K	88.99	$10^8 N/m^2$
Young's modulus	E	93.32	$10^8 N/m^2$
Shear modulus	G	35.21	$10^8 N/m^2$
Poisson's ratio	σ	.32521	1
Lamé constants	λ	65.51	$10^8 N/m^2$
	u	35.21	$10^8 N/m^2$

differential probability that the specified propagation direction of a sound wave would make an angle, γ, with the c axis of a crystal grain at some arbitrary point in the polycrystalline sample. With a nonuniform $p(\gamma)$, $\bar{V}_L$ and all subsequent derived elastic parameters become dependent on the direction of measurement. Working back from the measured elastic parameters of a polycrystalline ice sample would, in principle, facilitate at least partial analysis of an existing distribution of grain orientations. Such analysis would require good quality elastic (acoustic) measurements and would be greatly complicated by the presence of any inclusions in the ice. To date application of such a technique has not been reported in the literature.

(vii) Isothermal elastic constants

All elastic parameters quoted in Tables 6.3 and 6.5 as well as those quoted in the text to this point are dynamic or adiabatic (constant entropy) values. That is, they are appropriate in analyzing elastic strain which occurs so rapidly that a negligible amount of heat flows into or out of the strained region. Hence, entropy is conserved within the strained region. Adiabatic elastic constants are invariably measured when acoustic measurement techniques are used since the strain associated with sound propagation fluctuates over very short time intervals ($\sim 10^{-10}$ sec for the acoustic modes observed by Brillouin spectroscopy).

When analyzing quasi-static elastic strain, the assumption of negligible heat flow becomes invalid. Warming or cooling associated with the application of stress leads to heat flow across the boundary of the resultant strained region until thermal equilibrium is re-established, that is, until the temperature of the strained region

returns to its initial value. The static or isothermal (constant temperature) elastic constants, appropriate in analyzing such a deformation, differ from the adiabatic elastic constants by an amount sufficient to account for the contribution to the strain tensor of thermal expansion due to stress-induced temperature changes.

The mathematical relationships between the equations of thermodynamics and those of elasticity are discussed in detail by Huntington[10] and by Nye.[9] The analysis leads to the following equation linking the adiabatic and isothermal elastic compliances of an arbitrary monocrystalline medium:

$$s_{ijkl}^{(T)} = s_{ijkl}^{(S)} + \alpha_{ij}\,\alpha_{kl}\,T/(\rho C_p) \qquad (6\text{-}11)$$

In equation (6-11), $s^{(T)}$ denotes the isothermal elastic compliance tensor, $s^{(S)}$ denotes the adiabatic elastic compliance tensor, α denotes the thermal expansion tensor, T denotes the absolute temperature (in ^{o}K), ρ denotes the density and C_p denotes the heat capacity at constant stress.

Anisotropy in the thermal expansion of monocrystalline ice has been investigated by Butkovich[73] and by LaPlaca and Post.[72] Both experiments indicated relatively small or insignificant differences in the coefficients of linear expansion parallel and perpendicular to the crystal c axis. Thus, based on the data of Butkovich,[73] the thermal expansion tensor for ice at -16^{o}C was assumed isotropic and was taken to be $\alpha_{ij} = 50.83 \times 10^{-6}\,\delta_{ij}$ where δ_{ij} denotes the Kronecker delta. Measurements of the heat capacity of ice by Giauque and Stout[95] have been tabulated by Dorsey[24] and indicate a value for C_p of 1985.4 J/(kg.^{o}C) at -16^{o}C. With the density taken to be

919.5 kg/m^3 and the absolute temperature, 257.15°K, the adiabatic and isothermal compliances were found to be linked as indicated below:

$$s_{ij}^{(T)} = s_{ij}^{(S)} + .364 \times 10^{-12}\ m^2/N \quad ij = 11,12,13,33$$

$$s_{44}^{(T)} = s_{44}^{(S)} \qquad (6\text{-}12)$$

Accordingly, the isothermal elastic moduli of ice at -16°, based on the adiabatic values quoted in Table 6.3 were determined to be:

$$c_{11}^{(T)} = 136.75 \times 10^8\ N/m^2$$

$$c_{12}^{(T)} = 68.28 \times 10^8\ N/m^2$$

$$c_{13}^{(T)} = 55.14 \times 10^8\ N/m^2$$

$$c_{33}^{(T)} = 147.61 \times 10^8\ N/m^2$$

$$c_{44}^{(T)} = 30.14 \times 10^8\ N/m^2$$

The uncertainties in the above values are likely comparable to the corresponding uncertainties quoted for the adiabatic elastic moduli since the required correction was relatively small and was well determined by experimental data.

The isothermal (static) elastic moduli given above, in principle describe the elastic behaviour of ice in a situation where stress is applied gradually. In practice, nonelastic processes such as creep or plastic flow (for a review of these processes, see Glen[5]) may dominate the mechanical properties of ice under conditions of slow stress application. Thus, the isothermal elastic moduli are of considerably less relevance in interpreting the observed mechanical

properties of ice than are the adiabatic elastic moduli. Nevertheless, the values quoted above may find application in careful experiments aimed at separating the elastic and the nonelastic reaction of ice under the quasi-static application of load.

The isothermal bulk modulus of ice at $-16^{\circ}C$, determined via equation (6-2) from the isothermal elastic constants quoted above is $K^{(T)} = 86.47 \times 10^{8}\ N/m^{2}$. This value may be of future use in comparing the results of a static determination of bulk modulus with the present measurements. Among the various elastic parameters of ice, the bulk modulus is most amenable to precise measurement by static techniques since nonelastic deformation of a monocrystalline pure sample will not result from moderate changes in applied hydrostatic pressure.

(viii) Temperature corrections

The temperature dependence of the individual elastic constants of ice was not measured in connection with the present work. However, as mentioned previously, the present results may be corrected to correspond to various temperatures within a fairly wide range by using existing published data. The best data for this purpose are those of Dantl[35] who measured the elastic moduli of pure monocrystalline artificial ice at a large number of temperatures over the range $-0.7^{\circ}C$ to $-140^{\circ}C$. Least squares quadratic fits (linear for c_{13}) to the data yielded the temperature correction equations which have been reproduced below.[35]

$$c_{11}(T) = c_{11}(0^{\circ}C)\cdot[1-1.489 \times 10^{-3}T - 1.85 \times 10^{-6}T^2]$$

$$c_{12}(T) = c_{12}(0^{\circ}C)\cdot[1-2.072 \times 10^{-3}T - 3.62 \times 10^{-6}T^2]$$

$$c_{13}(T) = c_{13}(0^{\circ}C)\cdot[1-1.874 \times 10^{-3}T] \qquad (6\text{-}13)$$

$$c_{33}(T) = c_{33}(0^{\circ}C)\cdot[1-1.629 \times 10^{-3}T - 2.93 \times 10^{-6}T^2]$$

$$c_{44}(T) = c_{44}(0^{\circ}C)\cdot[1-1.601 \times 10^{-3}T - 3.62 \times 10^{-6}T^2]$$

In the above equations, T denotes temperature in $^{\circ}C$ and c_{ij} $(0^{\circ}C)$ denotes the value for an elastic constant at $0^{\circ}C$ obtained by extrapolation from measurements at lower temperatures. Anomolous behaviour in the temperature dependence of the elastic moduli at temperatures very near the freezing point has been noted by some authors.[29,30] More complex temperature correction relations than those given above would be required to account for such behaviour.

For the range of temperatures normally encountered in the natural environment, the equations (6-13) can be simplified without a significant loss of accuracy. This simplication results from neglecting the quadratic terms and assuming that all elastic parameters having units of pressure vary according to a common linear equation. The simplification leads to differences of less than 1% in the resultant implied values of the elastic moduli over the range $0^{\circ}C$ to $-30^{\circ}C$ versus the values calculated via (6-13).

A linear temperature correction equation can be determined from the present data either with or without application of the relations (6-13). The results of both calculations are included below for purposes of comparison. In the first instance, the weighted mean elastic moduli for ice at $-16^{\circ}C$ were calculated from the results

of the Brillouin experiments on Mendenhall ice, lake ice and sea ice. The elastic constant, $2\rho(\overline{V})^2$, (see following section for discussion and defining relation) believed to best represent the overall elastic properties was then calculated from the weighted mean elastic moduli. A second calculation of $2\rho(\overline{V})^2$, corresponding to Brillouin data at $-3^{\circ}C$, was made using the elastic moduli of artificial ice quoted in Chapter 3. The two values were then assumed to define a straight line thereby yielding the temperature correction equation given below:

$$X(T) = X(T_m) \cdot [1 - aT] / [1 - aT_m] \qquad (6\text{-}14)$$

where $a = 1.418 \times 10^{-3}/^{\circ}C$

In equation (6-14), X denotes an arbitrary elastic parameter (with units of pressure), T denotes temperature in $^{\circ}C$ and T_m denotes the temperature at which a measured value for the parameter, X, exists.

A second determination of the coefficient, a, in equation (6-14) was carried out using the temperature correction data of Dantl.[35] In this case, the weighted mean elastic constants of ice at $-16^{\circ}C$, listed in Table 6.3, were corrected to correspond to a temperature of $-3^{\circ}C$ via (6-13). Values of $2\rho(\overline{V})^2$ were determined for the data corresponding to both temperatures and were found to imply $a = 1.427 \times 10^{-3}/^{\circ}C$. This value differs by only 0.6% from the value obtained using just the Brillouin measurements. The agreement is much better than that obtained when comparing the present values of the elastic constants at a given temperature with the corresponding values determined by Dantl[35] (see following section).

Use of equation (6-14) in specifying the temperature dependence of an arbitrary elastic parameter of ice, for example Young's

modulus or bulk modulus, requires the assumption that ratios of elastic constants (with unit dimensions) do not vary with temperature. The Brillouin data suggest that this assumption is valid to within experimental uncertainty over the temperature range -16°C to -3°C. The data of Dantl[35] imply a similar result extending over at least the 30°C temperature range immediately below the freezing point. Thus, based on presently available data there does not appear to be a significant advantage in using the equations (6-13) for temperature correction of the elastic parameters of ice over the range of temperatures most commonly associated with ice in the natural environment. Rather, a much shorter expression of the form (6-14) can be used to yield approximately equivalent results while simplifying computations, particularly when correcting derived quantities such as Young's modulus or the bulk modulus or the polycrystalline averaged elastic parameters.

By way of analogous reasoning, sound velocities in pure ice can be adjusted for changes in temperature with an equation of the form (6-14). Based on the Brillouin data at -3°C and -16°C, the linear temperature correction equation for acoustic velocity was found to be:

$$V(T) = V(T_m) \cdot [1 - bT] \; / \; [1 - bT_m] \qquad (6\text{-}15)$$

where $b = 6.196 \times 10^{-4} \; / \; ^\circ C$

In equation (6-15), V denotes an acoustic velocity while the other parameters are defined as in (6-14). For reasons noted above, equation (6-15) can be expected to yield reliable results over at least the 30°C temperature range extending down from near the

freezing point.

6.3 Comparison with Previous Results

The results of the present work along with the results of all six previous experimental determinations of the full set of elastic moduli of ice which have been reported in the literature are given in Table 6.1. The present results apparently possess the smallest overall uncertainty of the various sets of measurements. This is in part due to the large volume of data (a total of 189 sound velocity measurements) obtained at two closely spaced temperatures. As well, the quasi-random distribution of the data over values of the angle γ leads to similar uncertainties in all five elastic constants. This contrasts with the results of conventional acoustic experiments where measurements at a small number of specially chosen orientations yield wide variations in the accuracy with which the five elastic constants are determined. In particular, conventional acoustic experiments tend to yield good values for c_{11}, c_{33}, c_{44} and c_{66} since these constants can be measured directly. The uncertainty in c_{12} is usually the combined uncertainty in c_{11} and c_{66} while the uncertainty in c_{13} is a complicated combination of the uncertainties in c_{11}, c_{33}, c_{44} and a sound velocity measurement at some value of γ intermediate between 0° and 90°.

Systematic error, that is, error common to all five elastic constants, will result from a common multiplicative error in a complete set of experimental sound velocity measurements. This type of error is less readily identified by empirical means than is non-systematic error which appears as scatter among the measured velocities and leads to relative variations in the values of the

elastic constants. As noted previously, the systematic error in Brillouin spectroscopic measurements results from error in laser wavelength, Fabry-Perot free spectral range, refractive index, scattering angle or density. As well, by way of arguments given in Sec. 6.2, error in sample temperature could give rise to systematic error in the elastic moduli. This source of error is insignificant in the present results, however. Each potential source of systematic error listed above has been accounted for in the present analysis (see Chapters 3 and 4). Since no other sources appear possible, differences beyond probable experimental uncertainty in the present results versus those of previous authors must be accounted for by one of three possibilities. These are (1) sample-to-sample variation in the elastic properties of ice, (2) dependence of the measured elastic moduli on frequency, or (3) unnoticed sources of error in previously published results.

In comparing the various sets of elastic moduli listed in Table 6.1, it was important to have a criterion for identifying possible systematic error. The parameter $2\rho(\bar{V})^2$ was chosen for this purpose. The value of $2\rho(\bar{V})^2$ was calculated directly from quoted elastic constants by numerically evaluating the integral given below:

$$2\rho(\bar{V})^2 = \{\frac{2}{3\pi} \int_0^{\frac{\pi}{2}} [(f_L(c_{ij},\gamma))^{\frac{1}{2}} + (f_{T1}(c_{ij},\gamma))^{\frac{1}{2}} + (f_{T2}(c_{ij},\gamma))^{\frac{1}{2}}] d\gamma\}^2 \tag{6-16}$$

In equation (6-16), f_L, f_{T1} and f_{T2} denote the right hand sides of equations (2-15), (2-17) and (2-16) respectively. The elastic constant $2\rho(\bar{V})^2$ thus equalled twice the density times the square of the

mean of the three acoustic velocities averaged uniformly over γ. The absence of the factor $\sin\gamma$ in the integrand of (6-16) (in contrast with polycrystalline velocity averages, see equation (6-8)) accounted for the distinctly nonrandom crystal orientations used by the various authors in determining the elastic moduli. In particular, a significant portion of the data shown in Table 6.1 resulted from sound velocity measurements along the c axis, that is, with $\gamma = 0$.

The elastic constant average, $2\rho(\bar{V})^2$, defined by equation (6-16), is strongly dependent on c_{11}, c_{33}, c_{44} and c_{66} and has positive derivative with respect to each of these parameters. Its dependence on c_{13} is weak and its dependence on c_{12} yields a negative derivative. Each of these properties makes $2\rho(\bar{V})^2$ a sensitive and reliable indicator of the overall trend in the five elastic constants, whether measured by Brillouin spectroscopy or by ultrasonic techniques. The value of this parameter has been calculated and quoted for all sets of elastic moduli listed in Table 6.1.

The quantity, 100 (1-d), listed in Table 6.1 for each set of elastic moduli, denotes the percentage by which the corresponding values for $2\rho(\bar{V})^2$ exceed a reference value, 122.33359×10^8 N/m^2, this being the value appropriate for the weighted mean of the four sets of Brillouin measurements (see Table 6.3). The parameter d is the ratio of 122.33359×10^8 to $2\rho(\bar{V})^2$. Multiplication of each of the five elastic constants in any set by the corresponding value for d thus yields a new set having $2\rho(\bar{V})^2$ equal to the reference value determined from the average of the Brillouin data. Such adjusted sets of elastic constants are listed for each experiment referenced in Table 6.1. Comparison of these adjusted sets excludes a large portion

of whatever systematic error may have been present in the initial measurements. However, it must be noted that real differences in elastic properties may also be obscured when comparing results in this manner.

The deviations of $2\rho(\overline{V})^2$ from the reference value are very small in the case of each of the four sets of elastic constants determined by Brillouin spectroscopy. These deviations are, in particular, considerably smaller than the uncertainties typically quoted in the individual elastic constants. Barring coincidental compensation of errors, this leads to the following conclusions. Firstly, the previous observation that the elastic properties of ice do not vary among the four samples is supported. Secondly, the use of $2\rho(\overline{V})^2$ as a mean value for comparing sets of five elastic constants eliminates a significant portion of the relative uncertainty in the moduli. This was an expected result since $2\rho(\overline{V})^2$ is basically an average of all sound velocity measurements used in the determination of the elastic constants. Finally, the scatter in the four $2\rho(\overline{V})^2$ values, presumably reflecting the systematic error in each determination, is smaller than the estimated systematic error (0.41%, see Chapters 3 and 4). Since the terms contributing significantly to systematic error varied randomly among the four determinations (see Sec. 6.1), the small observed scatter in $2\rho(\overline{V})^2$ implies that the estimated systematic error is sufficient.

A preliminary inspection of Table 6.1 reveals that the general agreement of the present results with those of previous authors is fairly good. In particular, of the 21 quoted elastic moduli with stated uncertainties, 13 agree with the average of the Brillouin

measurements to within ~1 standard deviation while 16 agree to within ~2 standard deviations. As well, those values of Brockamp and Querfurth[30] and of Proctor[32] which do not include stated uncertainties are in reasonably good agreement with the present values. The only obvious discrepancies are found in comparing c_{44} determined by Jona and Scherrer[26] and the full set of elastic moduli determined by Dantl[35] with the present results.

The agreement among values of $2\rho(\overline{V})^2$ is good for all sets of measurements except those of Dantl.[35] More specifically, deviations of $2\rho(\overline{V})^2$ from the reference value for the Brillouin spectroscopic results approximate, or are less than, the corresponding uncertainties in the individual elastic constants for three of the sets of previous measurements. The two sets lacking quoted uncertainties are also in good agreement in the sense that the indicated deviations are typical of the scatter present in the set of six values. It is also worth noting, but undoubtedly coincidental to some extent, that the average of the six values of $2\rho(\overline{V})^2$ determined from previously published data equals 122.48×10^8 N/m^2, in excellent agreement with the reference value for the Brillouin spectroscopic results.

Because the results of Dantl have been widely accepted as standard values for the elastic moduli of ice, their comparison with other measurements bears special significance. While the difference between the average sound velocities measured by Dantl[33,34,35] and those measured in the present instance and by other previous authors may be real, the possibility of an unnoticed systematic error must not be neglected. Error in the absolute determination of acoustic

velocity by pulse-echo techniques (as were employed by Dantl) is known to result from several effects. These include diffraction within the sample,[96] phase changes at the point of reflection and at the point of coupling to the transducer, multiple reflection and consequent pulse shape changes within the transducer or coupling, along with a variety of other effects stemming from the inherent acoustic complexity of the layered transducer-coupling-sample system.[36,37] Relative velocity measurements using a given ultrasonic setup are generally more reliable than absolute measurements since the effects noted above tend to influence each of a set of measurements in a consistent manner.

In theory, the factors contributing to absolute error in ultrasonic measurements can be analyzed and controlled or compensated. In practice, the procedure is difficult and often uncertain. Thus, Huntington[10] describes measured sets of dynamic elastic moduli of a given material to be in "essential agreement" when measurements from different laboratories agree to within 5%. A survey of the variations in nine acoustic velocity measurements from one sample was carried out by Einsprach and Truell.[97] A single sample of carefully prepared fused silica was circulated among nine laboratories, each of which measured the transit time for longitudinal vibrations at 10 MHz. The standard deviation of the measurements of 0°C was ±0.5%, corresponding to uncertainty of at least ±1% in determination of elastic modulus. Of course, possible error in measurement of the density or length of the sample would lead to larger uncertainty in modulus determination. The maximum variation in transit time measurement was 1.4% (2.8% in modulus determination), with those values showing

greatest deviation from the mean lying above the mean. Thus, the authors[97] note that "errors in measurement tend to produce results in velocity measurements which are too low." Finally, it should be noted that uncertainties quoted in association with the various measurements were not, in general, sufficient to account for the observed scatter, particularly in the case of those measurements lying furthest from the mean. This emphasizes the difficulty in accurately assessing the absolute uncertainty in ultrasonic measurements.

The uncertainties in the elastic moduli quoted by Dantl[33,34,35] were determined from the root mean square deviations of a large number (greater than 35) of individual determinations of the moduli at different temperatures. Mean values for the elastic moduli were specified by least squares temperature dependence curves (as in (6-13)). Apparently, no allowance was made for possible systematic error, this being assumed negligible. However, in connection with the application of the pulse-echo method, Dantl[35] notes that "variations of pulse shape due to multiple reflections cause relatively large errors in the determination of the absolute value of the moduli." A double pulse interference (pulse superposition) method was therefore used by Dantl[33] to check the absolute values of the moduli, c_{11}, c_{33} and c_{44}. The checks showed no detectable error in the initial determinations of c_{33} and c_{44} while c_{11} was found to be 1.16% low in the initial determination. This discrepancy was neglected and the final values for the moduli were taken to be those determined by the pulse-echo method.

In principle, the pulse superposition method can be made to yield longitudinal sound velocity measurements accurate to within

1 part in 10,000. However, the analysis of Williams and Lamb[36] leading to this assertion points out several acoustic parameters of the apparatus which must be carefully evaluated before the method can be expected to yield an accurate result. These include the thickness of the bond between transducer and sample, the acoustic impedances of the transducer and the sample, the resonance frequency of the transducer and the degree of electric loading of the transducer. Each of these factors influences the phase shift which occurs at the transducer-sample interface. This phase shift varies with applied frequency and becomes more difficult to estimate as the difference between the applied frequency and the resonance frequency of the transducer is increased. The pulse superposition method requires varying the applied frequency over a range determined by the acoustic transit time in the sample. With the apparatus used by Dantl,[33] this range corresponded to approximately the resonance halfwidth of the transducer. It was thus necessary to utilize applied frequencies deviating substantially from resonance.

The error analysis carried out by Dantl[33] in connection with the application of the double pulse interference technique parallels that of Williams and Lamb.[36] While this analysis leads to negligible error under near ideal experimental conditions, it does not specifically address the problem of estimating error under nonideal or uncertain experimental conditions. Hence, the analysis tends to yield a lower limit rather than an upper limit for the measurement error. The magnitudes and uncertainties of some of the parameters required for error analysis have not been quoted by Dantl.[33] As well, his ultrasonic apparatus differs in some respects from that discussed

by Williams and Lamb.[36] Thus, it does not appear possible to assess the validity of the error analysis of Dantl or the resulting conclusion of negligible uncertainty in velocities measured by the double pulse interference technique. The hypothesis of sample-to-sample variation in the elastic moduli of ice cannot be verified by comparison of the present results with those of Dantl.[33,34,35]

The significant percentage by which the value, $2\rho(\bar{V})^2$, determined from the data of Dantl lies below the other values quoted in Table 6.1 warrants further investigation. As discussed above, systematic error cannot be ruled out. In this respect, it is unfortunate that the results of Dantl did not include a specific test of the conclusions regarding the effect of age on the elastic moduli of ice. Ideally, such a test would utilize comparisons of velocity measurements from a control sample of unaged ice, prepared in a manner identical to that used in preparing the aged ice sample. A test of this kind might also have pointed out any possible effect of high sample purity on the elastic moduli of ice. The samples used by Dantl[35] may have had a higher purity than those used in connection with any of the other measurements reported in Table 6.1. An analysis, however, was not included with the quoted results.

When multiplied by d (see preceding discussion in this section) to compensate for possible systematic error, the results of Dantl[35] show closer agreement with the Brillouin mean results (see Table 6.3) than do the results of other previous measurements. A maximum discrepancy of 1.7 standard deviations (or less if allowance is made for error in d) occurs in the value of c_{33}. The average discrepancy is 0.95 standard deviations. It is thus concluded that no significant nonsystematic difference occurs in the present

results versus those of Dantl. A future investigation of the possible role of sample-to-sample elastic property variation in accounting for the disagreement of the present results with those of Dantl could thus concentrate on measurement of a single elastic parameter. For example, a set of measurements of static bulk modulus could be used. With x-ray crystallographic techniques analogous to those used by LaPlaca and Post[72] in measuring thermal expansion, isothermal bulk modulus could presumably be determined to within about 1% with applied hydrostatic pressures ranging up to 10^7 N/m^2 (0.1 kbar).

The data from Table 6.1 show small or insignificant acoustic dispersion in ice over frequencies ranging from 5 kHz to 10 GHz. As noted previously, the average of the values of $2\rho(\bar{V})^2$ obtained from ultrasonic measurements agrees well with the corresponding average from the present hypersonic measurements. Thus, it appears appropriate to look for possible dispersion in the relative values of the moduli, $d \cdot c_{ij}$, quoted in the lower five rows of Table 6.1. While the scatter in the measurements makes comparisons uncertain, a small variation (<3%) in the moduli, c_{11} and c_{44}, with frequency may be evident. In particular, c_{11} when determined at ultrasonic frequencies tends to have a value slightly less than the corresponding value determined by Brillouin spectroscopy. The converse is true for c_{44}. The measurements of Jona and Scherrer[26] yield a particularly high value for c_{44}. Comparison of this value with the other values for c_{44}, quoted in Table 6.1, suggests that unnoticed error in measurement might be at least in part responsible for the deviation. The error analysis given by Jona and Scherrer[26] is not sufficiently detailed to evaluate the possibility. Further experimental work is

required to test or substantiate the observations noted above regarding the slight apparent frequency dependence of the relative values of the elastic moduli of ice.

Comparison of the present results with the temperature corrected results of Proctor[32] shows surprisingly good agreement in view of the large difference in the temperatures of measurement. The temperature corrections were made using the data of Proctor[32] and the data of Dantl.[35] Proctor determined least squares quadratic temperature dependence equations for all five elastic moduli of pure artificial ice from data extending over the temperature range -213° to $-163^{\circ}C$. The values of the moduli determined from these equations at $-163^{\circ}C$ were corrected, using (6-13), to correspond to -16° thereby yielding the values quoted in Table 6.1. Extrapolation from measured data was required only over the interval $-163^{\circ}C$ to $-140^{\circ}C$. Barring coincidental compensation of errors, the following two conclusions can be drawn from the good agreement of the present results with those of Proctor.[32] Firstly, there is small or negligible systematic discrepancy between the present results and those of Proctor. In this respect it is important to note that the ultrasonic apparatus of Proctor was tested on several specially prepared samples of aluminum so as to verify accuracy of the method. Quoted uncertainties in the results ranged from .04% for c_{11} to 1.2% for c_{12}. Secondly, existing temperature dependence data appears reliable over the range $-213^{\circ}C$ to $-0.7^{\circ}C$ (combination of results of Proctor[32] and of Dantl[35]). The greatest uncertainty is likely in the temperature dependence equations for c_{13} since this elastic constant is subject to considerable relative uncertainty when determined by ultrasonic techniques.

Fig. 6.2 shows velocity versus γ curves specified by the present data and by the data of Jona and Scherrer[26] and of Dantl.[35] Equivalent curves comparing the present data with those of Proctor[32] and of Brockamp and Querfurth[30] are shown in Fig. 6.3. The systematic difference between the present results and those of Dantl[35] is clearly evident in Fig. 6.2 as is the disagreement in the value of c_{44} as measured by Jona and Scherrer[26] versus the value determined from the present data. The transverse mode velocity at $\gamma = 0^{o}$ is controlled by c_{44}. The principal difference between the present curves and those specified by both Proctor[32] and by Brockamp and Querfurth[30] is attributable to the lower values of c_{13} quoted in both these sets of results.

The present values determined for the elastic moduli of ice can be used to test the results of the simplifying assumptions of Penny[14] regarding ice structure and intermolecular forces. These assumptions led to three equations among the five elastic moduli thus facilitating calculation of all five elastic moduli from two experimentally determined elastic parameters. The equations, rearranged slightly to aid in comparisons with the present data, are reproduced below[14]:

$$[(c_{11}+c_{12}) / (c_{13}+c_{33})]-1 = 0$$

$$\{[2c_{44}(c_{33}-5c_{13}+4c_{12})]^{\frac{1}{2}} / (c_{33}-c_{13})\}-1 = 0 \qquad (6\text{-}17)$$

$$\{[c_{12}(15c_{13}+c_{33}+14c_{44})]^{\frac{1}{2}} / [12c_{13}^{2}+5c_{13}c_{33}-c_{33}^{2}+2c_{44}(5c_{13}+2c_{33})]^{\frac{1}{2}}\}-1 = 0.$$

Upon substituting values for the elastic constants from Table 6.3, the lefthand sides of the three above equations are found to equal,

Fig. 6.2. Comparative plots of sound velocity versus γ in ice. BR. AV. - weighted mean elastic constants from present measurements (Table 6.3); J. & S. - elastic constants measured by Jona and Scherrer[26] (see Table 6.1); DANTL - elastic constants measured by Dantl[35] (see Table 6.1).

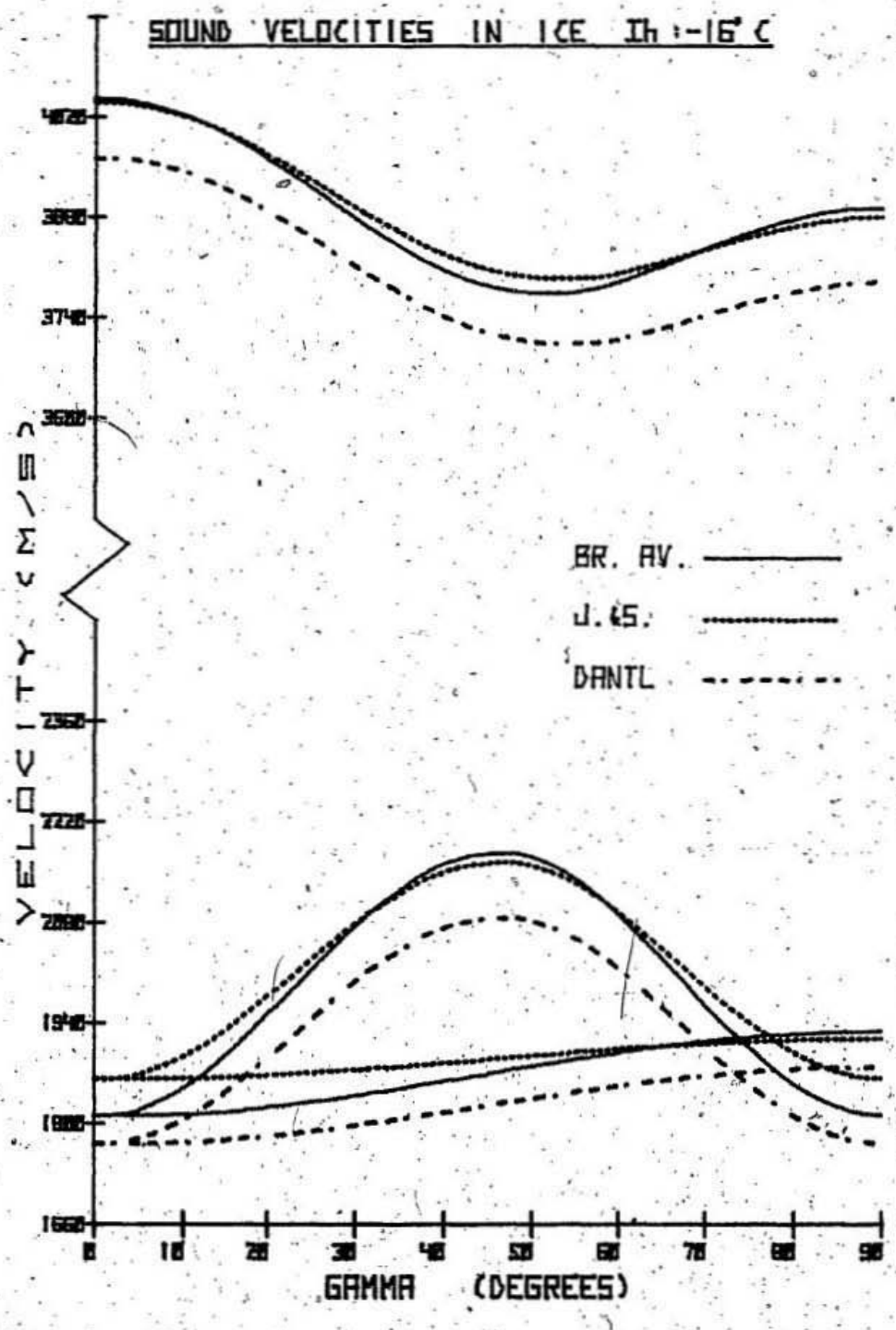
SOUND VELOCITIES IN ICE Ih :-16° C
VELOCITY (M/S)
BR. AV.
J.&S.
DANTL
GAMMA (DEGREES)

Fig. 6.2

Fig. 6.3. Comparative plots of sound velocity versus γ in ice. BR. AV. - weighted mean elastic constants from present measurements (Table 6.3); PROCTOR - temperature corrected (see text) elastic constants measured by Proctor[32] (see Table 6.1); B. & Q. - elastic constants measured by Brockamp and Querfurth[30] (see Table 6.1)

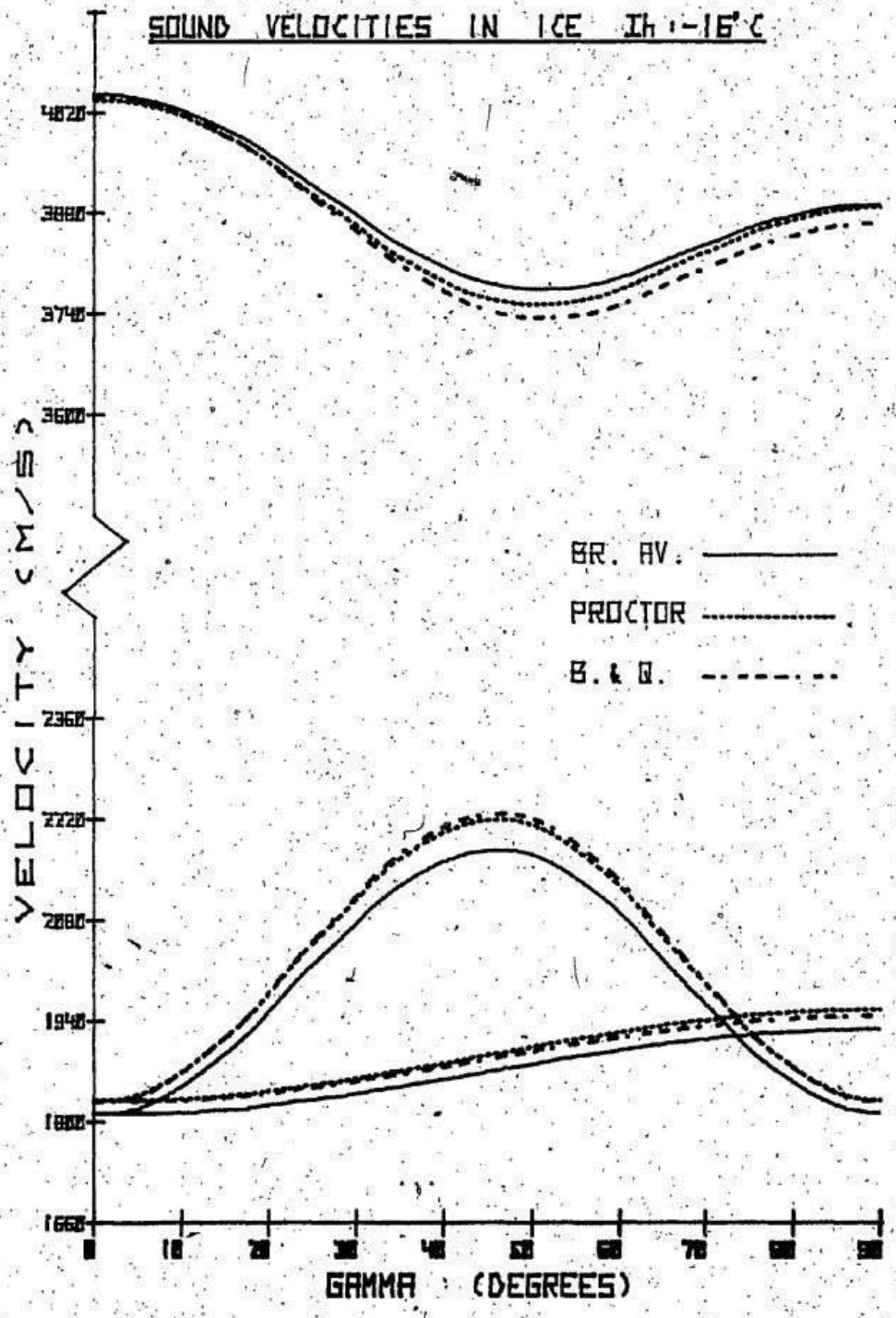
SOUND VELOCITIES IN ICE Ih : -16°C
VELOCITY (M/S)
4020
3880
3740
3600
2360
2220
2080
1940
1800
1660
BR. AV.
PROCTOR
B. & D.
GAMMA : (DEGREES)

Fig. 6.3

respectively:

$$(1.14 \pm .37)\%$$
$$(1.17 \pm .68)\% \qquad (6\text{-}17a)$$
$$(2.91 \pm .33)\%$$

The above values indicate that the agreement of the present results with the equations of Penny[14] is fairly good in absolute terms, although not within experimental uncertainty. The first of the equations (6-17) is equivalent to the condition that the linear compressibility of ice be isotropic (see equation (6-3)). Thus the equation relates to the restriction that the four nearest neighbours of an oxygen atom in the ice crystal structure lie at the vertices of a regular tetrahedron, giving rise to a constant c/a ratio of $(8/3)^{\frac{1}{2}}$. The second and third of equations (6-17) lack immediate physical significance.

The present results can be further compared with the theoretical results of Penny[14] by calculating elastic constants from the present data subject to the constraints, (6-17). This procedure appears more appropriate than simple comparison with the elastic constants quoted by Penny since these elastic constants were based in part on experimental data differing significantly from the present measurements. In particular, Penny utilized the dynamic measurements of Young's modulus and Poisson's ratio in quasi-isotropic polycrystalline ice, quoted by Northwood.[25] These values, 98×10^8 N/m^2 and 0.335 respectively, differ from those values quoted in Table 6.5, possibly as a result of preferred grain orientation in the polycrystalline samples. The values from Table 6.5 were thus used in

calculating elastic constants analogous to those calculated by Penny[14] so as to eliminate the effects of experimental error in comparisons with the present results. Accordingly, the atomic force constants α and β as defined by Penny[14] were found to have values $\alpha = 0.78227$ N/m, $\beta = 9.0289$ N/m thereby yielding the following values for elastic constants which satisfy the equations (6-17): $c_{11} = 138.57$, $c_{12} = 68.83$, $c_{13} = 59.55$, $c_{33} = 147.85$, $c_{44} = 31.08$ (units of 10^8 N/m^2). Velocity versus γ curves specified by these elastic constants are shown, along with the curves specified directly by the Brillouin data, in Fig. 6.4. It is hoped that the present measurements of elastic moduli will aid in the ongoing theoretical analysis of the molecular processes underlying the complex mechanical properties of ice.

In conclusion, it has been demonstrated that the technique of Brillouin spectroscopy is effective for determining the "local" elastic properties of ice. Furthermore, using this technique it was found that the local elastic constants of ice formed under very different conditions are basically the same. Consequently, the hypothesis of sample-to-sample variation (in particular, the correlation with sample age as suggested by Dantl[35]) has not been substantiated. Finally, it is believed that the elastic constants obtained in the present work are subject to smaller overall uncertainty than values measured previously. Because of this and because of the range of samples studied, the present results are the most reliable obtained to date for use in scientific or engineering applications involving artificial ice samples or ice formed in the natural environment.

Fig. 6.4. Comparative plots of sound velocity versus γ in ice. BR. AV. - weighted mean elastic constants from present measurements (Table 6.3); THEORY - elastic constants calculated using the theoretical relations of Penny[14] and values of polycrystalline Young's modulus and Poisson's ratio from present results (Table 6.5).

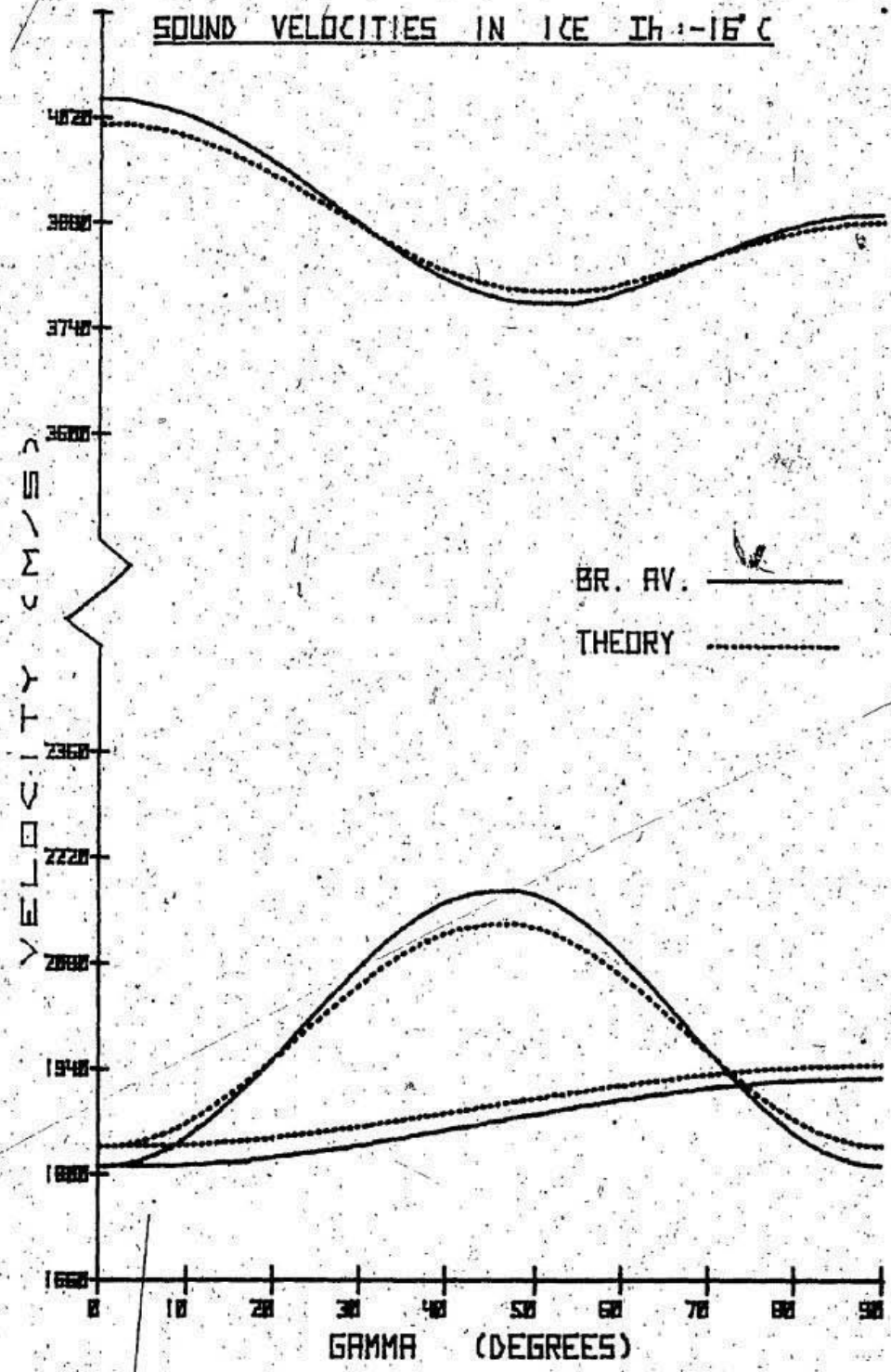
SOUND VELOCITIES IN ICE Ih :-16° C
VELOCITY M/S
4020
3840
3740
3600
2360
2220
2040
1940
1800
1660
BR. AV.
THEORY
0
10
20
30
40
50
60
70
80
90
GAMMA (DEGREES)

Fig. 6.4

REFERENCES

1. N.H. Fletcher. The Chemical Physics of Ice. Cambridge University Press, London. 1970.

2. P.V. Hobbs. Ice Physics. Oxford University Press, London. 1974.

3. J.W. Glen. The Physics of Ice. Cold Regions Science and Engineering. Pt. II, Sec. C2a. U.S. Cold Regions Research and Engineering Laboratory, Hanover, N.H. 1974.

4. E. Whalley. In Physics of Ice: Proceedings of the International Symposium on Physics of Ice, Munich, Germany. Edited by N. Riehl, B. Bullemer and H. Engelhardt. Plenum Press, New York. 1969. p. 19.

5. J.W. Glen. The Mechanics of Ice. Cold Regions Science and Engineering. Pt. II, Sec. C2b. U.S. Cold Regions Research and Engineering Laboratory, Hanover, N.H. 1975.

6. W. Weeks and A. Assur. The Mechanical Properties of Sea Ice. Cold Regions Science and Engineering. Pt. II, Sec. C3. U.S. Cold Regions Research and Engineering Laboratory, Hanover, N.H. 1967.

7. B. Michel. Ice Mechanics. Les Presses de l'Université Laval, Quebec. 1978.

8. L.D. Landau and Ye. M. Lifshitz. Theory of Elasticity. Pergamon Press, London. 1959.

9. J.F. Nye. Physical Properties of Crystals, Clarendon Press, Oxford. 1957.

10. H.B. Huntington. The Elastic Constants of Crystals. Academic Press, New York. 1958.

11. M.J.P. Musgrave. Crystal Acoustics. Holden-Day, San Francisco, 1970.

12. P.H. Gammon. M.Sc. Thesis. Memorial University of Newfoundland. 1978. (Unpublished).

13. W. Voigt. Lehrbuch der Kristallphysik. Teubner, Leipzig. 1910.

14. A.H.A. Penny. Proc. Cambridge Phil. Soc. 44, 423 (1948).

15. Yu. P. Doronin and D.E. Kheisin. Sea Ice. Amerind Publishing Co. Pvt. Ltd., New Delhi. 1977.

16. M.P. Langleben. Can. J. Phys. 40, 1 (1962).

17. L.W. Gold. Can. J. Phys. 36, 1265 (1958).

18. L.E. Malvern. Introduction to the Mechanics of a Continuous Medium. Prentice-Hall Inc., Englewood Cliffs, N.J. 1969.

19. H.J. McSkimin. In Physical Acoustics. Vol. 1, Pt. A. Edited by W.P. Mason. Academic Press, New York. 1964. p. 271.

20. J. Weertman. In Physics and Chemistry of Ice. Edited by E. Whalley, S.J. Jones and L.W. Gold. Royal Society of Canada, Ottawa. 1973. p. 320.

21. M.D. Coon, G.A. Maykut, R.S. Pritchard, D.A. Rothrock, and A.S. Thorndike. AIDJEX Bull. 24 (1974).

22. T.M. Haridasan and J. Govindarajan. Chem. Phys. Left. 4, 11 (1969).

23. B. Renker and P.V. Blanckenhagen. In Physics of Ice: Proceedings of the International Symposium on Physics of Ice, Munich, Germany. Edited by N. Riehl, B. Bullemer and H. Engelhardt. Plenum Press, New York. 1969. p. 287.

24. N.E. Dorsey. Properties of Ordinary Water-substance. Reinhold Publishing Corporation, New York. 1940.

25. T.D. Northwood. Can. J. Res., Sec. A, 25, 88 (1947).

26. F. Jona and P. Scherrer. Helv. Phys. Acta 25, 35 (1952).

27. R.E. Green and L. MacKinnon. J. Acous. Soc. Am. 28, 1292 (1956).

28. R. Bass, D. Rossberg and G. Ziegler. Z. Phys. 149, 199 (1957).

29. V.V. Bogorodskii. Sov. Phys. Acous. 10, 124 (1964).

30. B. Brockamp and H. Querfurth, Z. Polarforschung 5, 253 (1964).

31. A. Zarembovitch and A. Kahane. Compt. Rend. Hebd. Séance. Acad. Sci., Paris 258, 2529 (1964).

32. T.M. Proctor. J. Acous. Soc. Am. 39, 972 (1966).

33. G. Dantl. Thesis (Dr. rer. nat.) Technischen Hochschule Stuttgart. 1967.

34. G. Dantl. Phys. Kondens. Materie 7, 390 (1968).

35. G. Dantl. In Physics of Ice: Proceedings of the International Symposium on Physics of Ice, Munich, Germany. Edited by N. Riehl, B. Bullemer and H. Engelhardt. Plenum Press, New York. 1969. p. 223.

36. J. Williams and J. Lamb. J. Acous. Soc. Am. 30, 308 (1958).

37. H.J. McSkimin. J. Acous. Soc. Am. 33, 12 (1961).

38. E.J. Workman and S.E. Reynolds. Phys. Rev. 78, 254 (1950).

39. G. Dantl and I. Gregora. Naturwissenschaften 55, 176 (1968).

40. A. Deubner, R, Heise and K. Wenzel. Naturwissenschaften 47, 600 (1960).

41. B. Kamb. In Physics and Chemistry of Ice. Edited by E. Whalley, S.J. Jones and L.W. Gold. Royal Society of Canada, Ottawa. 1973. p. 28.

42. I. Teichmann and G. Schmidt. Phys. Stat. Sol. 8, K145 (1965).

43. T.R. Butkovich. J. Glaciol. 2, 553 (1955).

44. D.C. Ginnings and R.J. Corruccini. J. Res. Nat. Bur. Std. 38, 583 (1947).

45. P.R. Camp. J. Glaciol. 21, 703 (1978).

46. U. Mitzdorf and D. Helmreich. J. Acous. Soc. Am. 49, 723 (1971).

47. G.E. Durand and A.S. Pine. IEEE J. Quantum Electronics. QE4, 523 (1968).

48. J.R. Sandercock. RCA Review 36, 89 (1975).

49. B.P. Stoicheff. In Fundamental and Applied Laser Physics. Proceedings of the Esfahan Symposium. Edited by M.S. Feld, A. Javan and N.A. Kurnit. John Wiley and Sons, Inc., New York. 1973. p. 573.

50. B.P. Stoicheff. In Rare Gas Solids. Vol.2. Edited by M.L. Klein and J.A. Venables. Academic Press, New York. 1977, p. 979.

51. C. Kittel. Introduction to Solid State Physics. 5th Edition. John Wiley and Sons, Inc., New York. 1976.

52. G.B. Benedek and K. Fritsch. Phys. Rev. 149, 647 (1966).

53. H. Kiefte and M.J. Clouter. J. Chem. Phys. 62, 4780 (1975).

54. H. Kiefte and M.J. Clouter. J. Chem. Phys. 64, 1816 (1976).

55. P.H. Gammon, H. Kiefte and M.J. Clouter. J. Chem. Phys. 70, 810 (1978).

56. S.F. Ahmad, H. Kiefte and M.J. Clouter. J. Chem. Phys. 69, 5468 (1978).

57. A. Ermoleiff. Solid State Comm. 17, 1013 (1975).

58. J. Schwarz and W.F. Weeks. J. Glaciol. 19, 499 (1977).

59. C. Jaccard and L. Levi. Z. Angew. Math. Phys. 12, 70 (1961).

60. I.G. Young and R.E. Salomon. J. Chem. Phys. 48, 1635 (1968).

61. A. Kahane, J. Klinger and M. Philippe. Solid State Comm. 7, 1055 (1969).

62. J.L. Amoros, N.J. Buerger and M.C. de Amoros. The Laue Method. Academic Press, New York. 1975.

63. L.V. Azaroff. Elements of X-ray Crystallography. McGraw-Hill, New York. 1968.

64. B.D. Cullity. Elements of X-ray Diffraction. Addison-Wesley, Reading, Mass. 1956.

65. B. Mason and L.G. Berry. Elements of Minerology. W.H. Freeman and Company, San Francisco. 1968.

66. H. Goldstein. Classical Mechanics. Addison-Wesley, Cambridge. 1950.

67. S.F. Ahmad. Ph.D. Thesis. Memorial University of Newfoundland. 1980. (Unpublished).

68. P.H. Gammon, H. Kiefte, M.J. Clouter and W.W. Denner. J. Acous. Soc. Am. (in press for May, 1981).

69. G. Dahlquist and A. Bjork. Numerical Methods. Prentice-Hall, Englewood Cliffs, N.J. 1974.

70. P.H. Gammon, H. Kiefte and M.J. Clouter. J. Glaciol. 25, 159 (1980).

71. International Critical Tables. McGraw-Hill Book Co., Inc. New York. 1926-33.

72. S. LaPlaca and B. Post. Acta Cryst. 13, 503 (1960).

73. T.R. Butkovich. J. Appl. Phys. 30, 350 (1959).

74. D. Landheer. Ph.D. Thesis. University of Toronto. 1974. (Unpublished).

75. A. Higashi. In Physics of Ice: Proceedings of the International Symposium on Physics of Ice, Munich, Germany. Edited by N. Riehl, B. Bullemer and H. Engelhardt. Plenum Press, New York. 1969. p. 197.

76. G. Lemieux (private communication).

77. Handbook of Chemistry and Physics. Edited by R.C. Weast. 51st Edition. The Chemical Rubber Co., Cleveland, Ohio. 1970-71.

78. J.D. Jackson. Classical Electrodynamics. John Wiley and Sons, Inc., New York. 1975.

79. P.H. Gammon, H. Kiefte, M.J. Clouter and W.W. Denner, Solid State Comm. 37, 313 (1981).

80. A. Higashi. J. Glaciol. 21, 629 (1978).

81. N. Rowell and G.I. Stegeman. Phys. Rev. Lett. 41, 970 (1978).

82. G.I. Stegeman and N. Rowell. In Proceedings - VIIth International Conference on Raman Spectroscopy. Edited by W.F. Murphy. North-Holland Publishing Company, Amsterdam. 1980. p. 360.

83. J.R. Sandercock. In Proceedings - VIIth International Conference on Raman Spectroscopy. Edited by W.F. Murphy. North-Holland Publishing Company, Amsterdam. 1980. p. 364.

84. R. London. In Proceedings - VIIth International Conference on Raman Spectroscopy. Edited by W.F. Murphy. North-Holland Publishing Company, Amsterdam. 1980. p. 368.

85. W.C. Chang, S. Mishra and R. Bray. In Proceedings - VIIth International Conference on Raman Spectroscopy. Edited by W.F. Murphy. North-Holland Publishing Company, Amsterdam. 1980. p. 438.

86. N. Rowell and G.I. Stegeman. Phys. Rev. B 18, 2598 (1978).

87. R. Stoneley. Mon. Not. Roy. Ast. Soc. Geophys. Suppl. 5, 343 (1949).

88. R. Stoneley. Proc. Roy. Soc. A 232, 447 (1955).

89. N.H. Fletcher. Phil. Mag. 18, 1287 (1968).

90. S. Mantovani, S. Valeri, A. Loria and U. del Pinnino. J. Chem. Phys. 72, 1077 (1979).

91. H.H.G. Jellinek and K. Juznik. Phys. Stat. Sol. A. 2, 837 (1970).

92. T. Hondoh and A. Higashi. J. Glaciol. 21, 629 (1978).

93. D.R. Homer and J.W. Glen. J. Glaciol. 21, 429 (1978).

94. N. Maeno. In Physics and Chemistry of Ice. Edited by E. Whalley, S.J. Jones and L.W. Gold. Royal Society of Canada, Ottawa. 1973. p. 140.

95. W.F. Giauque and J.W. Stout. J. Am. Chem. Soc. 58, 1144 (1936).

96. A.E. Lord. J. Acous. Soc. Am. 40, 163 (1966).

97. N. Einspruch and R. Truell. J. Appl. Phys. 33, 3087 (1962).

END

14-04-82

FIN